Orthogonal Analytical Approaches for the Investigation of Specific Metabolic Pathways of 17α-Methyltestosterone with the Focus on Hydroxylation Reactions

Inaugural-Dissertation

to obtain the academic degree

Doctor rerum naturalium (Dr. rer. nat.)

submitted to the Department of Biology, Chemistry, Pharmacy

of Freie Universität Berlin

by

Felix Bredendiek

2021

Research of the present study was conducted from 2017 till 2020 under supervision of Prof. Dr. Maria Kristina Parr at the Institute of Pharmacy of the Freie Universität.

First Assessor:	Prof. Dr. Maria Kristina Parr
Second Assessor:	Prof. Dr. Francesco Botrè

Date of Defense: 17th May 2021

Acknowledgment

First of all, I would like to thank my supervisor Prof. Dr. Maria Kristina Parr, for the last three and a half years, her suggestions for new approaches in difficult times, and the excellent support she gave me. Without you, I would not be where I am now.

Further, I would like to thank Dr. Peter Witte. Because of you, teaching never felt like work for me.

Thanks to Steffen Loke, Sebastian Schmidtsdorff, Maxi Wenzel, Heike Scheffler, and Nora Reitner for the fun time in the practical laboratory course of the 5th semester.

Also, I would like to thank Anna Stoll and Oliver Schneider for the best coffee breaks in the past years (even if some were only online) and their support.

My grateful thanks to Bernhard Wüst for answering all my questions and all the knowledge you gave me about the instruments.

I thank all group members of the group of Prof. Parr for the supportive, friendly atmosphere.

Thanks to Dr. Xavier de la Torre and Prof. Dr. Francesco Botrè for measuring my samples in Rome, and Dr. Nils Schlörer for the time he invested in my NMR measurements.

I want to thank my friends and my family, especially my parents Jutta and Knut Bredendiek, and my brother Dr. Maximilian Bredendiek for their love and the non-ending support they gave me.

Finally, I want to thank you, Cindy, for being on my side every day, your love and affection. All this would not have been possible without you.

Table of content

I. Abbreviations III

1 Introduction 1

1.1 Steroid Hormones 1

1.1.1 Endogenous Steroids 3

1.1.2 Exogenous Steroids 5

1.2 Metabolism 6

1.2.1 Hydroxylation 6

1.2.2 Aromatization of Androgens 8

1.2.3 Metabolism of 17α-Methyltestosterone 10

1.3 Steroid Analysis 11

2 Aim of this Work 13

3 Material and Methods 15

3.1 Material 15

3.2 Methods 18

3.2.1 Liquid Chromatography 19

3.2.2 Supercritical Fluid Chromatography 22

3.2.3 Gas Chromatography 25

3.2.4 Synthesis of Reference Material 29

3.2.5 Structure Confirmation of Synthesized Products 31

3.2.6 Incubation Experiments 32

3.2.7 Human Urine Samples 33

4 Results and Discussion 34

4.1 Synthesis of 2α- and 2β-Hydroxy-17α-methyltestosterone 34

4.2 Synthesis of 4-Hydroxy-17α-methyltestosterone 46

4.3 Synthesis of 19-Hydroxy-17α-methyltestosterone..... 52

4.4 Analytical Method Development 57

4.4.1 GC-MS methods..... 57

4.4.2 LC-MS methods 61

4.4.3 SFC-MS methods 64

4.5 *In vitro* Hydroxylation of MT 67

4.5.1 Biotransformation of MT with HLM.....68

4.5.2 Biotransformation of MT with CYP2C19 71

4.5.3 Biotransformation of MT with CYP1A2 and CYP1B1 73

4.5.4 Biotransformation of MT with CYP19A1 77

4.5.5 Conclusion of the Biotransformation Studies of MT..... 79

4.6 *In vivo* Hydroxylation of MT 81

5 Summary and Outlook 86

6 Zusammenfassung und Ausblick..... 88

7 Curriculum Vitae 90

8 References 92

9 List of figures 101

10 List of tables.....109

11 Annex.....111

I. Abbreviations

$[M]^{\bullet+}$	Radical cation of the molecular ion
19OHAED	19-Hydroxyandrost-4-ene-3,17-dione
19OHMT	19-Hydroxy-17α-methyltestosterone
2αOHMT	2α-Hydroxy-17α-methyltestosterone
2βOHMT	2β-Hydroxy-17α-methyltestosterone
2ξOHMT	2ξ-hydroxy-17α-methyltestosterone
4OHMT	4-Hydroxy-17α-methyltestosterone, oxymesterone
5αDHT	5α-Dihydrotestosterone
5αTHMT	17α-Methyl-5α-androstane-3α,17β-diol
5βTHMT	17α-Methyl-5β-androstane-3α,17β-diol
6βOHMT	6β-Hydroxy-17α-methyltestosterone
AAF	Adverse analytical findings
AAS	Anabolic androgenic steroids
ACN	Acetonitrile
ACTH	Adrenocorticotropic hormone
AKR	Aldo-keto reductase
APCI	Atmospheric pressure chemical ionization
AR	Androgenic receptor
COSY	Heteronuclear correlation spectroscopy
CYP	Cytochrome P450
CYP11A1	Cytochrome P450 isoenzyme 11A1
CYP11B1	Cytochrome P450 isoenzyme 11B1
CYP11B2	Cytochrome P450 isoenzyme 11B2
CYP17A1	Cytochrome P450 isoenzyme 17A1
CYP19A1	Cytochrome P450 isoenzyme 19A1, aromatase
CYP1A2	Cytochrome P450 isoenzyme 1A2
CYP1B1	Cytochrome P450 isoenzyme 1A2

CYP21	Cytochrome P450 isoenzyme 21
CYP3A4	Cytochrome P450 isoenzyme 3A4
DCM	Dichloromethane
DEPT	Distortionless enhancement by polarization transfer
DHCMT	Dehydrochloromethyltestosterone
DMSO	Dimethyl sulfoxide
EI	Electron ionization
ESI	Electrospray ionization
GC	Gas chromatography
HLM	Human liver microsomes
HMBC	Hetero multiple bond correlation
HMQC	Heteronuclear multiple quantum coherence
HPLC	High performance liquid chromatography
HRMS	High resolution mass spectrometry
HSD	Hydroxysteroid dehydrogenase
LC	Liquid chromatography
MD	Metandienone
MRM	Multiple reaction monitoring
MS	Mass spectrometry
MSTFA	N-methyl-N-(trimethylsilyl)trifluoracetamide
MT	17α-Methyltestosterone
NADPH	Nicotinamide adenine dinucleotide phosphate
NMR	Nuclear magnetic resonance
PAPS	3'-Phosphoadenosin-5'-phosphosulfate
PED	Performance enhancing drugs
ppm	Parts per million
PREG	Pregnenolone
QQQ	Triple quadrupole
QTOF	Quadrupole time-of-flight

RT	Retention time
SFC	Supercritical fluid chromatography
SULT	Sulfotransferase
T	Testosterone
TMIS	Trimethyliodosilane
TMS	Trimethylsilyl
UGT	UDP-Glucuronosyltransferase
WADA	World Anti-Doping Agency
WM	Wagner-Mehrwein

1 Introduction

Steroids can be misused in sports to enhance the athlete's performance. Usually, the administration aims for the anabolic effects of androgenic steroids (anabolic androgenic steroids, AAS). Therefore, the use of AAS, as well as the use of aromatase inhibitors (steroidal and non-steroidal) and other performance enhancing drugs (PEDs; for example, growth factors), is prohibited by the World Anti-Doping Agency (WADA) [1]. The present work discusses various metabolic pathways for different steroids, such as testosterone (T) as one of the predominant male sex hormones, androstenedione (AED) as an endogenous prohormone, or 17α-methyltestosterone as an exogenous steroid. The investigation and identification of specific metabolomes for these substances are essential for future antidoping analysis. The following sections will give an overview of the characteristics of steroids, their metabolism, and analysis.

1.1 Steroid Hormones

Steroid hormones have a basic structure consisting of four fused ring systems (A, B, C, and D ring), which give an almost planar molecule structure [2]. For a better understanding, the numbering system of steroids is exemplified with cholestane (Figure 1). The substituents can be orientated above (β-space) or under (α-space) the paper level [3].

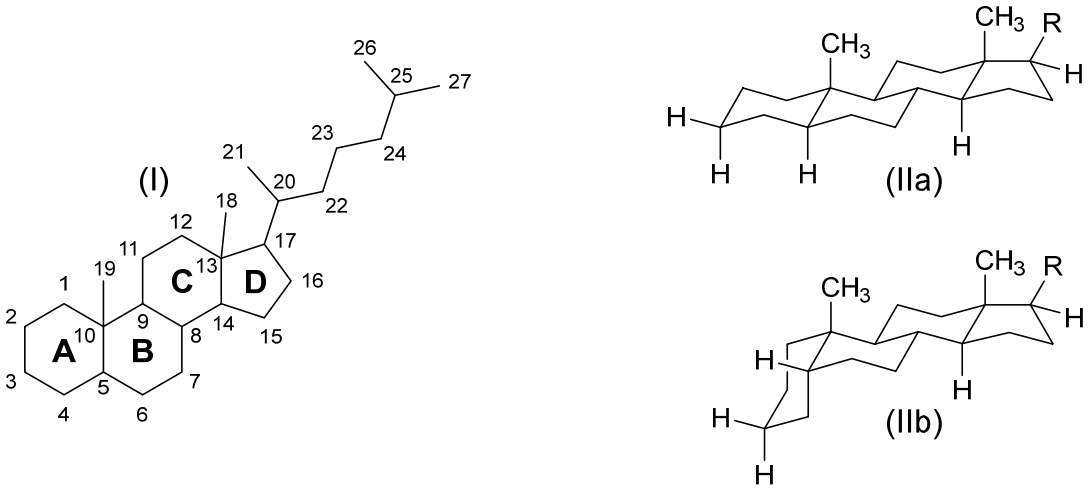

Figure 1: Numbering system of steroids exemplified with cholestane (I) and its spatial arrangement of 5α- (IIa) and 5β-configuration (IIb), adapted from [4]

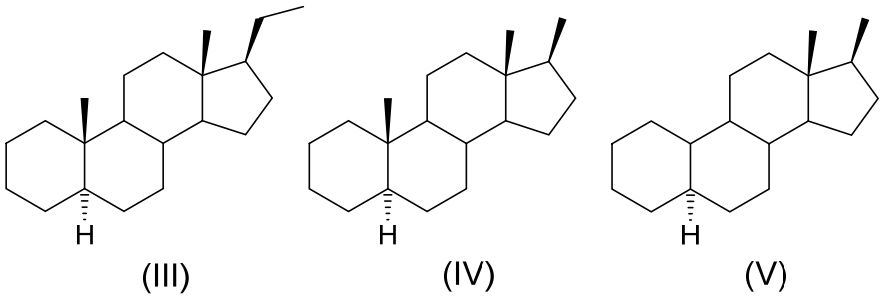

Figure 2: Basic structures of pregnans (C21-steroids, III), androgens (C19-steroids, IV), and estranes (C18-steroids, V)

Therefore, the configuration at position five has a significant influence on the spatial structure of the molecule. Figure 1 depicts this exemplarily for 5α-cholestane (IIa) and 5β-cholestane (IIb). The precursor for all sex hormones is pregnenolone (PREG), biosynthesized from cholesterol (C27-steroid) [5]. Cholesterol is a structural element of cell membranes, and therefore present in all humans and animals. The side chain of cholesterol is cleaved by cytochrome P450 isoform 11A1 (CYP11A1) in the mitochondria to give PREG, which belongs to the class of pregnanes (C21-steroids) [5]. The number of carbons classifies basic steroid structures. Figure 2 shows the fundamental structures of pregnanes (III, C21-steroids), androstanes (IV, C19-steroids), and estranes (V, C18-steroids) [2].

Another way of the biotransformation of cholesterol is the transformation into bile acids. Oxidoreductases targeting oxygens in positions 3 and 17 (HSD) and the 5α-reductase play an essential role in forming corticosteroids and sexual hormones [5]. Also, enzymes like CYP17A1 (microsomal, 17α-hydroxylase, 17,20-lyase), CYP11B1/2 (mitochondrial, 11β-hydrolase/aldosterone synthase), CYP19A1 (microsomal, aromatase), and CYP21 (microsomal, 21-hydroxylase) are essential in the formation of glucocorticoids, gestagenes, androgens, mineralocorticoids, and estrogens [5, 6]. Figure 3 shows the essential biosynthetic pathways for the formation of PREG, AED, cortisol, aldosterone, and estrone.

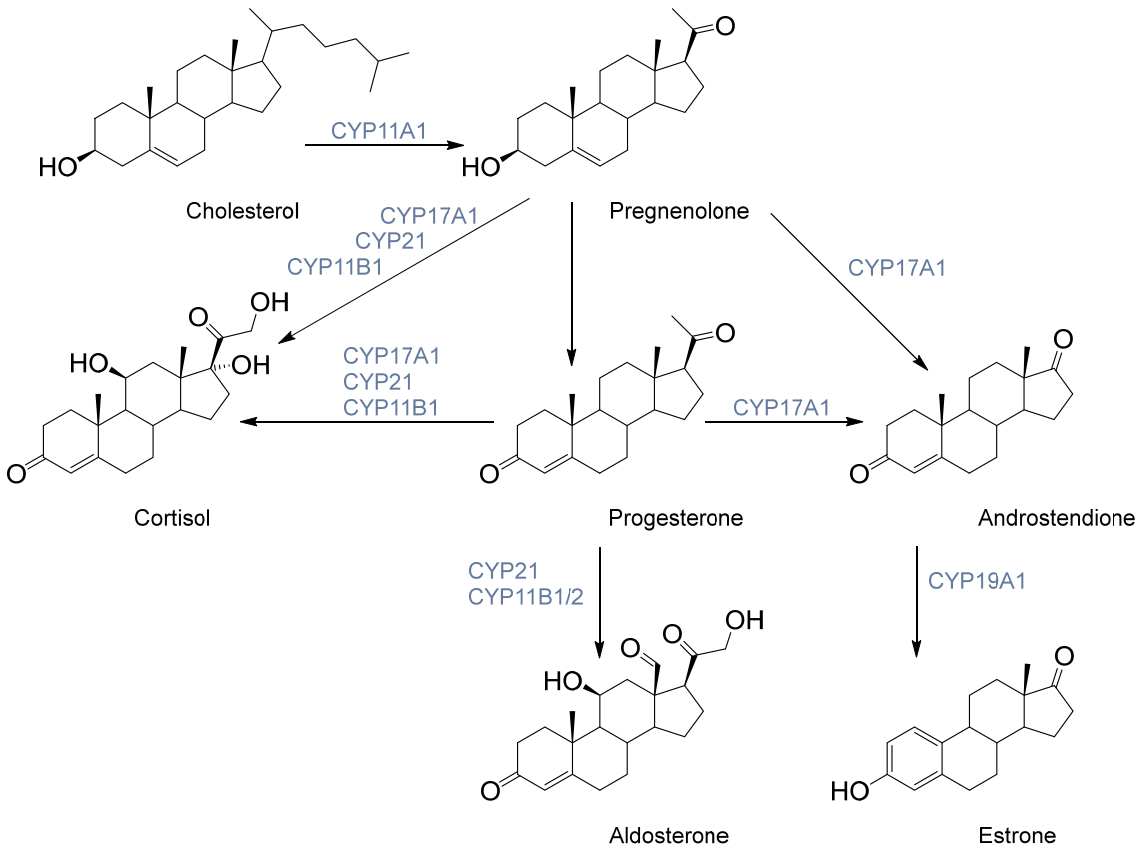

Figure 3: Essential biosynthetic pathways in the formation of pregnanes (pregnenolone), glucocorticoids (cortisol), gestagens (progesterone), androgens (androstenedione), mineralocorticoids (aldosterone), and estrogens (estrone) with involved CYP enzymes, starting from cholesterol; partially adapted from [4] and [6]

1.1.1 Endogenous Steroids

All androgens (male sex hormones) are structure-based to 5α-androstane (Figure 2, IV). They show effects on the strength and mass of muscles (anabolic) and the sexual maturation (androgenic). Male sex hormones are also present in women but show higher concentrations and a higher impact on humans with male sex organs. The most dominant androgen in men is T. It is mainly formed in the testicles (Leydig cells) via the intermediates PREG and AED. Enzymes involved in this formation are CYP17A1, 3α-hydroxysteroid dehydrogenase (HSD3B2), and the aldo-keto reductase 1C3 (AKR1C3), reducing the oxo function at C17 into the corresponding C17 hydroxy group (Figure 4). T is binding to the nuclear androgenic receptor (AR), mostly in the brain, muscles, and sex organs. Its metabolite 5α-dihydrotestosterone (5αDHT) has a higher affinity to the ARs. Therefore, 5αDHT is synthesized from T by the 5α-reductase

(SRD5A1/2) in the effector organ (Figure 4) [7]. This pathway is described as the "front-door-pathway". The literature also describes a second pathway for 5αDHT formation from allopregnanolone, called the "back-door-pathway" (not displayed in Figure 4) [8]. The formation of weak androgens, like AED, in the adrenal cortex is controlled by the adrenocorticotropic hormone (ACTH) and present in males and females.

Estrogens are formed from androgens (T, AED, and 16-hydroxyandrostendion) by CYP19A1 (Figure 4, aromatase) in, for example, the placenta, ovaries, fat tissue, or growing bones. Compared to androgens in men, estrogens in women have an impact on female sexual maturation. Estrogens like estradiol, estrone, or estriol also control the menstrual cycle regulation and pregnancy. Figure 4 shows essential biosynthetic pathways in the formation of important androgens and estrogens.

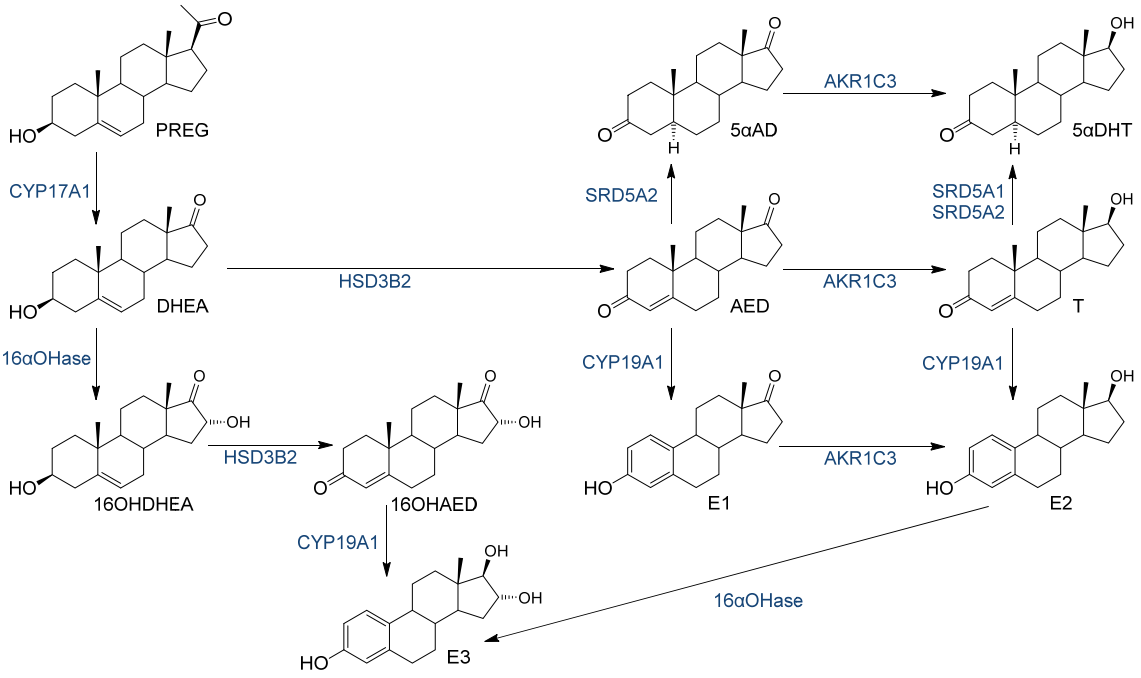

Figure 4: Biosynthetic pathways including the formation of dihydrotestosterone (front-door-pathway) and estrogens (including involved enzymes): pregnenolone (PREG), dehydroepiandrosterone (DHEA), 16-hydroxydehydroepiandrosterone (16OHDHEA), 16-hydroxyandrostendione (16OHAED), androstenedione (AED), 5α-androstanedione (5αAD), testosterone (T), 5α-dihydrotestosterone (5αDHT), estrone (E1), estradiol (E2), estriol (E3), hydroxysteroid dehydrogenase (HSD), aldo-keto reductase (AKR), SRD5A (5α-reductase); partially adapted from [8-10]

1.1.2 Exogenous Steroids

T can be synthetically modified to avoid unwanted side effects or change pharmacokinetics. The medical use and misuse of endogenous and exogenous steroids can cause different side effects. Androgenic side effects caused by aromatization can be, for example, gynecomastia or alterations in the menstrual cycle [11]. Other unwanted side effects described in the literature are high blood pressure, problems in liver- and kidney function, and heart diseases [7, 11]. These synthetically modified substances are foreign to the human body; therefore, they are called exogenous steroids. Typical modifications are exemplified in Figure 5. As the bioavailability is too low for oral application, T is typically applied intramuscular or topical [12, 13]. The introduction of a methyl group in position 17, as seen in 17α-methyltestosterone (MT), metandienone (MD), dehydrochloromethyltestosterone (DHCMT), and stanozolol, increases the bioavailability by hindering the oxidation of the C17 hydroxy group and enables oral administration [14]. A double bond in position 1 (MD, DHCMT) can be introduced to reduce androgenic side effects by preventing the aromatization process with CYP19A1. Another way to prevent the aromatization process is a missing C19 methyl group (nandrolone) [14] (the effect of the C19 methyl group in the aromatization will be explained in 1.2.1). The use of aromatase inhibitors is a third option to avoid androgenic side effects caused by aromatization.

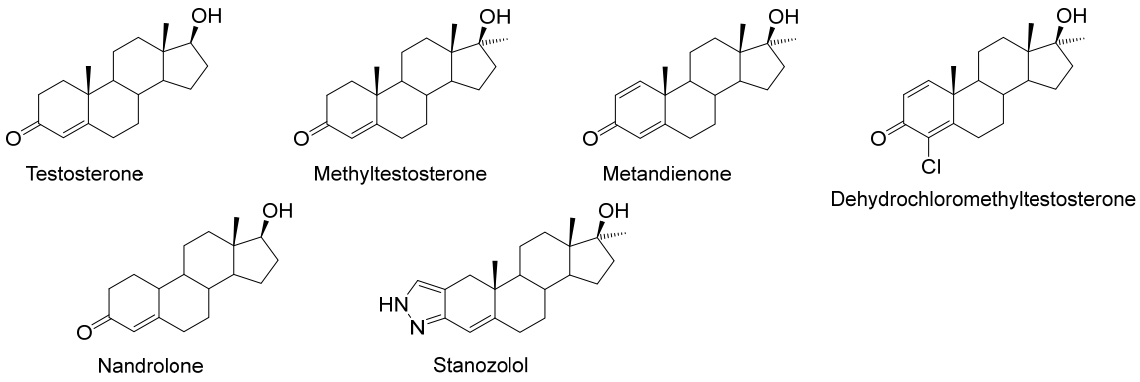

Figure 5: Typical modifications of T resulting in methyltestosterone, metandienone, dehydrochlormethyltestosterone (DHCMT), nandrolone, stanozolol

1.2 Metabolism

Most of the endogenous and exogenous (xenobiotics) steroids are lipophilic. They are predominantly converted into more hydrophilic substances to be excreted from the body. The conversion of the parent compound can lead to more active metabolites (for example, 5αDHT) or less active substances [15]. Hydroxylation, oxidation, hydrolyzation, and reduction are common reactions in phase-I-metabolism [7]. These reactions lead to more hydrophilic metabolites, which are excreted faster. The oxidation reactions in metabolism are often correlated to cytochrome P450 enzymes (CYPs) or occur due to the autoxidation of the parent compound. CYP3A4 is one of the most dominant enzymes involved in human metabolism. Especially in steroid metabolism, the 5α-reductase and HSD_3 play an essential role in forming reduced metabolites [15, 16].

Typically, the parent compound or the phase-I-metabolites will be conjugated to sulfate or glucuronic acid in phase-II-metabolism [7]. Phase-II-metabolites are even more hydrophilic than the corresponding aglycons (phase-I-metabolites) or the parent compounds. UDP-Glucuronosyltransferase (UGT) enzymatically binds glucuronic acid to functional groups in the molecule. The reaction to glucuronidated metabolites shows the predominant way of phase-II-metabolization in the human body [17]. Sulfotransferase (SULT) and the co-factor 3'-phosphoadenosin-5'-phosphosulfate (PAPS) catalyze sulfonation of phase-I-metabolites and parent compounds [7]. Other phase-II-reactions such as methylation or acetylation [17] are not much described for steroid metabolism.

1.2.1 Hydroxylation

The hydroxylation of steroids is one of the pathways in the metabolization process. Various CYP enzymes are involved in steroid hydroxylation [16]. The oxygen transfer to the molecule, catalyzed by CYP enzymes, is a mono-oxygenation. Hence, cytochrome P450 enzymes are assigned to the class of monooxygenases. The CYP structure consists of a minimum of two protein substructures. First, the heme protein, containing iron as

the central atom, and second the NADPH-CYP oxidoreductase, which transfers electrons to the heme system [18].

Hydroxylation reactions for T are described in positions 1β, 2, 6, 11, 15 (all α and β) and 16β [19-25]. Yamazaki *et al.* described five different hydroxy metabolites of progesterone after CYP2C19 incubation (2β, 6β, 16α, 17α, and 21) [19]. The predicted mechanism for the hydroxylation is exemplified for T in the 6β position in Figure 6. Renidc *et al.* predicted that the iron(IV)-oxo porphyrin radical is the active species in this reaction (compound I) [26]. This substructure can activate the C-H bond in the steroid molecule. The abstraction of one hydrogen atom yields an alkyl radical [27]. After that, the formed hydroxy group reorientates, and a C-O bond is formed. This reaction ends in the hydroxylated metabolite and an oxygen-free heme system. Binding oxygen, two electron transfers, and water loss after protonation, the so-called "oxygen rebound", reactivate the monooxygenase [28, 29].

CYP3A4 is one of the dominant enzymes expressed in the liver and other tissues involved in the metabolization of xenobiotics. Due to its variable binding site, CYP3A4 is a relatively unspecific enzyme and hence plays a role in the formation route of many metabolites.

CYP1A2 and CYP1B1 were shown to be involved in forming A-ring hydroxylation in estrogens [30]. Hydroxylated intermediates in the aromatization process are also described in the literature [4, 31].

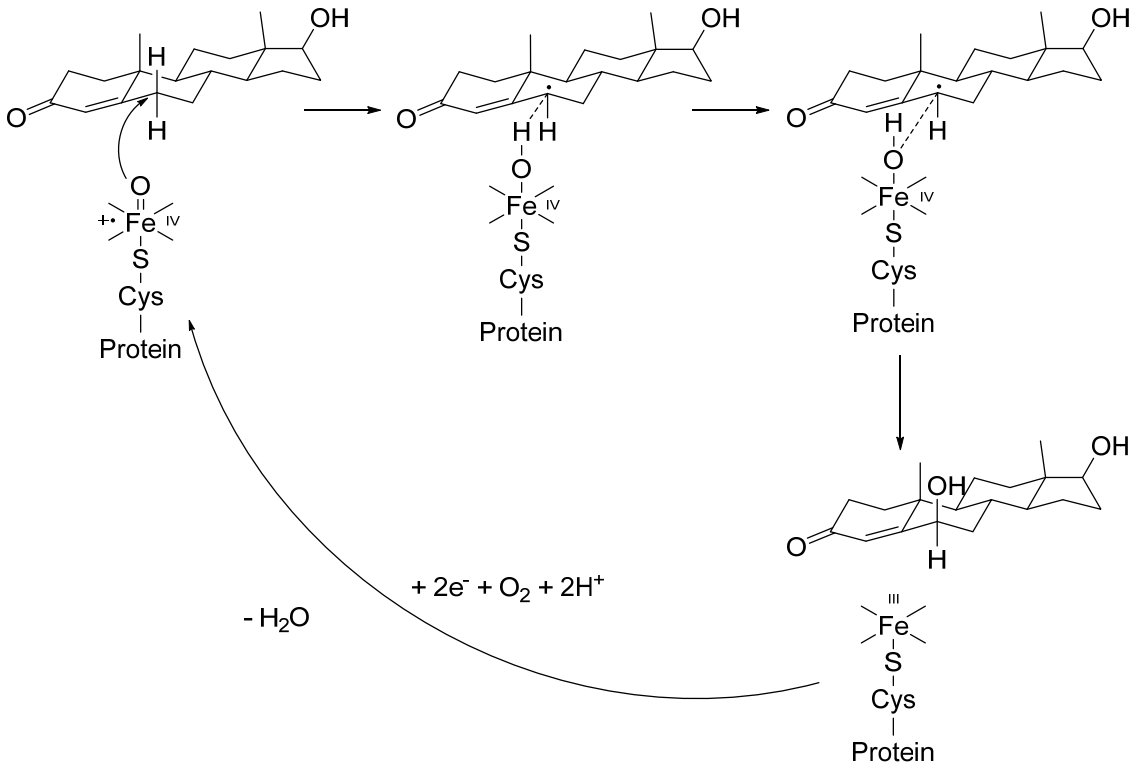

Figure 6: Proposed mechanism of the hydroxylation of 3-oxo-4-ene-steroids with CYP, exemplified on the formation of 6β-hydroxymethyltestosterone; adapted from [26]

1.2.2 Aromatization of Androgens

Aromatase is a specific enzyme because of its tight binding site. Only planar substrates can be metabolized [32]. Sugimoto *et al.* showed that the C19 methyl group of AED is orientated directly to the enzyme's heme group [33].

CYP19A1 catalyzes the formation of estrogens from androgens. Three hydroxylation processes are involved in the aromatization process [34]. The estradiol formation from T, depicted in Figure 7, exemplifies this reaction. In the first step, C19 is hydroxylated to result in the primary alcohol. After a second hydroxylation at C19 and the loss of water, the intermediate aldehyde is formed. These two monooxygenations follow the hydrogen abstraction/oxygen rebound mechanism described in 1.2.1 (Figure 6) [29]. The first step is considered as the rate-limiting factor [35]. The third step of aromatization is the elimination of C19. The mechanism which ends in the loss of formic acid and aromatization of the A-ring is discussed controversially in the literature. The three proposed mechanisms are shown in Figure 8. Yoshimoto and Guengerich proposed two

different pathways that are shown in Figure 8 [34]. Pathway I describes ferric peroxide as the mechanism's active iron species. The second hypothesis (pathway II) shows compound I as active iron species, as in the first two aromatization steps. In both pathways, the 1β-proton and the 19 methyl group (as formic acid) are cleaved from the molecule. Those two positions seem essential for the aromatization process [34, 36].

Hosoda *et al.* described the last step to be not enzymatically catalyzed. In their hypothesis (Figure 8, III), the existence of 2β-hydroxylated compounds in the aromatization builds the third proposed pathway [31, 37]. The hydroxylation in position 2β results in the 2β-hydroxy-19-aldehyde intermediate. This structure undergoes a complete conversion to estrogen after a basic attack at C19 (loss of water [C2] and formic acid [C19]) [31].

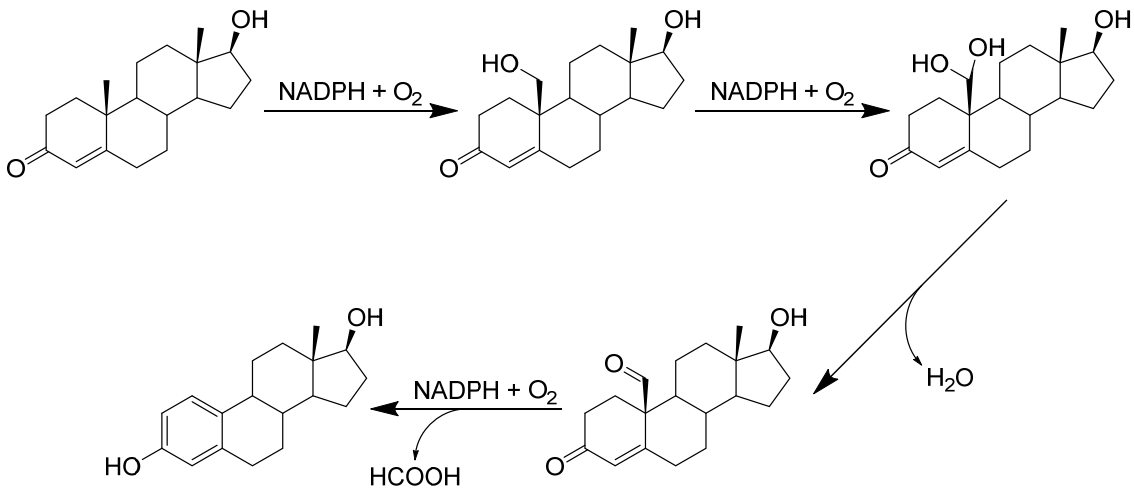

Figure 7: Aromatization process of testosterone; every hydroxylation consumes one oxygen and NADPH molecule; C19 methyl group is finally cleaved off as formic acid

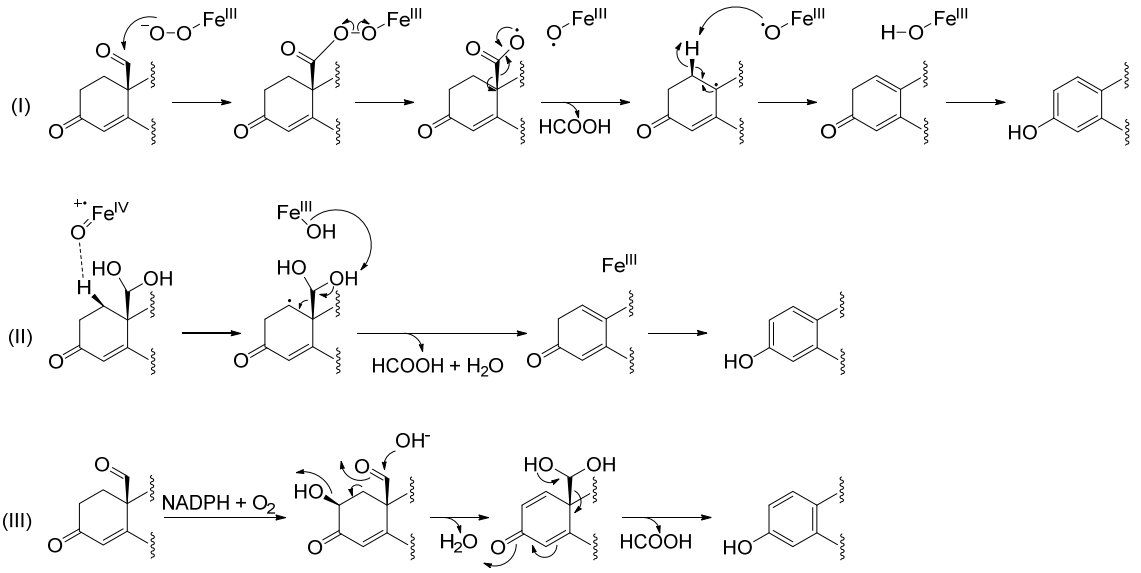

Figure 8: The three discussed pathways for the third step in the aromatization process, described by Yoshimoto et al. (I + II) and Hosoda et al. (III) [31, 34]

1.2.3 Metabolism of 17α-Methyltestosterone

The model substance of this project is MT. As described in 1.1.2, MT is an exogenous steroid. The methylation in position 17 allows the oral administration. MT intake, as a performance enhancing drug (PED) in sport, is prohibited by the WADA in and out of competition (prohibited at all times) [1]. Therefore, the metabolism plays an important role in the detection of MT abuse. Several metabolites are already described, albeit mainly in animals (horse, greyhound, heifer) [38-44]. Besides some small amounts of hydroxylated compound (in position C6, C16, C17), the reduction to dihydrogenated (dihydromethyltestosterone, DHMT) and fully reduced (tetrahydromethyltestosterone, THMT) metabolites showed to be the main metabolization pathway. Furthermore, the combination as a reduced and hydroxylated compound and epimerization in position 17 are also described [42].

The metabolome of MT in human, however, is not thoroughly investigated. Pozo *et al.* described the two fully reduced metabolites 17α-methyl-5β-androstane-3α,17β-diol (5βTHMT) and 17α-methyl-5α-androstane-3α,17β-diol (5αTHMT) as main metabolites in the human metabolism [45]. This was done by investigations on mice with humanized liver and confirmed in humans. Typically, MT administration in antidoping analysis is traced by these two reduced metabolites using GC-MS analysis after cleavage of the

phase-II-glucuronides [46]. Earlier this year, Martinez-Brito *et al.* reported the excretion of 2ξ-hydroxy-17α-methyltestosterone (2ξOHMT), 4-hydroxy-17α-methyltestosterone (4OHMT), and 6β-hydroxy-17α-methyltestosterone (6βOHMT) in small amounts beside the main metabolites 5αTHMT and 5βTHMT in man, after the administration of 10 mg MT [47].

1.3 Steroid Analysis

To detect the use of performance enhancing drugs (PED) [48], typically gas chromatographic (GC) or liquid chromatographic (LC) systems coupled to a mass-spectrometric detector are used (GC-MS[/MS], LC-MS[/MS]) [49, 50]. Both systems have their advantages and disadvantages. Today, GC-MS methods show high selectivity and resolution for complex matrices. Therefore, mostly GC-MS(/MS) methods are used in routine antidoping analysis for steroids. The major disadvantage of these methods is laborious sample preparation. As phase-II-metabolites are poorly or not detectable in GC-MS analysis, the sample preparation generally includes the cleavage of glucuronides. After extraction of free and liberated compounds, the samples are derivatized to TMS derivatives, as shown in 3.2.3.1, partially leading to derivatization artifacts (for example, hydroxylation in C6 at MT; MT reference compound showed minor amounts of 6-hydroxy-17α-methyltestosterone after TMIS derivatization, results have been omitted for the sake of brevity). However, the derivatization also shows the advantage of a better separation and hence reliable identification of possible PED. After electron ionization (EI), trimethylsilylated compounds show a specific fragmentation pattern suitable for structure elucidation/identification [51]. The observation of specific fragmentation patterns of the compounds (MS/MS experiments) lowers the background noise. Therefore, tandem mass spectrometry is typically used to lower the limit of detection (triple-quadrupole-MS [QQQ-MS]).

LC-MS(/MS) methods are often used in endocrinological investigations [52-54]. Compared to the standard GC-MS(/MS) methods, the detection of thermolabile substances and intact phase-II-metabolites is possible in LC-MS analysis [55, 56].

Usually, the run time is shorter than in GC-MS analysis, and the derivatization step is often not necessary [56]. Nevertheless, the easier sample preparation and improvement in run time typically go along with a lower separation efficiency than GC-MS methods. Compared to EI, the electrospray ionization (ESI) often used in LC-MS analysis [besides atmospheric pressure chemical ionization (APCI) and atmospheric pressure photo ionization (APPI)] may result in decreased sensitivity for some compounds and metabolites. For example, fully reduced metabolites as 5α/βTHMT are poorly ionized with ESI [56].

For the untargeted approach, high-resolution MS (HRMS, GC-EI-(Q)TOF, LC-ESI-(Q)TOF) is the method of choice [57]. Accurate mass together with tandem mass spectrometry is a useful tool in the structure elucidation of unknown compounds.

2 Aim of this Work

MT belongs to the class of exogenous steroids and is prohibited by the WADA at all times [1], as described in 1.2.3. MT administration was detected in about 1% of all adverse analytical findings (AAF) for AAS in the past years. Figure 9 depicts the number of AAF for MT from 2014 to 2019.

Mainly, MT is metabolized similarly to its endogenous analogon T, resulting in 5αTHMT and 5βTHMT. To detect its misuse, MT is mainly identified by detection of these reduced metabolites. GC-MS analysis is the method of choice because of the low ionization of these substances with ESI. Only recently, the U.S. cycling athlete Barbara Gicquel (80 years) was tested positive for 5αTHMT and 5βTHMT [46].

Hydroxylated metabolites of MT with intact 3-oxo-4-ene substructure might be a possible way to identify MT abuse with an ESI-MS/(MS) coupled method. The advantage of such a method would be faster analysis times, much faster sample preparation, and complementary data to GC-MS of THMT as long term marker. Several hydroxylation reactions for different AAS are discussed in literature (see 1.2.1). For example, Joseph found 2β-hydroxyandrost-4-ene-3,17-dione to be the major hydroxylated metabolite after AED administration to one healthy male volunteer [4]. In this project, a method able to separate and identify different hydroxy metabolites of MT shall be developed.

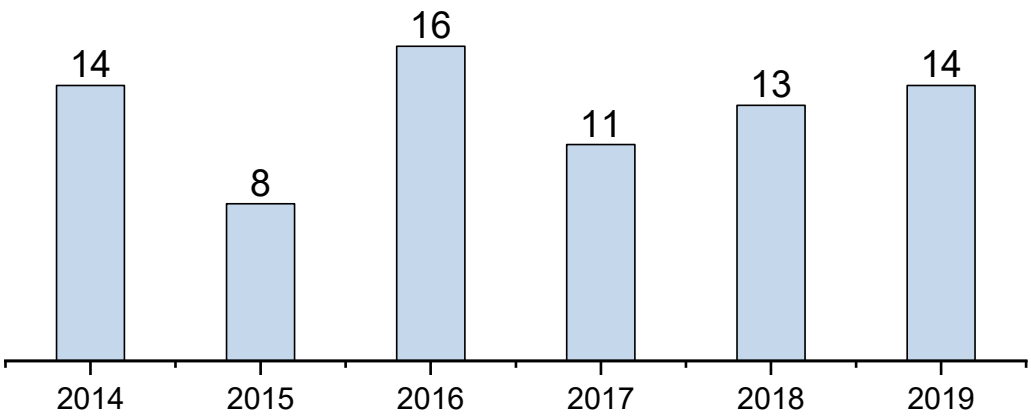

Figure 9: Number of adverse analytical findings of MT from 2014 to 2019 reported by the WADA laboratories (Testing Figures Report 2014-2019)

Based on literature results for other AAS, 2β-hydroxy-17α-methyltestosterone (2βOHMT), 2α-hydroxy-17α-methyltestosterone (2αOHMT), 4-hydroxy-17α-methyltestosterone (4OHMT, oxymesterone), and 6β-hydroxy-17α-methyltestosterone (6βOHMT) were selected as target analytes after enzymatic hydroxylation. As 2βOHMT and 2αOHMT are not commercially available, they had to be synthesized and characterized (chapter 4.1) before further *in vitro* and in *vivo studies*. 4OHMT is commercially available, but as it is a byproduct of the 2α/βOHMT synthesis, it was also synthesized in house.

Orthogonal analytical approaches were tested to achieve the best selectivity for the separation of hydroxylated metabolites of MT. For this purpose, the common systems for steroid analysis, GC-MS/(MS) after derivatization and LC-MS(/MS), together with supercritical fluid chromatography (SFC) as orthogonal techniques, were investigated to be used as the chromatographic separation system (chapter 4.4).

In vitro studies with CYP3A4, CYP2c19, CYP1A2, and CYP1B1 shall investigate the formation of four different hydroxy metabolites, focusing on the formation of 2βOHMT as a possible long-term marker for MT abuse (chapter 4.5.1-4.5.3). In addition to these *in vitro* studies, an *in vivo* study was implemented to show the impact of hydroxylated metabolites in human metabolism of MT (chapter 4.6).

The second project investigated the influence of 2βOHMT in the third step of the aromatization of MT (1.2.2). 19-hydroxy-17α-methyltestosterone (19OHMT) was synthesized and characterized for this project. This study focused on the formation of 2βOHMT and 19OHMT after MT incubation with CYP19A1 (chapter 4.5.4).

3 Material and Methods

3.1 Material

Table 1: Steroids and reference material

17α-Methyltestosterone	Sigma Aldrich (Taufkirchen, Germany)
19-Hydroxyandrost-4-ene-3,17-dione	Carbosynth Ltd. (Compton, United Kingdom)
2α-Hydroxyandrost-4-ene-3,17-dione	in house synthesized
2β-Hydroxyandrost-4-ene-3,17-dione	in house synthesized
4-Hydroxy-17α-methyltestosterone	TRC (North York, USA)
6β-Hydroxy-17α-methyltestosterone	Steraloids (Newport, USA)
Androst-4-ene-3,17-dione	VWR (Dresden, Germany)
Mefruside	BOC Science (New York, USA)
Metandienone	Sigma Aldrich (Taufkirchen, Germany)
Testosterone-d3	Sigma Aldrich (Taufkirchen, Germany)
Testosterone-d3-Gluc	TRC (North York, USA)

Table 2: Solvents, reagents, and materials

Acetone	VWR (Dresden, Germany)
Acetonitrile LC-MS grade	Fisher (Schwerte, Germany)
Acetonitrile p.a.	VWR (Dresden, Germany)
Acetyl chloride	Sigma Aldrich (Taufkirchen, Germany)
Ammonium fluoride	Sigma Aldrich (Taufkirchen, Germany)
Ammonium iodide	Sigma Aldrich (Taufkirchen, Germany)
Argon	Air liquide (Düsseldorf, Germany)
Cyclohexene	Sigma Aldrich (Taufkirchen, Germany)
CYP19A1 + oxidoreductase	Corning Supersomes (New York, USA)
CYP1A2	Corning Supersomes (New York, USA)
CYP1B1	Corning Supersomes (New York, USA)
CYP2C19	Corning Supersomes (New York, USA)
Dichloromethane	VWR (Dresden, Germany)
DMSO	Merck (Darmstadt, Germany)
Ethanethiole	Sigma Aldrich (Taufkirchen, Germany)
Ethanol	VWR (Dresden, Germany)
Ethyl acetate	VWR (Dresden, Germany)
Formic acid, LC-MS grade	Sigma Aldrich (Taufkirchen, Germany)
Glacial acetic acid	Merck (Darmstadt, Germany)
Helium	Air liquide (Düsseldorf, Germany)
HLM pooled from 50 donors	BD Bioscience (Milan, Italy)
Hydrochloric acid	Fisher (Schwerte, Germany)
Hydrogen peroxide 30 %	Sigma Aldrich (Taufkirchen, Germany)
Methanol MS quality	Fisher (Schwerte, Germany)
Methanol p.a.	VWR (Dresden, Germany)
Methylmagensium bromide solution (3N)	Sigma Aldrich (Taufkirchen, Germany)

MSTFA	Chemische Fabrik Karl Bucher (Waldstetten, Germany)
NADPH regenerating system solution A	Corning Gentest (New York, USA)
NADPH regenerating system solution b	Corning Gentest (New York, USA)
Nitrogen	Air liquide (Düsseldorf, Germany)
Phosphate-buffer-system 0.5 M	BD Bioscience (Milan, Italy)
Potassium carbonate	Sigma Aldrich (Taufkirchen, Germany)
Potassium hydrogencarbonate	Sigma Aldrich (Taufkirchen, Germany)
Potassium iodide	Sigma Aldrich (Taufkirchen, Germany)
Pyridine	VWR (Dresden, Germany)
Sodium hydroxide	Sigma Aldrich (Taufkirchen, Germany)
Sulfuric acid 96 %	Merck (Darmstadt, Germany)
TBME	AppliChem (Darmstadt, Germany)
Tetrahydrofuran	Sigma Aldrich (Taufkirchen, Germany)
Water LC-MS grade	LaboStar 2-DI/-UV ultrapure water system; SG Wasseraufbereitung und Regenerierstation GmbH (Barsbüttel, Germany)
β-Glucuronidase from *Escherichia coli* (>140 U/mL)	Roche Diagnostics (Mannheim, Germany)

3.2 Methods

Table 3 depicts a short overview of the methods used in this thesis. The methods details will be introduced in subsections 3.2.1-3.2.3.

Table 3: Overview of the used methods, showing the used instruments, their field of application in this thesis, and the method shortcut

Instrument	**Field of Application**	**Method**
LC-UV	Purification	a)
HPLC-ESI-MS	Synthesis monitoring	b)
HPLC-ESI-QTOF-MS	Structure elucidation	c)
SFC-ESI-QQQ-MS	*In vitro*/*in vivo* studies (MT)	d)
SFC-ESI-QQQ-MS	*In vitro* studies (AED)	e)
GC-EI-MS	Synthesis monitoring	f)
GC-EI-MS	Synthesis monitoring	g)
GC-EI-QTOF-MS	Structure elucidation	h)

3.2.1 Liquid Chromatography

3.2.1.1 LC-UV

The LC-UV system was used for the semipreparative separation of 2α/β- and 4-hydroxy-17α-methyltestosterone. Therefore, a fraction collector was used to collect the fractions of interest. The sample was loaded on silica and placed on top of the column. Separation was achieved using the following method.

Table 4: Parameters for LC purification method a)

Device	Biotage Isolera One (Uppsala, Sweden)
Column	Biotage SNAP Ultra 10 g (Uppsala, Sweden)
Solvent A	Hexane
Solvent B	Ethyl acetate
Gradient	40% *B* for 2 column volumes (CV) to 60% *B* at 15 CV 60% *B* for 2 CV
Flow rate	12 mL/min
UV parameters	254 nm Threshold 15 mAU
Fraction collector	Peak based; automatically

3.2.1.2 HPLC-ESI-MS

HPLC-ESI-MS was used to monitor the synthesis progress. Therefore 10 µL aliquots of the reaction mixture were diluted with methanol to a resulting 10 ppm solution. Test samples from synthesis raw product were prepared by diluting a ~1000 ppm stock solution (in methanol).

Table 5: HPLC-ESI-MS parameters for method b)

Device	Agilent 1260 Infinity System (Santa Clara, USA) Agilent 6130B Single Quadrupole MS System (Santa Clara, USA)
Column	Agilent ZORBAX Eclipse Plus RP C18 (1.8 µm, 2.1 x 100 mm)
Temperature	25 °C ± 0.8 °C
Injection volume	1 µL
Solvent A	H_2O/FoOH (99.9:0.1; v:v)
Solvent B	ACN/FoOH (99.9:0.1; v:v)
Gradient	5% *B* at 0 min 95% *B* at 10 min 95% *B* at 11 min 5% *B* at 11.5 min 5% B at 12 min
Flow rate	0.250 mL/min
MS parameters	Full scan mode 70-1000 (m/z) Gas temperature 350°C Gas flow 12 L min Nebulizer pressure 35 psi Capillary voltage 3000 V

3.2.1.3 HPLC-ESI-QTOF-MS

HPLC system equipped with a high-resolution quadrupole time-of-flight mass spectrometer (QTOF) with ESI was used to obtain the accurate masses of underivatized substance. Therefore methanolic solutions (1 ng/mL) of the compounds were prepared.

Table 6: HPLC-ESI-QTOF-MS parameters for method c)

Device	Agilent 1290 Infinity II (Santa Clara, USA) Agilent 6550 iFunnel QTOF-MS (Santa Clara, USA)
Column	Agilent Poroshell 120 Chrial-V (2.7 µm, 2.1 x 100 mm)
Temperature	30 °C ± 0.8 °C
Injection volume	10µL
Solvent A	H_2o/FoOH (99.9:0.1; v:v) + 1mM NH_4F
Solvent B	ACN/H2O/FoOH (97.4:2.5:0.1; v:v:v) + 1 mM NH_4F
Gradient	10% B at 0 min 40% B at 8 min 95% B at 10 min 95% B at 12 min 10% B at 13 min
Flow rate	0.800 mL/min
MS parameters	Gas temperature 200°C Gas flow 13 L/min Nebulizer pressure 35 psi Sheath gas temperature 375 °C Sheath gas flow 11 L/min Capillary voltage 3500 V Nozzle voltage 500 V

3.2.2 Supercritical Fluid Chromatography

3.2.2.1 SFC-ESI-QQQ-MS

SFC-ESI-QQQ-MS was used for *in vivo* and *in vitro* study investigation. Method d) (MT) and method e) (AED) only differ in the target analytes and their ion transitions monitored (Table 8 and Table 9).

Table 7: SFC-ESI-QQQ-MS parameters, method d) + e)

Device	Agilent 1260 Infinity II SFC System Agilent 6495B Triple Quadrupole
Column	Agilent Poroshell 120 Chrial-V (2.7 µm, 2.1 x 100 mm)
Temperature	23 °C ± 0.8 °C
Injection volume	10 µL (double loop overfill)
Solvent A	CO_2 (precompressed)
Modifier	Methanol
Gradient	10% *Modifier* at 0 min 20% *Modifier* at 6 min 30% *Modifier* at 8 min 10% *Modifier* at 10 min
Flow rate	1.200 mL/min
Makeup solvent	MeOH/H2O/FoOH (97.4:2.5:0.1; v:v:v) + 1mM NH_4F
Makeup flow rate	0.150 mL / min
MS parameters	Gas temperature 210°C Gas flow 17 L/min Nebulizer pressure 40 psi Sheath gas temperature 350 °C Sheath gas flow 11 L/min Capillary voltage 4000 V Nozzle voltage 500 V

Table 8: Precursor and product ions of 17α-methyltestosterone, its hydroxy metabolites and internal standards for MRM experiments, method d)

Compound	**Precursor (m/z)**	**Product ion (m/z)**
17α-Methyltestosterone	303.2	→ 109.1 → 97
2α-Hydroxy-17α-methyltestosterone	319.2	→ 283.1 → 121 → 107.1
2β-Hydroxy-17α-methyltestosterone	319.2	→ 283.1 → 121 → 107.1
4-Hydroxy-17α-methyltestosterone	319.2	→ 189 → 125 → 113
6β-Hydroxy-17α-methyltestosterone	319.2	→ 283.2 → 225.1 → 173.1
19-Hydroxy-17α-methyltestosterone	319.2	→ 283.1 → 157
Testosterone-d3	292.2	→ 109 → 97
Gluc-testosterone-d3	468.3	→ 109 → 97 → 84.9
Mefruside	383	→ 284.9 → 81
Metandienone	301.2	→ 149 → 121

Testosterone-d3, gluc-testosterone-d3, and mefruside were used as internal standards in the urine samples. MD was used as an internal standard in the incubation studies.

Table 9: Precursor and product ions of androst-4-ene-3,17-dione, its hydroxy metabolites, and the internal standard MD for MRM experiments; method e)

Compound	**Precursor (m/z)**	**Product ion (m/z)**
Androst-4-ene-3,17-dione	287.2	→ 109.1 → 97
2α-Hydroxy-androst-4-ene-3,17-dione	303.2	→ 267.1 → 158.9 → 93
2β-Hydroxyandrost-4-ene-3,17-dione	303.2	→ 267.1 → 171 → 95
6β-Hydroxyandrost-4-ene-3,17-dione	303.2	→ 226.9 → 209.1 → 97
19-Hydroxyandrost-4-ene-3,17-dione	303.2	→ 255.2 → 156.9 → 97
Metandienone	301.2	→ 149 → 121

MD was used as an internal standard in the incubation studies.

3.2.3 Gas Chromatography

Gas chromatography, coupled with mass spectrometric detection, was used for product identification and characterization. The samples were measured underivatized, as mono-TMS or per-TMS derivative.

3.2.3.1 Derivatization

For GC analysis of steroids, two different derivatization-methods were used to yield the per-TMS (derivatization with catalyst) or mono/bis-TMS (derivatization without catalyst) derivatives. A mixture of N-methyl-N-(trimethylsilyl)trifluoracetamide (MSTFA), ammonium iodide (NH_4I) and ethanethiol (1000:2:3, v/w/v) was used to generate trimethyliodosilane (TMIS) *in situ* and form the per-TMS derivatives. Figure 10 shows the reaction mechanism. Donike *et al.* and Geyer *et al.* introduced this well-described method used in antidoping laboratories worldwide [58, 59]. The trimethylsilyl ethers were formed directly from the corresponding hydroxy group, the trimethylsilyl enol ethers after enolization of the oxo function. Ethanethiol reacts with iodine to form hydrogen iodide (antioxidant).

Derivatization with MSTFA without any catalyst yielded the derivatization of sterically unhindered hydroxy groups. Position 17 of MT was not derivatized because the hydroxy group is sterically hindered. Generally, only hydroxy and not oxo groups form the corresponding trimethylsilyl ethers.

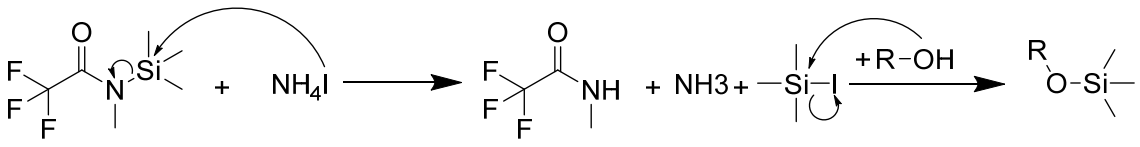

Figure 10: In situ formation of TMIS from MSTFA/NH4I/ethanethiol (1000:2:3, v/w/v)

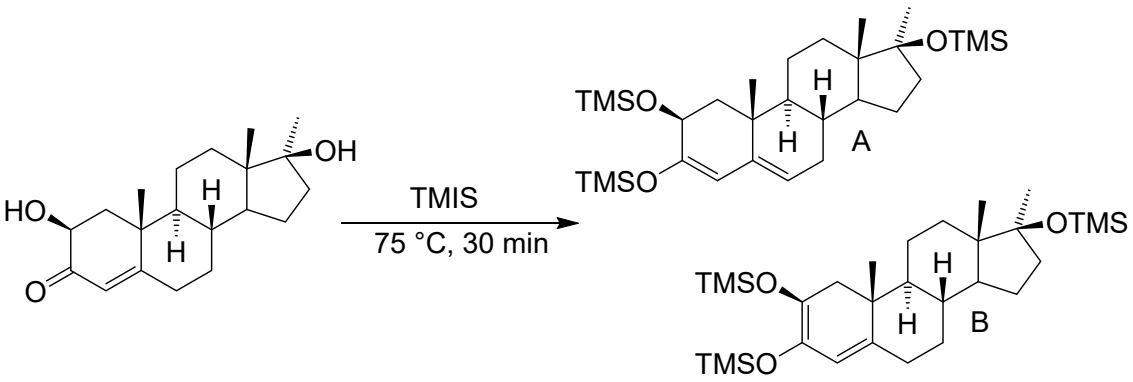

Figure 11: Reaction scheme of derivatization of 2βOHMT with TMIS; the resulting per-TMS derivatives 3,5-diene-2,3,17-triol tris-TMS (A) and 2,4-diene-2,3,17-triol tris-TMS (B) from the reaction of 2β-hydroxy-17α-methyltestosterone

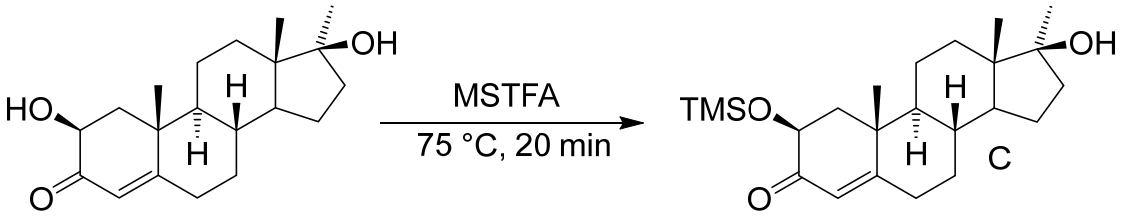

Figure 12: Reaction scheme of derivatization of 2βOHMT with MSTFA; the resulting mono-TMS derivative 4-ene-2,17-diol-2-TMS (C) from the reaction of 2β-hydroxy-17α-methyltestosterone

The resulting mono- (**C**) and per-TMS derivatives (**A** and **B**) are exemplified with 2β-hydroxy-17α-methyltestosterone and shown in Figure 11 and Figure 12.

For TMIS derivatization, 10 µL (1000 µg/mL) of the steroid solution was transferred into a test tube and dried. An amount of 90 µL MSTFA and 10 µL of derivatization solution (MSTFA/NH_4I/ethanethiol; 100:2:3, v/w/v) were added, and the solution was heated to 75 °C for 30 minutes.

For MSTFA derivatization, 10 µL of the steroid solution (1000 µg/mL) was transferred into a test tube and dried. An amount of 100 µL MSTFA was added, and the solution was heated to 75 °C for 20 minutes. The sample was dried under nitrogen at 75 °C, and the residue was dissolved in 100 µL ethyl acetate.

3.2.3.2 GC-EI-MS/QTOF-MS

For the characterization of synthesis products, a gas chromatograph coupled to a single quadrupole mass selective detector was used [Agilent 5975C MSD, method f) & g)]. High-resolution mass spectrometry [Agilent 7200 accurate mass QTOF, method h)] was used to identify the products. Both systems were equipped with an EI source. Method g) uses a different oven temperature program to separate per-TMS derivatives; all other parameters are like method f).

Table 10: GC-EI-MS parameters applied in method f)

Device	Agilent 7890A gas chromatograph (Santa Clara, USA) Agilent 5975C mass selective detector (MSD) (Santa Clara, USA)
Column	Agilent HP1-Ultra (17 m, 200 µm, 0.11 µm) (Santa Clara, USA)
Injection volume	2 µL
Carrier gas	Helium at 1 mL/min, constant flow
Inlet parameters	Split injection 1:10, temperature 300 °C
Oven temperature program	183 °C, 3 °/min to 232 °C, 40 °C/min to 310 °C, 2 min hold
MS parameters	Electron ionization with 70 eV at 230 °C Full scan mode 40-750 m/z

Table 11: GC-EI-MS parameters applied in method g)

Device	Agilent 7890A gas chromatograph (Santa Clara, USA) Agilent 5975C mass selective detector (MSD) (Santa Clara, USA)
Column	Agilent HP1-Ultra (17 m, 200 µm, 0.11 µm) (Santa Clara, USA)
Injection volume	2 µL
Carrier gas	Helium at 1 mL/min, constant flow
Inlet parameters	Split injection 1:10, temperature 300 °C
Oven temperature program	150 °C, 50 °/min to 240 °C, 3 °C/min to 266 °C, 50 °C to 310 °C, 3 min hold
MS parameters	Electron ionization with 70 eV at 230 °C Full scan mode 40-750 m/z

Table 12: GC-EI-QTOF-MS parameters applied in method h)

Device	Agilent 7890B gas chromatograph (Santa Clara, USA) Agilent 7200 accurate mass selective QTOF (Santa Clara, USA)
Column	Agilent HP1-Ultra (17 m, 200 µm, 0.11 µm) (Santa Clara, USA)
Injection volume	0.2 µL
Carrier gas	Helium at 1 mL/min, constant flow
Inlet parameters	Split injection 1:10, temperature 280 °C
Oven temperature program	200 °C, 1 °/min to 245 °C, 40 °C/min to 310 °C 2 min hold
MS parameters	Electron ionization with 70 eV at 230 °C Full scan mode 40-750 m/z Scan speed 50 Hz (200 ms/spectrum)

3.2.4 Synthesis of Reference Material

3.2.4.1 2α/β- and 4-Hydroxy-17α-methyltestosterone

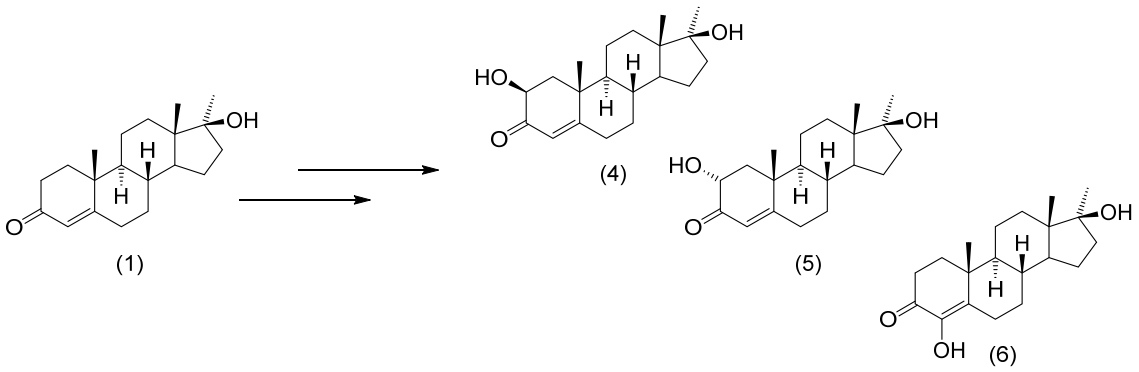

Figure 13: Chemical structures of the educt 17α-methyltestosterone (1) and the three desired products 2β-hydroxy-17α-methyltestosterone (4), 2α-hydroxy-17α-methyltestosterone (5) and 4-hydroxy-17α-methyltestosterone [oxymesterone] (6)

The synthesis of 2α-, 2β-, and 4-hydroxy-17α-methyltestosterone started from the commercially available MT [60]. An amount of 1.66 g MT (0.005 mol) was dissolved in 110 mL methanol and cooled to 0 °C. A solution of 2.3 mL sodium hydroxide (6 N) and 1.8 mL hydrogen peroxide 30% was added dropwise. The temperature was controlled to be in-between 0 and 5 °C. After stirring the solution for 24 hours at 0 °C, the reaction was stopped by adding 25 mL of water. The reaction mixture volume was decreased to about 50 mL by evaporation of the solvent under reduced pressure and extracted three times, with 50 mL of dichloromethane (DCM). The combined organic phases were washed two times with 50 mL of water and dried with sodium sulfate. After evaporation under reduced pressure, 1.3431 g (77%) of white powder were yielded.

An aliquot of 0.392 mg residue was dissolved in 16 mL acetone, and 0.8 mL sulfuric acid 25% was added slowly. The reaction mixture was stirred at room temperature for 72 hours. After addition of 100 mL water, the resulting solution was extracted three times with 50 mL DCM. The organic phases were combined, washed with 100 mL water, dried with sodium sulfate, and evaporated under reduced pressure. LC purification [method a), 3.2.1.1] of the resulting oily residue yielded 18 mg 4-hydroxy-17α-methyltestosterone (0.06 mmol) and 56 mg of the 2α/β-hydroxy-17α-methyltestosterone mixture (0.17 mmol).

3.2.4.2 19-Hydroxy-17α-methyltestosterone

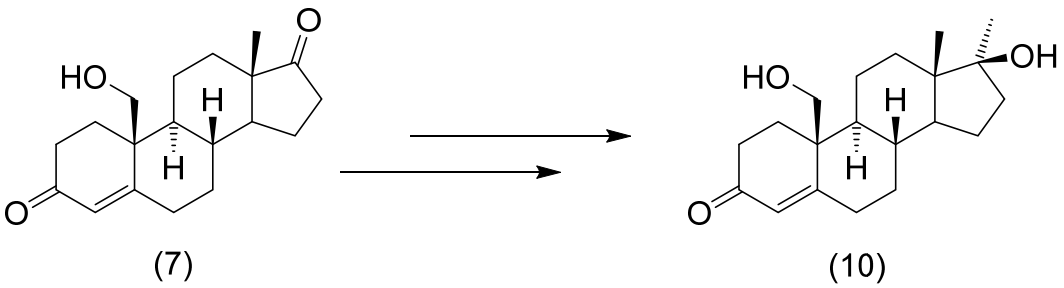

Figure 14:Chemical structures of 19-hydroxyandrost-4-ene-3,17-dione (left) and the expected product 19-hydroxy-17α-methyltestosterone (right)

19-Hydroxy-17α-methyltestosterone (19OHMT) was synthesized from 19-hydroxyandrost-4-ene-3,17-dione (19OHAED). The synthesis steps were adapted from Liao *et al.* [61] and are shown in Figure 14. Methanol (10 mL) was cooled to 0 °C and 1 g of acetyl chloride was slowly added dropwise. The solution was stirred for 15 minutes at 0 to 5 °C. An amount of 1.00 g 19OHAED (0.003 mol) was added to this solution, and the reaction was carried out for five hours at 0 °C. After this, the reaction mixture was poured into 75 mL water containing 2.5 g potassium carbonate, which was previously cooled to 0 °C. After one hour of stirring, the obtained residue was separated by suction filtration and washed with water.

The residue was dissolved in 10 mL toluene containing 38 µL of pyridine and heated under reflux for one hour. After cooling the solution to room temperature, the water phase was separated from the organic reaction mixture. The reaction temperature was held between 10 and 15 °C when a solution of 6.6 mL CH3MgBr (0.05 mol/L in diethyl ether) and 3.4 mL of dry tetrahydrofuran was added dropwise. After 24 hours of stirring at 40 to 45 °C, the reaction was stopped by cooling the solution to 15 °C, adding 1 mL of water, and 10 mL methanol dropwise. After that, a solution of 1.5 mL concentrated hydrochloric acid (36%) and 10 mL water was slowly added to the reaction mixture and adjusted to pH=2. The temperature of the solution was held at 50 to 55 °C for two hours and cooled down to 30 °C after this. The solution was concentrated under reduced pressure, then added to previously cooled water (0 °C) and this reaction mixture was

stirred for one hour. The residue was separated by suction filtration, washed until the residue had a neutral pH, and dried over potassium hydroxide. This reaction yielded 487 mg of yellow-brown crude product. The residue was purified by washing it with ethyl acetate to give ~3 mg of yellowish crystals (0,01 mmol, most of the residue seemed to be unconsumed educt).

3.2.5 Structure Confirmation of Synthesized Products

Nuclear magnetic resonance spectroscopy (NMR) was used to confirm the structure of the synthesized references 2αOHMT, 2βOHMT, and 4OHMT.

High-resolution mass spectrometry (HRMS) was used to identify the elementary composition of the synthesized reference compounds.

3.2.5.1 NMR

NMR spectra (500 Hz [^{1}H] and 125 Hz [^{13}C]) were measured at 298 K on a Bruker Avance III 499 instrument. The 5 mm inverse probe head was actively shielded with a z-gradient coil. Deuterated chloroform or DMSO was used as solvent.

The following experiments were measured for the structure confirmation:

^{1}H, ^{13}C, DEPT (Distortionless Enhancement by Polarization Transfer), ^{1}H,^{1}H-COSY (Heteronuclear Correlation Spectroscopy), HMQC (Heteronuclear Multiple Quantum Coherence), and HMBC (Hetero Multiple Bond Correlation).

3.2.5.2 HRMS

LC-HRMS data was obtained using an Agilent 6550 iFunnel QTOF-MS. Permanently performed mass axis calibration and a high resolution (> 10,000) achieved high mass accuracy.

GC-HRMS was carried out on an Agilent 7200 accurate mass QTOF-MS. The calibration of the mass axis was performed prior to each run.

3.2.6 Incubation Experiments

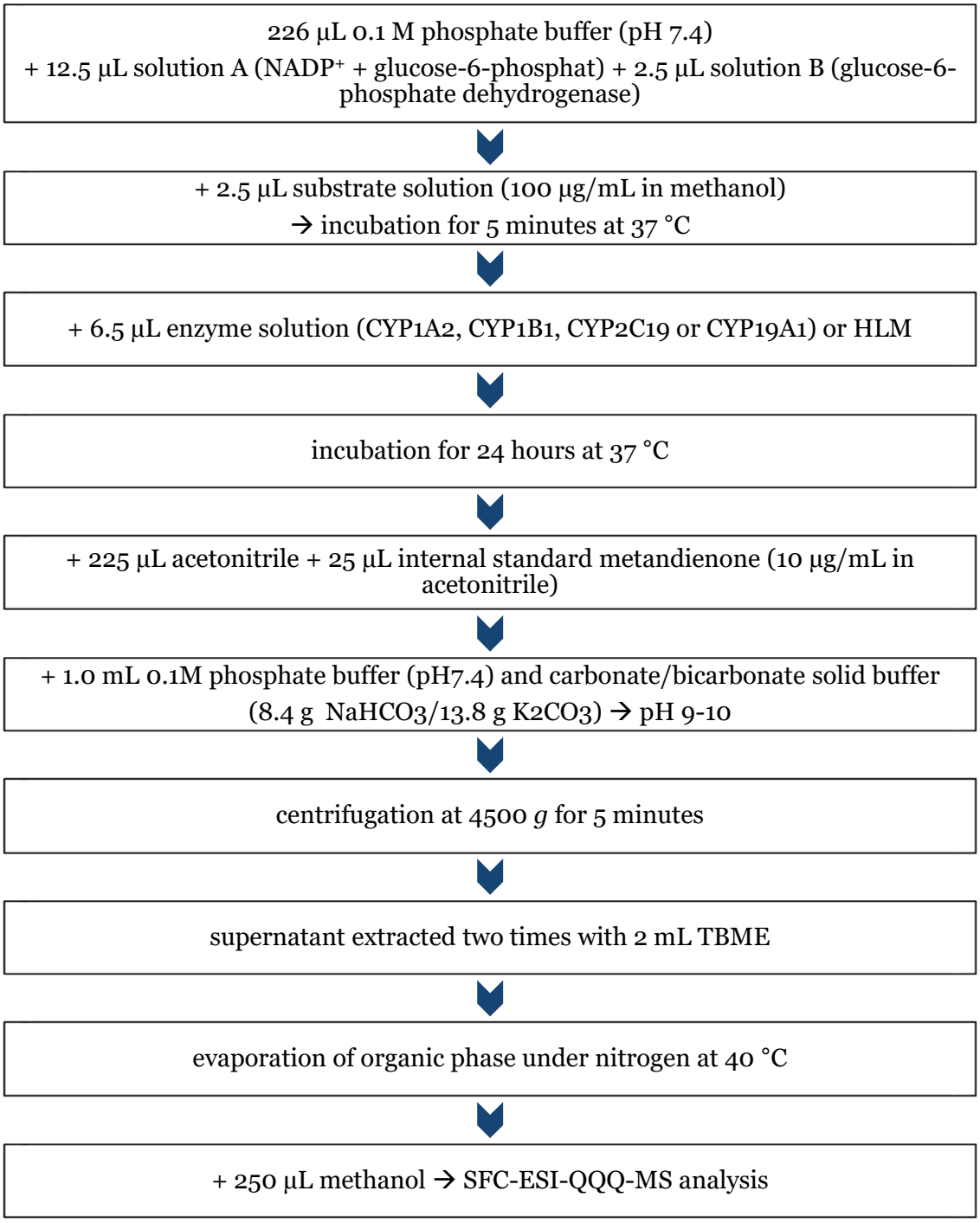

Figure 15: Incubation protocol for the in vivo studies adapted from [62]

Incubation studies were performed with MT. AED served as positive control. A control sample (negative) without any enzyme was prepared for every compound.

3.2.7 Human Urine Samples

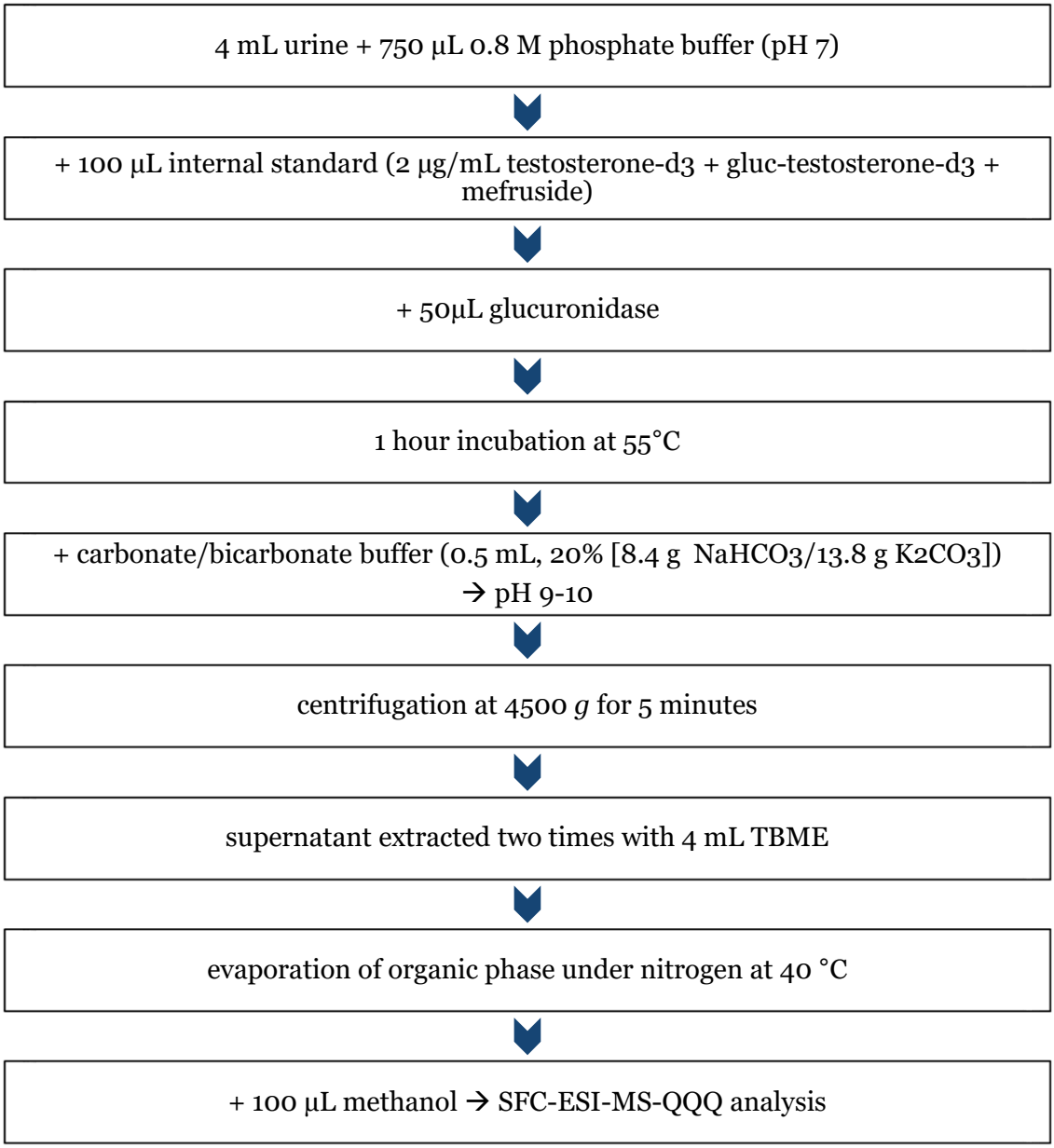

Figure 16: Protocol for the sample preparation of urine analysis

The protocol for steroid extraction from urine samples was adapted from Mareck *et al.* [63].

4 Results and Discussion

4.1 Synthesis of 2α- and 2β-Hydroxy-17α-methyltestosterone

The synthesis of 2αOHMT, 2βOHMT, and 4OHMT consists of two steps, shown in Figure 17. To obtain 2αOHMT (**5**), 2βOHMT (**4**), and 4OHMT (**6**), commercially available MT (**1**) was used as educt. In the first step, MT was treated with sodium hydroxide and hydrogen peroxide to obtain a mixture (7:3 peak area ratio from GC-MS) of 4β,5β-epoxy-17α-methyltestosterone (**2**) and 4α,5α-epoxy-17α-methyltestosterone (**3**) (chromatogram Figure 18). GC-EI-MS identified the two isomers with no derivatization by comparison with reference mass spectra of 4ξ,5ξ-epoxyandrostane-3,17-dione, and calculated mass shifts of relevant fragments (Figure 19 and Figure 20).

Because the intention was to synthesize all three hydroxy metabolites of MT in one synthesis, no further purification of the epoxides was performed before the second step. Afterwards, the epoxide mixture was dissolved in acetone, and a 25% aqueous solution of sulfuric acid was added dropwise. The solution was stirred at room temperature for 72 hours. Extension of the reaction time and variation of the amount of sulfuric acid showed no difference in the synthesis outcome.

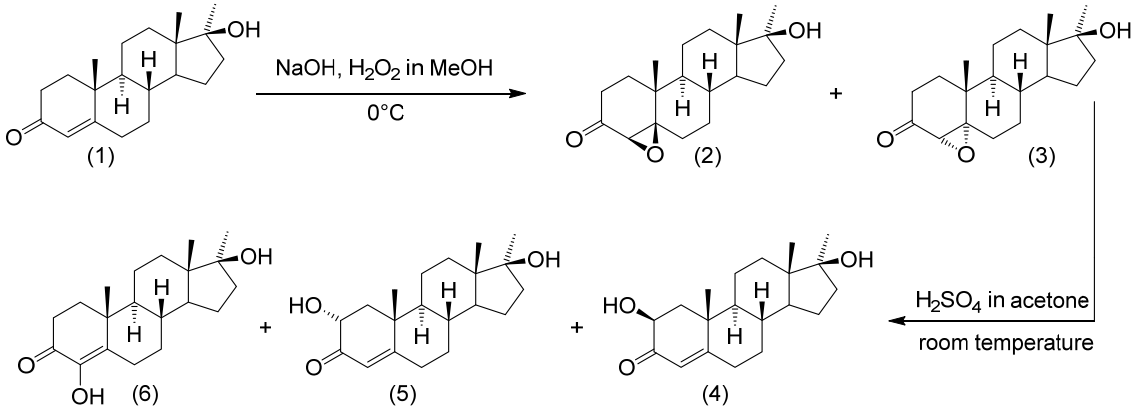

Figure 17: Two-step synthesis of the three hydroxylated metabolites 2α-hydroxy-17α-methyltestosterone (5) 2β-hydroxy-17α-methyltestosterone (4) and 4-hydroxy-17α-methyltestosterone (6) starting from 17α methyltestosterone (1)

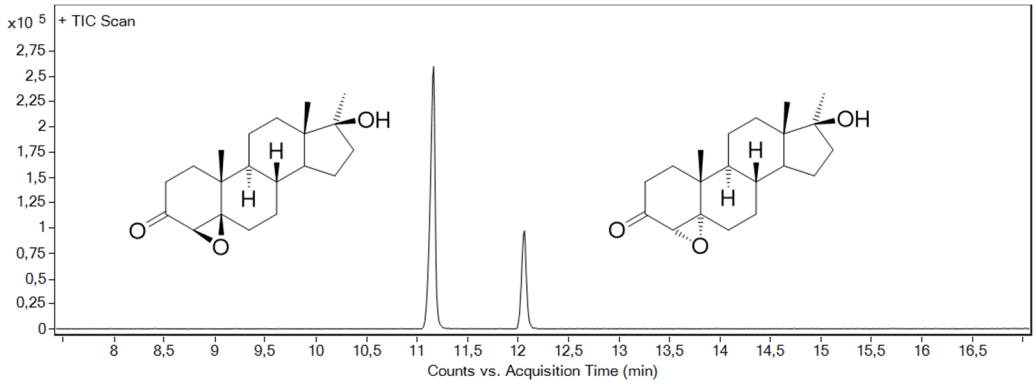

Figure 18: GC-EI-MS total ion current (TIC) chromatogram of underivatized 4β,5β-epoxy-17α-methyltestosterone (2) and 4α,5α-epoxy-17α-methyltestosterone (3)

Literature describes that the acid-catalyzed ring opening of 4β,5β-epoxyandrostane-3,17-dione will mainly yield 2α-hydroxyandrostane-3,17-dione, where the α,α-epoxide will open to 4-hydroxyandrostane-3,17-dione [64]. Similarities for the ring opening of (**2**) and (**3**) were expected (Figure 21).

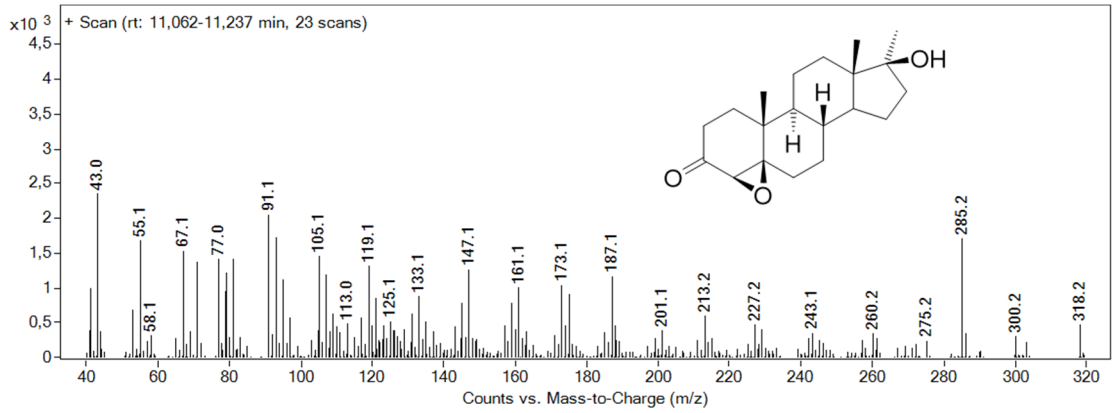

Figure 19: GC-EI-MS spectra of 4β,5β-epoxy-17α-methyltestosterone at 70 eV $[M]^{\bullet+}$= 318.2

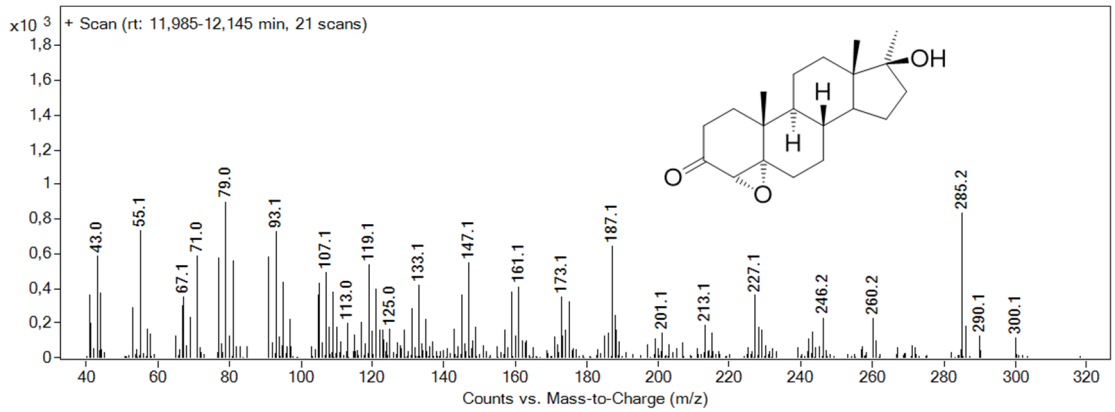

Figure 20: GC-EI-MS spectra of 4α,5α-epoxy-17α-methyltestosterone at 70 eV $[M]^{\bullet+}$= 318.2

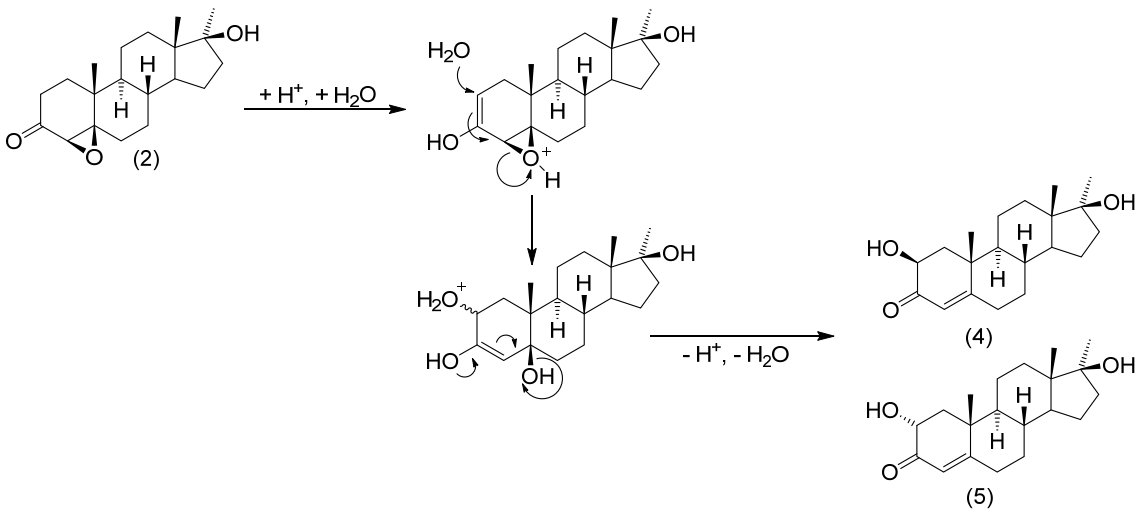

Figure 21: The predicted chemical reaction of the ring-opening in acid conditions exemplified by 4β,5β-epoxy-17α-methyltestosterone (2) to 2α-hydroxy-17α-methyltestosterone (5) and 2β-hydroxy-17α-methyltestosterone (4)

Step two of the synthesis yielded 4OHMT, 2ξOHMT, and small amounts of byproducts, which were not identified. As no separation of the per-TMS derivatives with GC-EI-MS was achieved, the reaction mixture was analyzed with LC-ESI-MS [method b)]. 4OHMT was identified using commercial reference standard. It eluted later than the coeluting 2ξOHMT isomers. Separation of the 2-hydroxy isomers could not be achieved with method b). The byproduct with m/z 319 may be another hydroxy-17α-methyltestosterone, m/z 317 might be an oxidized hydroxy-17α-methyltestosterone. The expected byproduct 6βOHMT coelute with the 2-hydroxy isomers, as a later investigation with commercial reference standard of 6βOHMT showed (Figure 22).

The predicted opening mechanism to obtain (2ξOHMT) – adapted from Tomoeda *et al.* [60] – is shown in Figure 21. A nucleophilic attack at C2 triggers the ring-opening via the 2,3-enol. The elimination of the resulting hydroxy group at C5 yielded the two 2-hydroxy isomers of MT [(**4**) and (**5**)]. The α-form is described as the thermodynamically more stable isomer, and the β-form can undergo an inversion [65]. The methyl group at C19 cause sterical complications in the β-form because both large substitutes are orientated in the same direction. Burnett *et al.* showed that 2β substituents switch the A-ring into the inverted chair form [64] (Figure 23; 2αOHMT chair form, 2βOHMT inverted chair form).

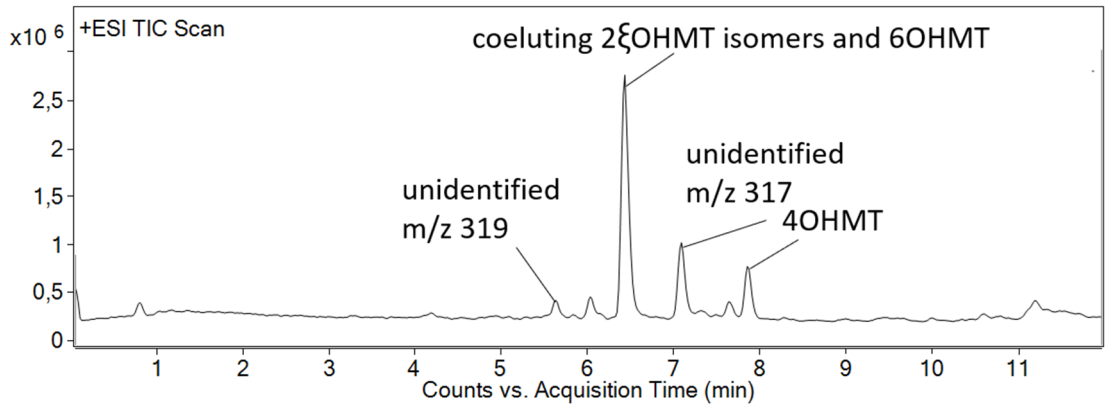

Figure 22: LC-ESI-MS total ion chromatogram of the product mixture showing 2OHMT, 4OHMT, 6OHMT, and unidentified byproducts

The products (0.392 mg) were separated in a semipreparative approach using method a) to obtain pure fractions for 4OHMT (18 mg, 0,06 mmol) and 2ξOHMT (56 mg, 0.17 mmol). GC-EI-MS spectra of the mono- and per-TMS derivatives of both fractions for structure verification were received using method g). Separation of the per-TMS derivatives of 2ξOHMT was achieved with method h) (Figure 63, annex).

Derivatization with MSTFA and injection out of ethyl acetate resulted in the mono-TMS derivatives of 2αOHMT and 2βOHMT; no bis-TMS derivative was visible in the chromatogram. MSTFA only at 70 °C was found to be not strong enough to derivatize the sterically hindered hydroxy group at C17, as also reported in literature [66]. The MS spectrum of 2αOHMT as mono-TMS shows the base peak at m/z 375.2, which shows a direct loss of one CH_3 group compared with the molecular ion's theoretical mass ($[C_{22}H_{35}O_3Si]^+$, Figure 66 annex). The fragment m/z 357.2 is derived from a water loss ($[M\text{-}CH_3\text{-}H_2O]^+$).

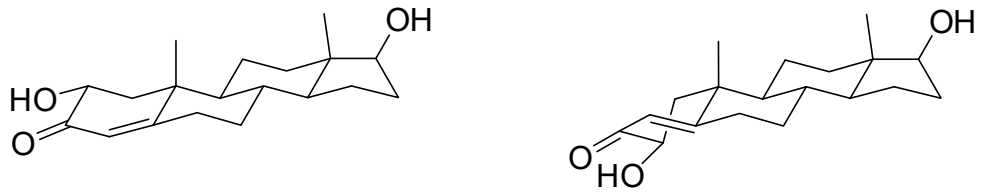

Figure 23: Structures of 2αOHMT (left) and 2βOHMT (right), showing the tension in the A-ring of 2βOHMT

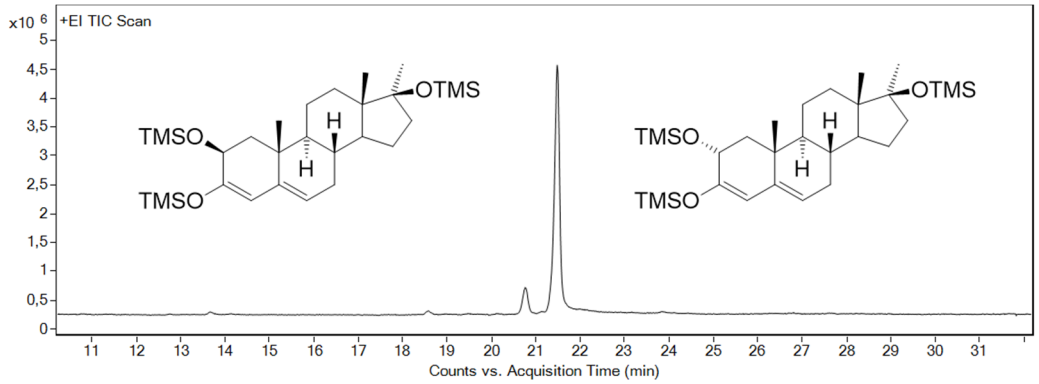

Figure 24: GC-EI-QTOF-MS chromatogram (TIC) of per-TMS derivatives of 2α-hydroxy-17α-methyltestosterone and 2β-hydroxy-17α-methyltestosterone, method h)

The spectrum of the mono-TMS derivative of 2βOHMT shows a similar fragmentation pattern as 2αOHMT ($[C_{22}H_{35}O_3Si]^+$, $[M\text{-}CH_3\text{-}H_2O]^+$, Figure 67 in annex). Only minor differences in the fragments were observed. Differentiation of the two hydroxy isomers as mono-TMS spectra was not possible by EI-MS. Figure 69 shows the spectra of 2αOHMT as a per-TMS derivative with the molecular ion $[M]^{\bullet+}$ = m/z 534. The loss of $[CH_3]^\bullet$ results in the fragment m/z 519. Further fragmentation yield m/z 444 after the cleavage of one TMSOH group ($[M\text{-}TMSOH]^{\bullet+}$) and 429 after the loss of TMSOH and $[CH_3]^\bullet$ ($[M\text{-}CH_3\text{-}TMSOH]^+$). The fragment with the m/z 147 is indicative for vicinal TMS groups ($[TMS\text{-}O\text{-}DMS]^+$) [67, 68]. D-ring fragmentation gives m/z 143, also specific for 17-methyl steroids [68].

Similar to the mono-TMS derivatives, 2βOHMT (Figure 70) as per-TMS derivative shows a similar fragmentation as 2αOHMT. Chromatographic separation was needed to discriminate between the two 2-hydroxy isomers (Figure 24).

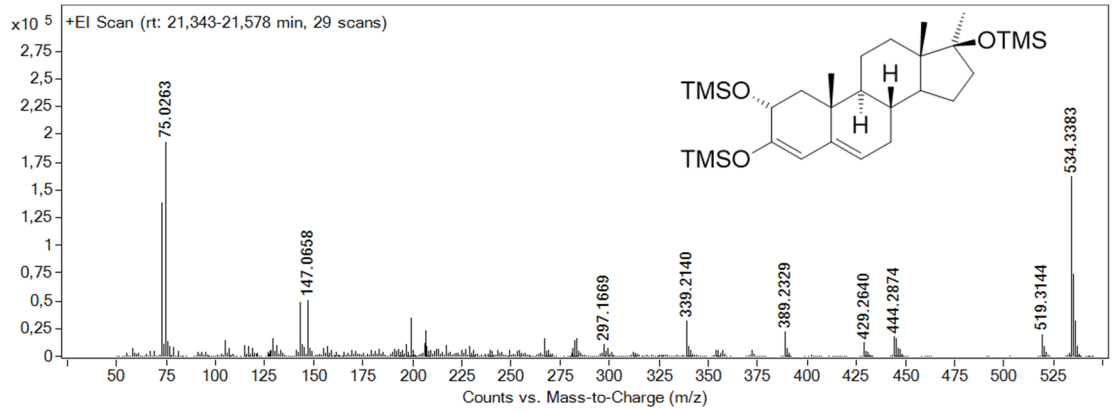

Figure 25: GC-EI-QTOF-MS spectra of 2α-hydroxy-17α-methyltestosterone as per-TMS derivative $[M]^{\bullet+}$=534.3383

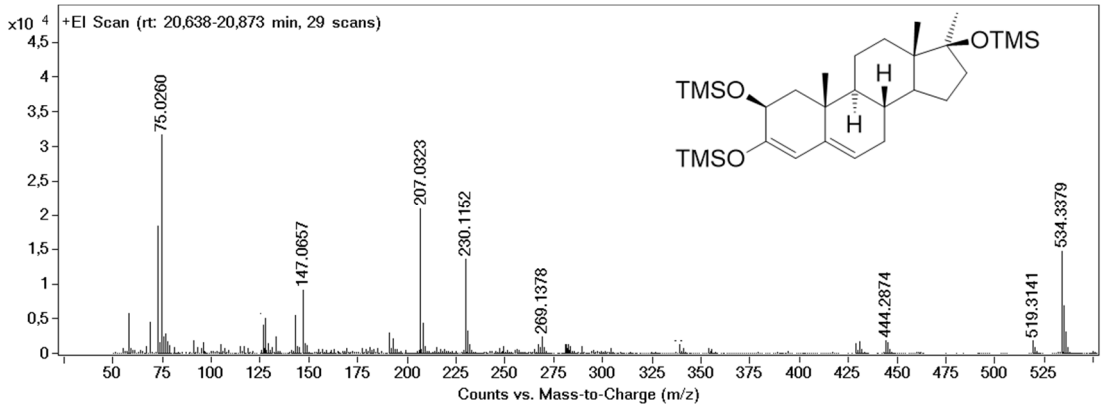

Figure 26: GC-EI-QTOF-MS spectra of 2β-hydroxy-17α-methyltestosterone as per-TMS derivative $[M]^{\bullet+}$=534.3379

GC-EI-QTOF-MS was used to identify the elementary composition and origin of the fragments discussed before. All fragments (elementary composition, exact mass, accurate mass, and mass error) of both enantiomers are displayed in Table 13 and Table 14. Additionally, it was used for structure confirmation, together with LC-HRMS (LC-ESI-QTOF-MS) and NMR spectroscopy.

Figure 25 represents the mass spectra obtained after analysis of 2αOHMT as per-TMS on the GC-QTOF-MS in scan mode (method g). The $[M]^{\bullet+}$ ion m/z 534.3383 is the most abundant peak in the spectrum ($[C_{29}H_{54}O_3Si_3]^{\bullet+}$, mass error 1.50 ppm). The loss of $[CH_3]^{\bullet}$ results in m/z 519.3144 ($[M\text{-}CH_3]^+$, mass error 0.58 ppm). As reported for 2OHAED, it may be assigned to the loss of the methyl group at C19, C18, or a loss of a methyl group of TMS [67]; for 2OHMT, also a loss of C20 is possible. Further fragmentation yields $[M\text{-}CH_3\text{-}TMSOH]^+$ with m/z 429.2640 (mass error 0.00 ppm). The loss of one OTMS group and $[H]^{\bullet}$ results in the fragment $[M\text{-}TMSOH]^+$ m/z 444.2874 with a mass error of 0.00 ppm. After D-ring fragmentation (loss of $[C_7H_{17}OSi]^{\bullet}$), the fragment m/z 389.2329 is obtained. It can be explained as the fragment $[M\text{-}C_4H_8\text{-}TMSOH]^+$, having a mass error of 0.51 ppm [68]. The loss of two TMSOH groups and one methyl group yields $[M\text{-}195]^+$ and is shown as m/z 339.2140 ($[M\text{-}CH_3\text{-}2x\ TMSOH]^+$, mass error 0.29 ppm). For 2OHAED, Kollmeier *et al.* describe the fragment m/z 267 as an A-ring fragment containing two TMS groups [67]. The fragment with m/z 267.1728 in the spectrum of 2αOHMT ($[C_{13}H_{23}O_2Si_2]^+$) has a mass error of 0.37 ppm. A fragment often seen in hydroxylated steroids with vicinal TMS groups in the A-ring is m/z 147.0656. Because of

the proximity of the two TMS groups, the fragment $(CH_3)_2=O^+$-$Si(CH_3)_3$ can be formed and is well described in literature [67-69]. This fragment is visible with m/z 147.0656 (mass error -1.36 ppm). The D-ring fragment with the theoretical mass of 143.0878 (mass error -6.29 ppm), which indicates the structure of 17-hydroxy-17-methyl-steroids, is also present in the spectra beside the non-specific fragment of the TMS group with m/z 73.0468 (mass error 0.00 ppm) [68]. Another fragment described for oxymesterone by Parr *et al.* is m/z 296.1622, which is correlated with fragmentation in the B-ring (loss of $[C_{14}H_{26}OSi]^{\bullet}$) [68]. In the spectrum of 2αOHMT, a fragment with m/z 297.1669 is visible and may be the postulated fragment with an additional proton ($[M\text{-}C_{14}H_{25}OSi]^+$) having a mass error of -10.77 ppm.

The spectrum of 2βOHMT (Figure 26) shows similar fragments to the ones described above for its enantiomer 2αOHMT. Most likely due to low abundance, m/z 389 and m/z 297 are not detected). Only the fragment m/z 269.1378 ($[C_{13}H_{25}O_2Si_2]^+$, mass error -3.72 ppm) shows a two proton shift, compared to 2αOHMT. This fragment is also described for oxymesterone by Kollmeier *et al.* [67].

HRMS using ESI provided accurate masses of the non-derivatized isomers. The elementary composition of 2αOHMT ($C_{20}H_{30}O_3$), $[M+H]^+$ accurate mass 319.2265 (mass error -0.94 ppm), and 2βOHMT ($C_{20}H_{30}O_3$), $[M+H]^+$ accurate mass 319.2267 (mass error -0.31 ppm), was verified (Figure 72 and Figure 73, annex).

Table 13: Postulated fragments, their exact mass, accurate mass, and the resulting mass errors for tris-TMS derivatives of 2α-hydroxy-17α-methyltestosterone (GC-QTOF-MS)

Postulated fragment	**Exact mass [m/z]**	**Accurate mass (experimental) [m/z]**	**Mass error [ppm]**
$[M]^{\bullet+}$	534.3375	534.3383	1.50
$[M\text{-}CH_3]^+$	519.3141	519.3144	0.58
$[M\text{-}TMSOH]^{\bullet+}$	444.2874	444.2874	0.00
$[M\text{-}CH_3\text{-}TMSOH]^+$	429.2640	429.2640	0.00
$[M\text{-}C_3H_5\text{-}CH_3\text{-}TMSOH]^+$	389.2327	389.2329	0.51
$[M\text{-}CH_3\text{-}2xTMSOH]^+$	339.2139	339.2140	.029
$[M\text{-}C_3H_5\text{-}CH_3\text{-}TMSOH]^+$	297.1701	297.1669	-10.77
$[C_{13}H_{23}O_2Si_2]^{\bullet+}$	267.1231	267.1230	0.37
$[TMS\text{-}O\text{-}DMS]^+$	147.0656	147.0658	1.36
$[C_7H_{15}OSi]^+$	143.0887	143.0878	-6.29
$[TMS]^+$	73.0468	73.0468	-0.00

Table 14: Postulated fragments, their exact mass, accurate mass, and the resulting mass differences for tris-TMS derivatives of 2β-hydroxy-17α-methyltestosterone (GC-QTOF-MS)

Postulated fragment	**Exact mass [m/z]**	**Accurate mass (experimental) [m/z]**	**Mass error [ppm]**
$[M]^{\bullet+}$	534.3375	534.3379	0.75
$[M\text{-}CH_3]^+$	519.3141	519.3141	0.00
$[M\text{-}TMSOH]^{\bullet+}$	444.2874	444.2874	0.00
$[M\text{-}CH_3\text{-}TMSOH]^+$	429.2640	429.2634	-1.40
$[M\text{-}CH_3\text{-}2xTMSOH]^+$	339.2139	339.2140	0.29
$[C_{13}H_{25}O_2Si_2]^{\bullet+}$	269.1388	269.1378	-3.72
$[TMS\text{-}O\text{-}DMS]^+$	147.0656	147.0657	0.68
$[C_7H_{15}OSi]^+$	143.0887	143.0880	-4.89
$[TMS]^+$	73.0468	73.0467	-1.37

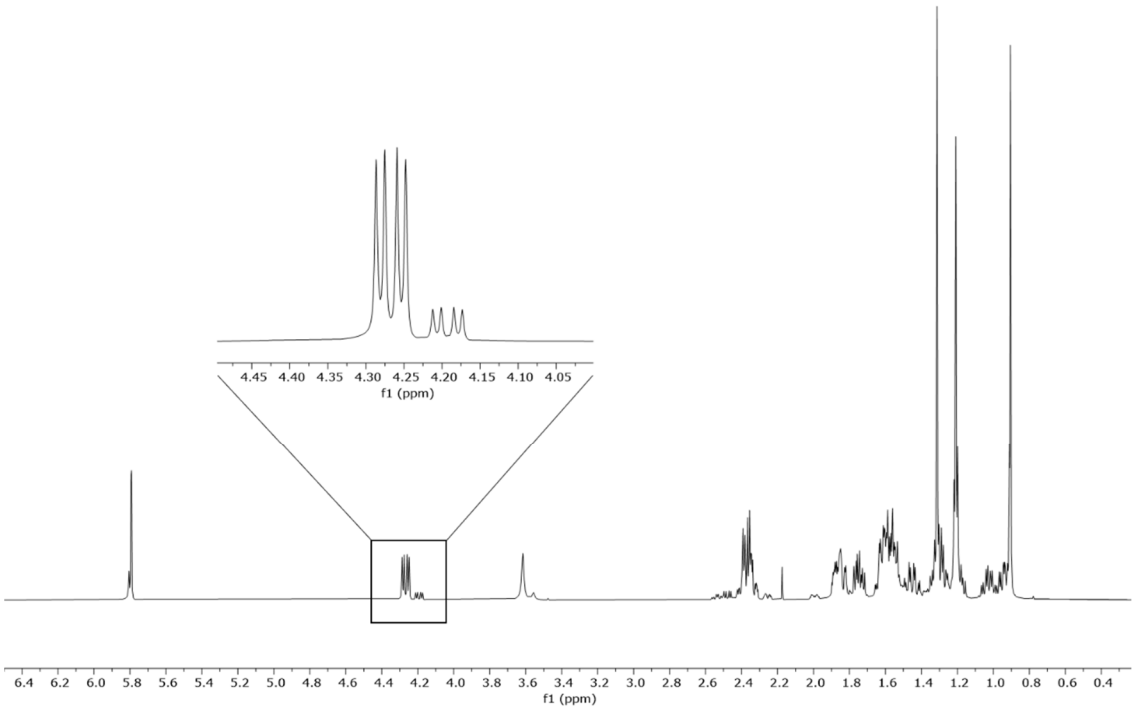

Figure 27: ^{1}H-NMR spectrum of 2ξ-hydroxy-17α-methyltestosterone enantiomers in $CDCl_3$, insert shows zoom at 4.00 - 4.50 ppm

NMR data was obtained from a solution of 5 mg purified 2ξOHMT in deuterated chloroform at 298 K. The spectra were recorded at 500 Hz (^{1}H) and 125 Hz (^{13}C), respectively. 2D-NMR experiments (^{1}H,^{1}H-COSY, ^{1}H,^{13}C-HSQC, ^{1}H,^{13}C-HMBC) were implemented for structure elucidation. Figure 27 shows the ^{1}H spectrum of a mixture of the two isomers (2ξOHMT, chemical shifts of the protons in the molecule are displayed in parts per million [ppm]). The zoomed region (4.00 ppm to 4.50 ppm) shows the proton's chemical shifts at C2. The 2α-proton (4.19 ppm, dd) is correlated to 2βOHMT. At 4.27 ppm (dd), the chemical shift of the 2β-proton of 2αOHMT is located. Double bond protons are typically shifted to the downfield region. The proton at C4 was assigned to the chemical shift at 5.8 ppm. Figure 28 presents the ^{13}C-NMR DEPTQ spectrum of 2ξOHMT (chemical shifts of the carbon atoms in the molecule are also displayed in ppm). The peak at 199.64 was assigned to C3. Carbonyl functions are typically shifted downfield. The peaks at 173.07 (C5) and 120.17 (C4) were assigned to the double bond (4-en). Similar to the shifts of the 2α/β protons in the ^{1}H-NMR spectrum, C2 shows two different chemical shifts for 2βOHMT (68.55 ppm) and 2αOHMT (69.42 ppm). The

positive peaks at 13.89 ppm (C18), 18.03 ppm (C19), and 25.88 ppm (C20) represent the three methyl groups of the molecule. For structure confirmation of 2βOHMT and 2αOHMT 2D-NMR experiments were used. $^{1}H,^{13}C$-HSQC was used to assign the protons to the corresponding carbons in the molecule. The 2α-proton at 4.27 ppm couples to the carbon at 69.42 ppm, while the 2β-proton at 4.19 ppm couples to the carbon at 68.55 ppm. $^{1}H,^{1}H$-COSY (Figure 76, annex), and $^{1}H,^{13}C$-HMBC (Figure 77, annex) spectra were used to validate the structure. The NMR results were also compared with the predicted values of ChemDraw Professional V19.1 and literature data for 2ξ-hydroxytestosterone [70, 71]. The corresponding values are shown in Table 15. The assignment of C atoms in the A-ring, C17 (CH_3), C18, and C19, was confirmed with the literature data. The predicted values from ChemDraw were comparable to the measured and literature values. Only the prediction for C2 was significantly higher than the value found in the sample. The predicted and literature values also confirmed the proton assignment for 2ξOHMT.

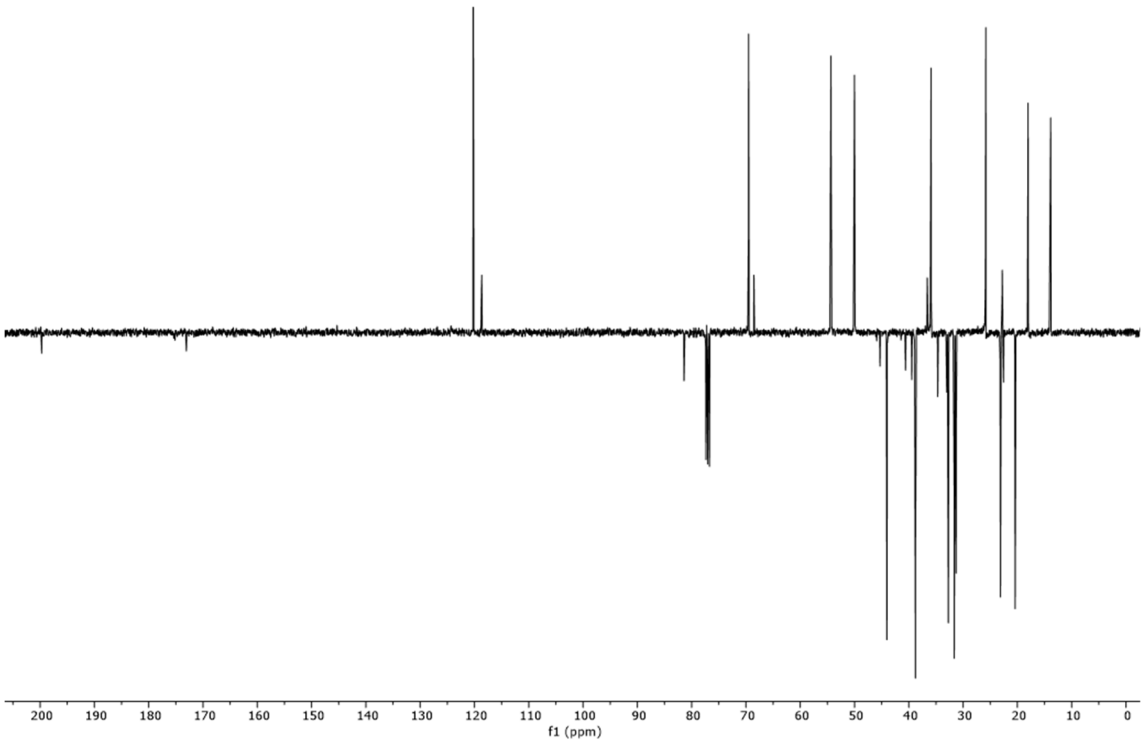

Figure 28: ^{13}C-NMR DEPTQ spectrum of 2ξ-hydroxy-17α-methyltestosterone enantiomers in $CDCl_3$

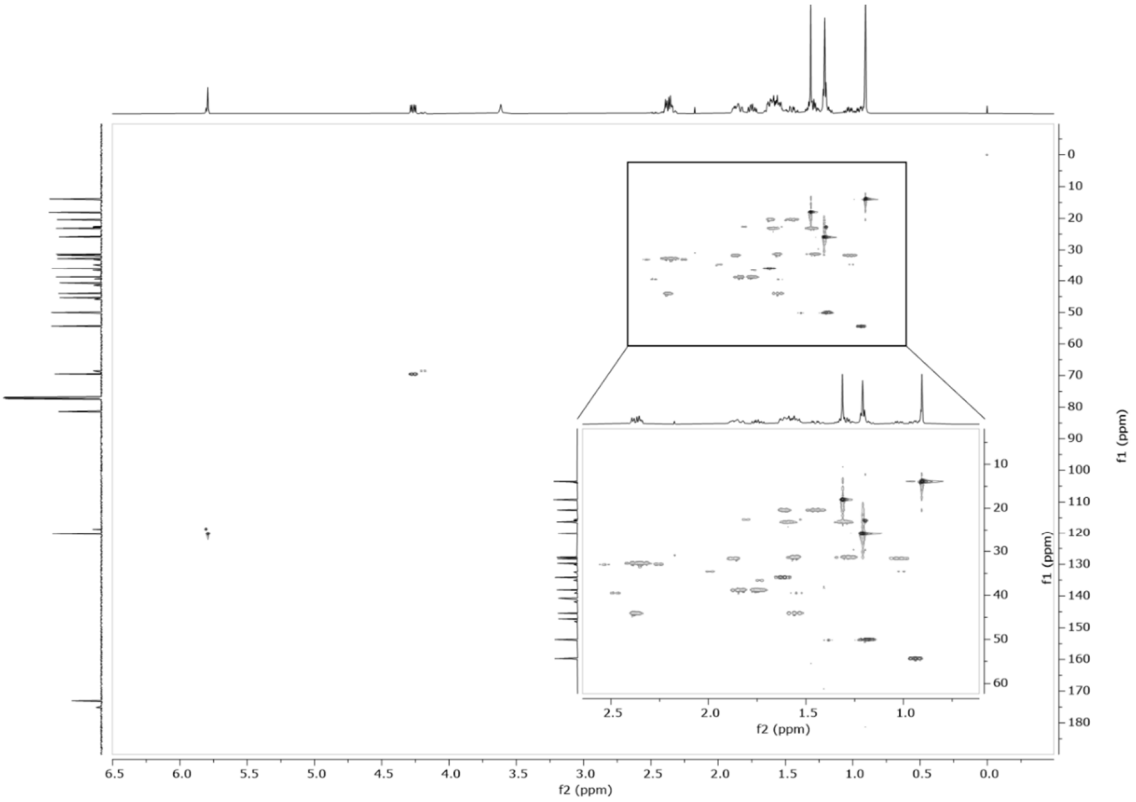

Figure 29: $^{1}H,^{13}C$-HSQC spectrum of 2ξ-hydroxy-17α-methyltestosterone in $CDCl_3$, zoomed area of 0.75 - 2.5 ppm and 5 - 60 ppm

The ^{1}H-NMR spectrum (Figure 27) was also used to calculate the ratio of the two isomers. The isomer mix used to obtain the NMR spectra contained 15% 2βOHMT and 85% 2αOHMT. The isomer ratio was determined by comparing the C2 proton integrals of both isomers in the ^{1}H-NMR spectra (Figure 27).

To increase the amount of the 2β-isomer Mitsonobu rearrangement was performed [72, 73] but did not give the desired outcome. Another synthesis approach by obtaining 2βOHMT via bromination of C6 with N-bromosuccinimide followed by an acetoxylation to obtain the 2ξ-acetoxy derivatives, which then were hydrolyzed to the hydroxy metabolites as reported by Rao *et al.* [65], did not yield the desired products.

*Table 15: Chemical shifts of 2ξ-hydroxy-17α-methyltestosterone (^{1}H-NMR and ^{13}C-NMR) in comparison to predicted values and chemical shifts of 2ξ-hydroxytestosterone from literature [70, 71]; *value for 4-hydroxytestosterone [71]*

Position	Own synthesis [$CDCl_3$]		ChemDraw prediction		Literature values for ^{13}C 2α-hydroxyandrostendione [71] ^{1}H 2ξ-hydroxytestosterone [70] [$CDCl_3$]	
	δ_C [ppm]	δ_H [ppm]	δ_C [ppm]	δ_H [ppm]	δ_C [ppm]	δ_H [ppm]
1	44.08	1.53 2.36	42.2	1.34 1.59	n.a.	1.59 / 1.54 2.38 / 2.49
2	2α: 69.42 2β: 68.55	2α: 4.27 -OH 5.80 2β: 4.19 -OH 5.80	85.1	5.48 -OH 5.48	69.2	2α: 4.27 2β: 4.19
3	199.73	----------	197.0	----------	199.6	----------
4	120.17	5.75	120.8	5.85	120.4	5.81 / 5.80
5	173.07	----------	175.2	----------	172.3	----------
6	32.68	2.24 2.34	32.5	2.32 2.42	n.a.	2.34 /2.26 2.41 / 2.53
7	31.68	1.00 1.85	31.6	1.72 1.97	n.a.	1.02 / 1.01 1.86 / 1.98
8	35.94	1.59	36.0	1.14	n.a.	1.57 / 1.71
9	54.41	0.92	50.3	1.17	n.a.	0.95 / 1.40
10	40.61	----------	41.4	----------	n.a.	----------
11	20.46	1.43 1.60	21.4	1.38 1.62	n.a.	1.44 / 1.53 1.60 / 1.80
12	31.32	1.25 1.53	38.5	1.31 1.56	n.a.	1.08 /1.14 1.87 / 1.89
13	45.26	----------	32.8	----------	n.a.	----------
14	50.06	1.16	49.7	1.04	n.a.	0.97 / 1.00
15	23.18	1.30 1.58	22.9	1.65 1.90	n.a.	1.31 / 1.31 1.62 / 1.59
16	38.82	1.82 1.82	31.4	1.48 1.73	n.a.	1.49 / 1.49 2.08 / 2.08
17	81.32	----------	82.8	-OH 4.49	220.2 *81.5**	3.65 / 3.67
18	13.89	0.89	16.2	0.89	13.8	0.80/ 0.80
19	18.03	1.28	19.3	1.24	17.9	1.31 / 1.19
20	25.88	1.18	25.8	1.20	x	x

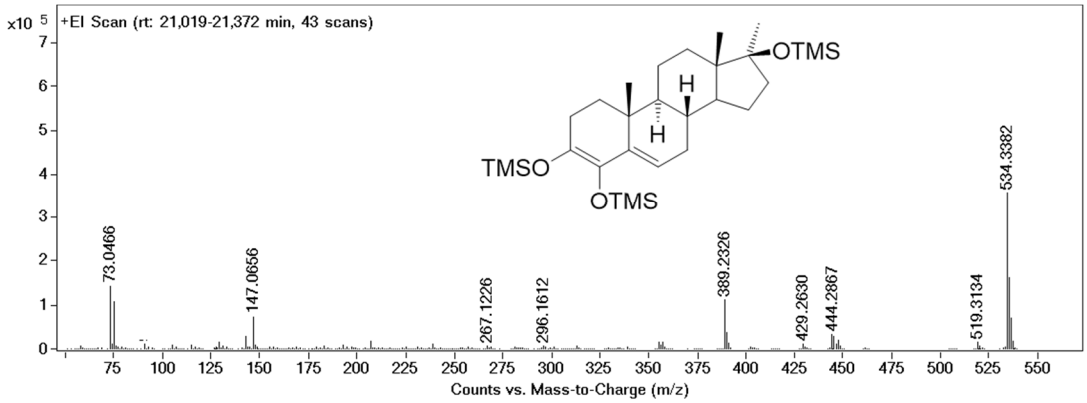

Figure 30: GC-EI-QTOF-MS spectra of 4-hydroxy-17α-methyltestosterone as per-TMS derivative $[M]^{\cdot+}$= 534.3382

4.2 Synthesis of 4-Hydroxy-17α-methyltestosterone

4OHMT was synthesized from commercially available MT as described in 3.2.4.1. The steps of synthesis are described in the section for 2ξOHMT (4.1). An amount of 18 mg pure 4OHMT was obtained after the semipreparative purification of the product mixture with method a). Spectra of 4OHMT as mono- (Figure 68, annex) and per-TMS (Figure 71) derivatives showed a similar fragmentation pattern to the 2ξOHMT isomers. The spectrum of the 4OHMT per-TMS-derivative as TOF scan experiment (GC-EI-QTOF, method g) is shown in Figure 26. The fragments are similar to the fragments already discussed in the section above for 2ξOHMT. Table 16 shows all fragments of 4OHMT, which are discussed in this section. The base peak of m/z 534.3382 is correlated to the $[M]^{\cdot+}$ ion (mass error 1.31 ppm). The loss of $[CH_3]^{\cdot}$ results in m/z 519.3134 (mass error -1.35 ppm) [67]. A subsequent loss of [TMSOH] gives $[M\text{-}CH_3\text{-}TMSOH]^{+}$ with m/z 429.2630 (mass error -2.33 ppm). The fragment m/z 444.2867 may be explained by the loss of one TMSOH group resulting in the fragment $[M\text{-}TMSOH]^{\cdot+}$ with a mass error of -1.58 ppm. The loss of $[C_7H_{17}OSi]^{\cdot}$ from the D-ring structure yields the fragment m/z 389.2325. It can be explained as the fragment $[M\text{-}C_4H_8\text{-}TMSOH]^{+}$, having a mass error of -0.51 ppm [68]. After the loss of two TMSOH groups and one methyl group, the fragment $[M\text{-}CH_3\text{-}2xTMSOH]^{+}$ m/z 339.2082 (mass error -16.80 ppm) is detected. The A-ring fragment with m/z 267.1226 ($[C_{13}H_{23}O_2Si_2]^{\cdot+}$) has a mass error of -1.87 ppm. The fragment m/z 147.0656 is present in the spectrum and represents vicinal TMS groups in

the A-ring (mass error 0.00 ppm). A well-described fragment of oxymesterone is m/z 296.1622, which is correlated with fragmentation in the B-ring (loss of $[C_{14}H_{26}OSi]^{\bullet}$) [68]. This fragment ($[M\text{-}C_{14}H_{26}OSi]^{+}$, m/z 296.1611, mass error -3.71 ppm) has a very low abundance but can be observed in the spectra. The characteristic D-ring fragment of 17-methyl steroids with the accurate mass of 143.0872 (mass error -10.48 ppm) is also present in the spectrum besides the non-specific fragment of the TMS group with m/z 73.0466 (mass error -2.74 ppm) [68]. The elementary composition of 4OHMT ($C_{20}H_{30}O_3$) was verified by LC-HRMS (accurate mass $[M+H]^{+}$ 319.2268, mass error 0.00 ppm).

NMR experiments were obtained from a solution of 5 mg purified 4OHMT in deuterated DMSO at 298 K. The spectra were recorded at 500 Hz (^{1}H) and 125 Hz (^{13}C), respectively. 2D-NMR experiments ($^{1}H,^{1}H$-COSY, $^{1}H,^{13}C$-HSQC, $^{1}H,^{13}C$-HMBC) were implemented for structure elucidation. As explained in the discussion for 2ξOHMT, integrating the ^{1}H-NMR spectra and proton assignment was only achieved with 2D-NMR experiments.

Table 16: Postulated fragments, their exact mass, accurate mass, and the resulting mass differences for 4-hydroxy-17α-methyltestosterone, GC-QTOF-MS of per-TMS derivative

Postulated fragment	**Exact mass [m/z]**	**Accurate mass (experimental) [m/z]**	**Mass error [ppm]**
$[M]^{\bullet+}$	534.3375	534.3382	1.31
$[M\text{-}CH_3]^{+}$	519.3141	519.3134	-1.35
$[M\text{-TMSOH}]^{\bullet+}$	444.2874	444.2867	-1.58
$[M\text{-}CH_3\text{-TMSOH}]^{+}$	429.2640	429.2630	-2.33
$[M\text{-}C_3H_5\text{-}CH_3\text{-TMSOH}]^{+}$	389.2327	389.2325	-0.51
$[M\text{-}CH_3\text{-2xTMSOH}]^{+}$	339.2139	339.2082	-18.28
$[M\text{-}C_3H_5\text{-}CH_3\text{-TMSOH}]^{+}$	296.1622	296.1611	-3.71
$[C_{13}H_{23}O_2Si_2]^{\bullet+}$	267.1231	267.1226	-1.87
[TMS-O-DMS]$^{+}$	147.0656	147.0656	0.00
$[C_7H_{15}OSi]^{+}$	143.0887	143.0872	-10.48
$[TMS]^{+}$	73.0468	73.0466	-2.74

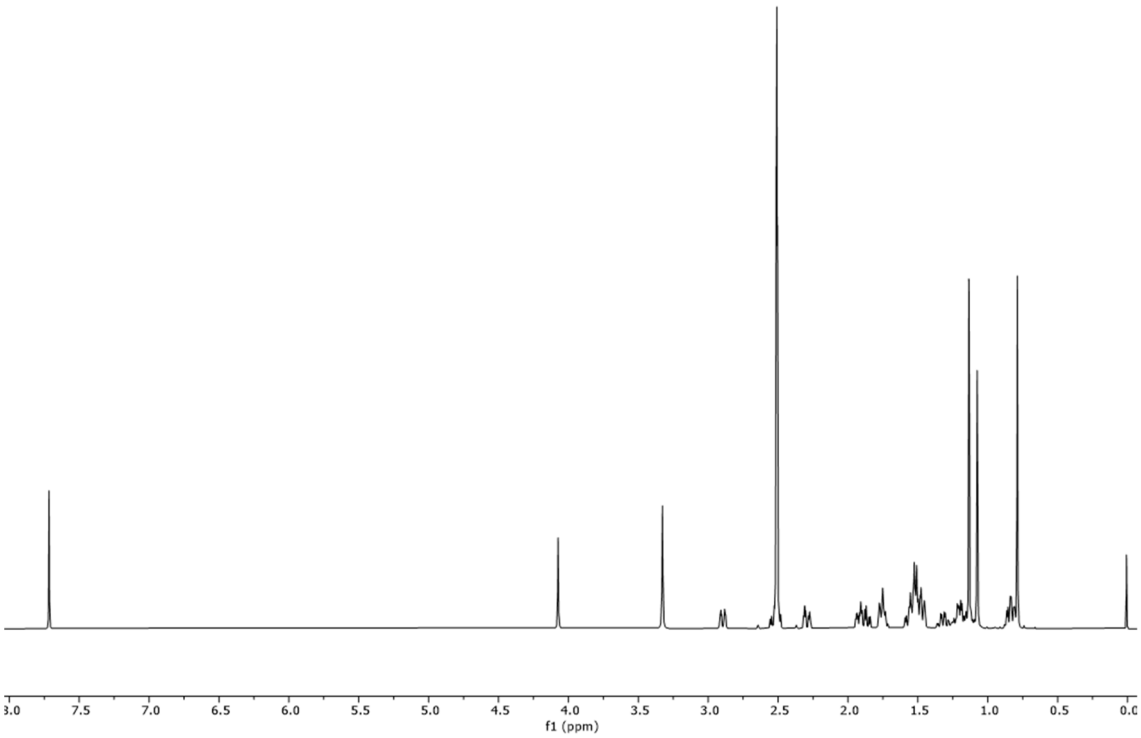

Figure 31: ^{1}H-NMR spectrum of 4-hydroxy-17α-methyltestosterone in DMSO-d_6

The ^{1}H-NMR spectrum of 4OHMT is displayed in Figure 31 and shows the protons' chemical shifts in the molecule. The proton of the hydroxy group at C4 is shifted downfield to 7.72 ppm. The proton of the second hydroxy group at C17 is located at 4.07 ppm. The three methyl groups (C18, C19, C20) were assigned to 0.79 ppm, 1.13 ppm, and 1.07 ppm. Figure 32 shows the ^{13}C-NMR spectrum of oxymesterone. Similar to 2ξOHMT, C3 is shifted downfield to 199.39 ppm. Carbons related to the double bond are also shifted downfield to 141.94 ppm (C4) and 139.85 ppm (C5). C17 is shifted to 80.08 ppm because of the proximity to the hydroxy group. The correlation between protons and carbons in the molecule is displayed in Figure 33 (^{1}H,^{13}C-HSQC). The four quaternary carbons (C3, C4, C5, and C17) show no proton binding, as expected. C18, C19, and C20 show highly intense signals (14.47 ppm – 0.79 ppm / 17.47 ppm – 1.13 ppm / 26.57 ppm- 1.07 ppm). To strengthen the structure confirmation, ^{1}H,^{1}H-COSY (Figure 78, annex), and ^{1}H,^{13}C-HMBC (Figure 79, annex) were used together with the prediction of ChemDraw V19.1 and formestane data from the literature [71] as shown in Table 17. Minor deviations between measured and literature values were expected due to different solvents (DMSO-d_6 [sample] vs. $CDCl_3$ [literature]). Nevertheless, the

assignment of all C atoms was confirmed with the literature data. Only the value for C17 was different (220 ppm [literature] – 80 ppm [measured]) but was expected because of the 17-oxo group of 4-hydroxyandrost-4-ene-3,17-dione (formestane). The value for 4-hydroxytestosterone from the same reference showed a comparable value of 83 ppm to the found 80 ppm (both structures have a 17-hydroxy group). The predicted values from ChemDraw were comparable to the measured and literature values but differed for C2 and C17. The predicted and literature values also confirmed the proton assignment for 4OHMT.

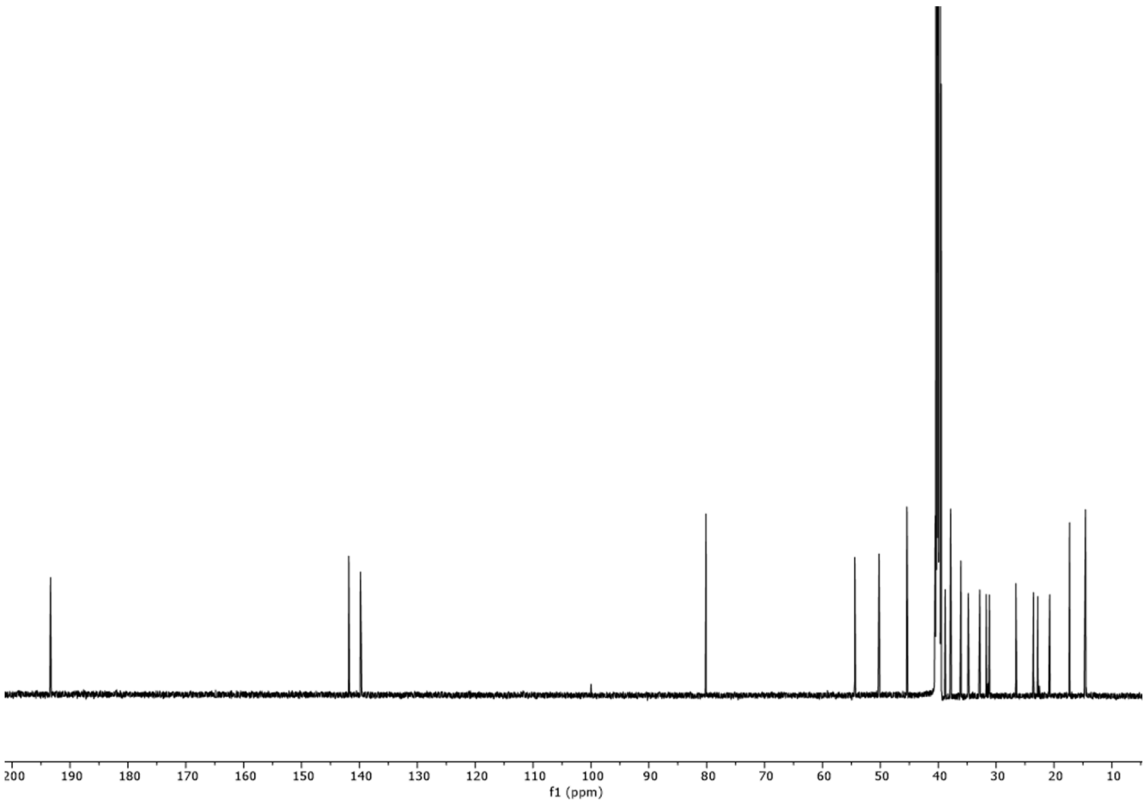

Figure 32: ^{13}C-NMR spectrum of 4-hydroxy-17α-methyltestosterone in DMSO-d_6

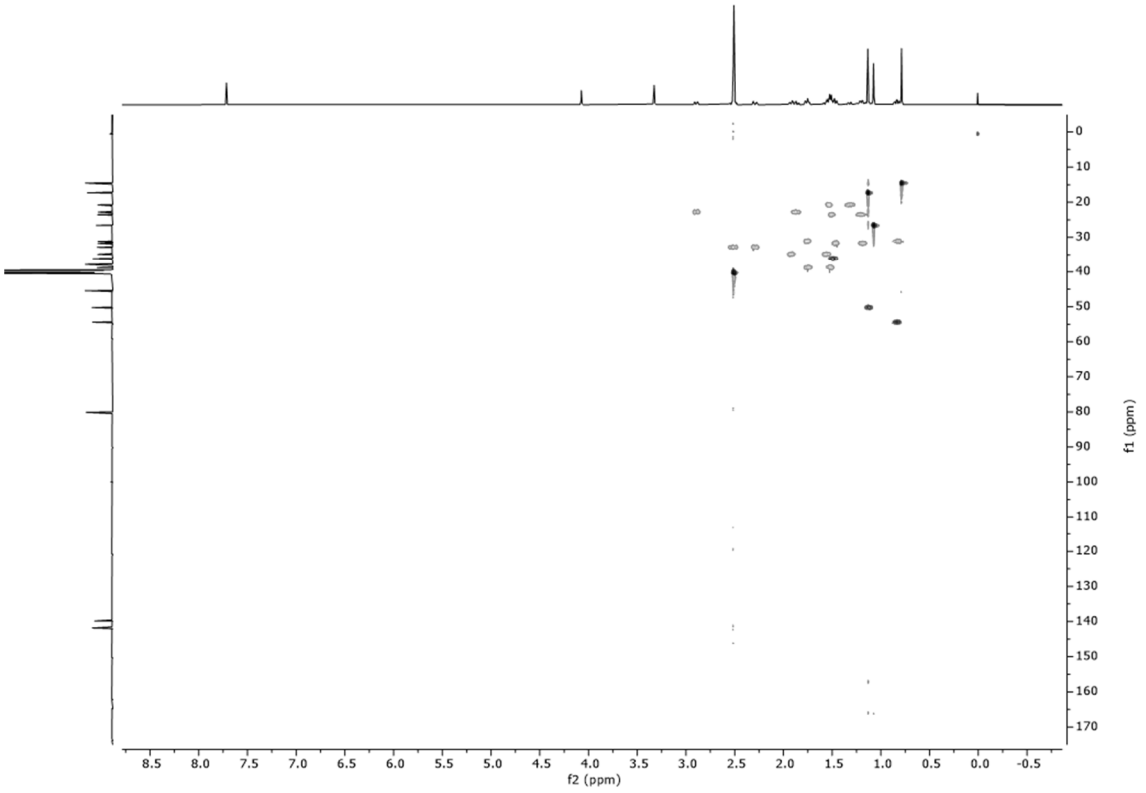

Figure 33: $^{1}H,^{13}C$-HSQC spectrum of 4-hydroxy-17α-methyltestosterone in DMSO-d_6

*Table 17: Chemical shifts of 4-hydroxy-17α-methyltestosterone (^{1}H-NMR and ^{13}C-NMR) in comparison to predicted values and chemical shifts of 4-hydroxyandrost-4-ene-3,17-dione from literature [70, 71], *value for 4-hydroxytestosterone [71]*

Position	Synthesis [DMSO-d_6]		ChemDraw prediction		Literature values for ^{13}C / ^{1}H 4-hydroxyandrost-4-ene-3,17-dione [71] [$CDCl_3$]	
	δ_C [ppm]	δ_H [ppm]	δ_C [ppm]	δ_H [ppm]	δ_C [ppm]	δ_H [ppm]
1	34.79	1.56 1.92	35.5	1.20 1.45	34.5	1.70 2.04
2	32.81	2.29 2.52	27.9	2.87 2.97	31.6	2.52 2.58
3	199.39	----------	193.0	----------	193.2	----------
4	141.94	-OH 7.72	142.9	-OH 10.68	141.4	-OH 6.16
5	139.85	----------	142.2	----------	139.3	----------
6	22.79	1.87 2.89	22.3	2.32 2.42	22.5	2.03 3.07
7	31.13	0.82 1.76	31.9	1.72 1.97	29.7	1.09 2.00
8	36.07	1.49	36.0	1.14	34.6	1.65
9	54.41	0.83	54.0	1.17	54.1	1.01
10	37.87	----------	33.0	----------	37.7	----------
11	20.71	1.32 1.53	21.4	1.38 1.62	20.1	1.44 1.70
12	31.65	1.19 1.46	38.5	1.31 1.56	31.1	1.30 1.88
13	45.39	----------	45.4	----------	47.3	----------
14	50.22	1.13	49.7	1.04	50.8	1.30
15	23.54	1.21 1.51	22.9	1.65 1.90	21.6	1.58 2.00
16	38.80	1.52 1.75	31.4	1.48 1.73	35.6	2.16 2.52
17	80.08	-OH 4.07	82.8	-OH 4.49	220.4 *81.5**	n.a.
18	14.47	0.79	16.2	0.89	13.8	0.92
19	17.26	1.13	19.3	1.24	17.1	1.20
20	26.57	1.07	25.8	1.20	x	x

4.3 Synthesis of 19-Hydroxy-17α-methyltestosterone

19OHMT was synthesized from commercially available 19OHAED via a Grignard reaction at position 17. Prior protection of position 3 was performed by stirring a methanolic solution of 19OHAED in the presence of acetyl chloride. The stages of chemical synthesis are shown in Figure 34. In the first step, acetyl chloride was used to eliminate the resulting water from the ketalization of position three. As acetyl chloride is very reactive, the hydroxy group at position 19 might be acetylated to give the first intermediate product (**8**). As the raw product of the first step was directly used for step two of the synthesis, this structure (**8**) is only postulated but not verified. The postulated ester in position 19 was cleaved during the Grignard reaction, as displayed in Figure 35. Further investigation of this prediction was not performed, as the protection of the C19 hydroxy group would not influence the structure of the product. In the second step, (**8**) was treated with methyl magnesium bromide to introduce the methyl group in position 17.

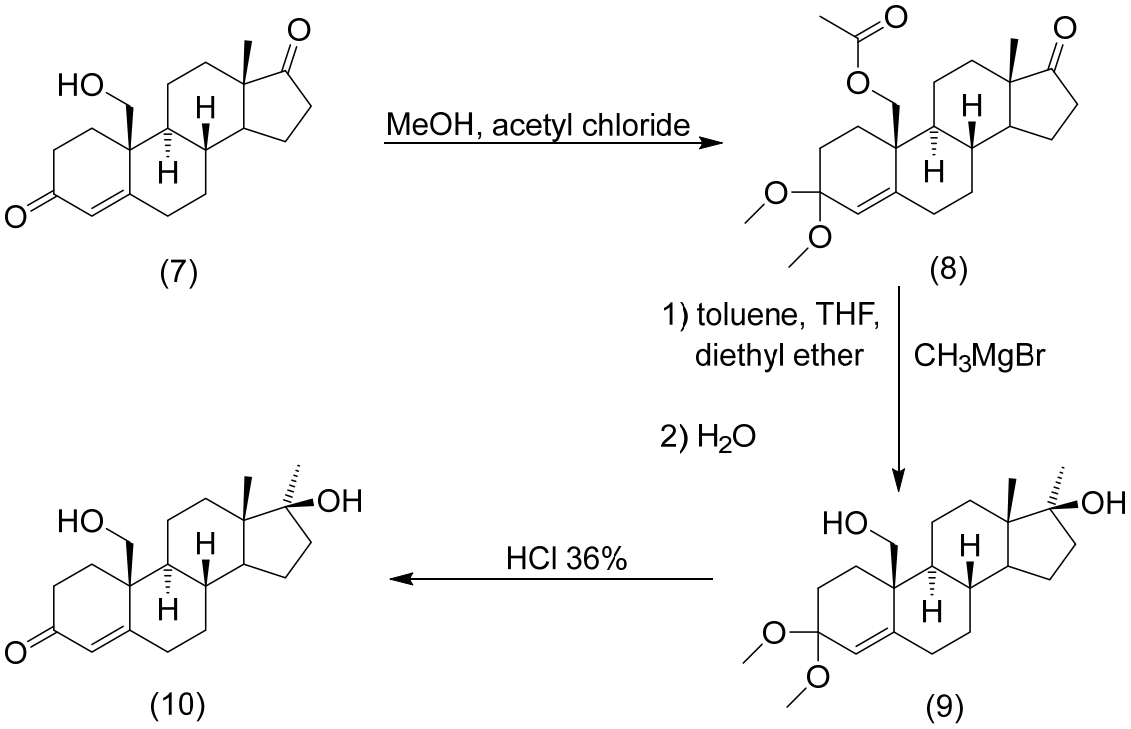

Figure 34: Steps of the chemical synthesis of 19-hydroxy-17α-methyltestosterone (10) using 19-hydroxyandrost-4-en-3,17-dione (7) as educt; first intermediate product (8) after the protection of position 3 and second intermediate product (9) after Grignard reaction and hydrolysis with water

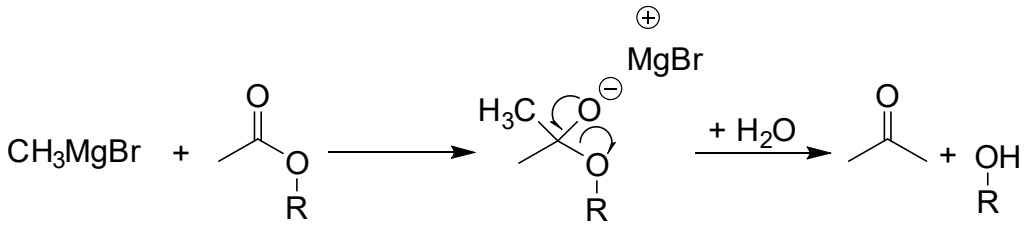

Figure 35: Anticipated reaction mechanism of C19 ester with CH_3MgBr to give the unprotected hydroxy group

Liao *et al.* described that this step mainly gives the 17α-methyl product (19-hydroxy-3,3-dimethoxy-17α-methyltestosterone, **9**) as generally obtained in 17-methylation of steroids [61].

The isomer 19-hydroxy-3,3-dimethoxy-17β-methyltestosterone may be one byproduct but was not detected with the used GC-MS method. Cleavage of the protection group at position 3 with hydrochloric acid in methanol gave the desired product 19OHMT (**10**).

Figure 36 depicts the GC-EI-MS chromatogram after derivatization of the product mixture (GC-EI-MS, method f). 19OHAED has a retention time of 16.3 min and m/z of 518 (spectrum is displayed in annex Figure 80). The educt spectrum shows the characteristic fragment loss of 103 daltons, which correspond with the loss of $[CH_2\text{-OTMS}]^{\cdot}$ (C19) [74]. Most of the educt did not react in the synthesis. Protection of both oxo groups (3 and 17) instead of only protecting position 3 might explain this. 19OHMT, as the desired product, has a retention time (RT) of 17.3 min and m/z 534.

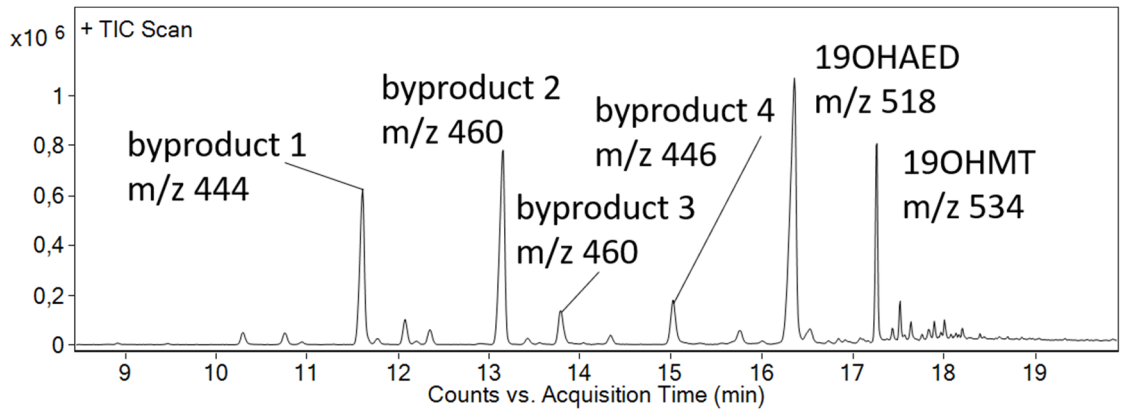

Figure 36: GC-MS chromatogram after TMIS derivatization showing 6 main products unidentified byproduct 1 (m/z 444, RT 11.6), unidentified byproduct 2 (m/z 460, RT 13.1 min), unidentified byproduct 3 (m/z 460, RT 13.8 min), unidentified byproduct 4 (m/z 446, RT 15.0) min, 19OHAED (m/z 518, RT 16.3 min, educt) and 19OHMT (m/z 534, RT 17.3, product)

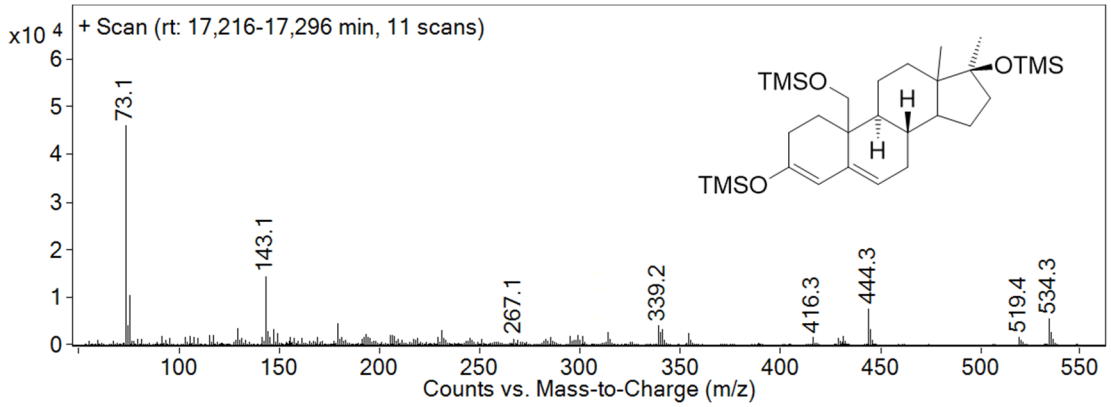

Figure 37: GC-EI-MS spectra of 19OHMT as per TMS derivative at 70 eV $[M]^{\bullet+}$= 534.3

The spectrum of 19OHMT, displayed in Figure 37, shows specific fragments for the 19-hydroxy group ($[M-103]^+$) and the introduced methyl group in position 17 (m/z 143, D-ring fragment of 17-methyl-steroids).

Other fragments already described for 2ξOHMT and 4OHMT in sections 4.1 and 4.2 are also found in the spectrum of 19OHMT. For example, the loss of one TMSOH group resulting in $[M-90]^{\bullet+}$ with m/z 444, or the loss of $[CH3]^{\bullet}$ resulting in m/z 519 ($[M-15]^+$). Also, the fragment $[C_{13}H_{23}O_2Si_2]^{\bullet+}$ with m/z 267 and m/z 339 showing the fragment $[M-CH_3-2xTMSOH]^+$ (similarities to 2ξOHMT) were used to identify the structure of 19OHMT.

Two main byproducts were produced with $[M]^{\bullet+}$ of m/z 444 and m/z 460. Both peaks (RT 11.6 min and 13.1 min, Figure 80 and Figure 81) show a loss of m/z 103 that correlates to an intact 19-hydroxy group. The first byproduct (substance 1, RT 11.6 min, Figure 81) did not show the fragment with m/z 143, which indicates a missing 17-methyl-17-hydroxy structure. The $[M]^{\bullet+}$ of m/z 444 and the missing fragment of m/z 143 indicate a possible Wagner-Mehrwein (WM) rearrangement in the D-ring. Therefore, substance 1 (RT 11.6 min) was proposed to be the WM product of 19OHMT, produced during the acid catalyzed cleavage of the protection group in position 3. The second byproduct (RT 13.1 min, substance 2, Figure 82) shows the specific D-ring fragment for 17-methyl-17-hydroxy steroids of m/z 143. With m/z 460 at RT 13.8 min, the third byproduct (substance 3, Figure 83) shows a similar spectrum and may be an isomer of substance 2. Fragmentation pattern and molecule peak in the spectra of substance 2 and substance 3

may result from an oxidated isomer of 19OHMT as bis-TMS derivative. The molecular peak of byproduct 4 (substance 4, Figure 84) at RT 15.0 min shows an m/z of 446, which may be explained by the bis-TMS derivative of the educt.

Nevertheless, the spectrum of substance 4 (Figure 84) also shows both characteristic fragments for 19-hydroxy and 17-methyl groups ($[M-103]^+$ and m/z 143), which counterfeits the 17-oxo function of 19OHAED. Therefore, no identification of substance 4 was possible. For an exact confirmation of the byproduct structures, further purification and separation of the product mixture and NMR analysis of the pure fractions are advisable. As the intention was to synthesize 19OHMT as analytical reference for CYP19A1 *in vitro* study of MT (RT and MRM), no further investigation of the byproducts was performed.

After purifying the product mixture by washing it with ethyl acetate, only a small amount of ~3 mg of 19OHMT was obtained. The amount was too small for additional structure investigation methods, such as NMR experiments.

The product, after cleaning, showed a bad solubility in methanol. After filtration, the methanolic solution was used to investigate the RT and multiple reaction monitoring and source optimization for method d).

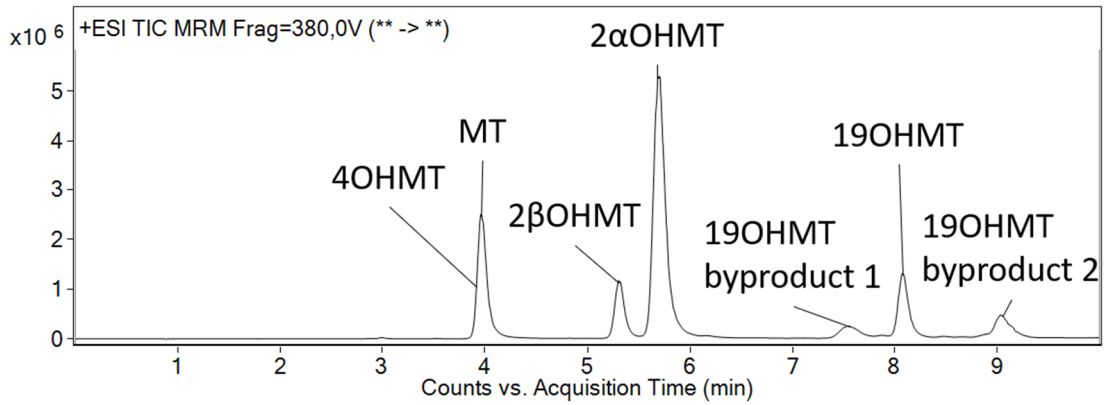

Figure 38: SFC-QQQ-MS chromatogram of the steroid mix (4OHMT, MT, 2βOHMT, 2αOHMT, 19OHMT [including two unidentified byproducts]) using method d)

Figure 38 shows the chromatogram of a mixture of 2ξOHMT, 4OHMT, MT, 19OHMT, and its two synthesis byproducts. The product gave three peaks with the same MRM (showed as 19OHMT, 19OHMT byproduct 1, and 19OHMT byproduct 2). Later investigation of the *in vitro* study showed the peak at 8.1 min to be the desired 19OHMT.

The product with RT 17.3 min was postulated to be the desired 19OHMT, taking into account the reaction mechanism, the fragmentation pattern of the per-TMS derivative, and the chromatographic behavior in SFC (AED-19OHAED/MT-19OHMT).

19OHMT could be synthesized in small amounts using an adapted method of Liao *et al.* [61]. However, optimization of this method has to be performed to increase this synthesis outcome to obtain enough substance for further characterization of the products.

4.4 Analytical Method Development

One central part of the project was developing a chromatographic method, which can separate OHMT isomers of interest. Therefore, the well-established systems GC-MS(/MS) (section 4.4.1) and LC-MS(/MS) (section 4.4.2) were compared to the orthogonal technique of SFC-MS/MS (section 4.4.3).

4.4.1 GC-MS methods

Three different GC-MS methods were used in this project. Two of these methods used a single quadrupole MS as a detector (method f and g in section 3.2.3.2). HRMS on a GC-QTOF-MS was performed at the anti-doping laboratory in Rome, using a standardized method (method h in section 3.2.3.2). All three methods used identical Agilent HP1-Ultra columns (17 m, 200 µm, 0.11 µm) due to its proven success for steroid-TMS separation. Method f) was already established for the detection of several underivatized and trimethylsilylated steroids. It used a long two gradient from 183 °C to 232 °C with a ramp of 3 °C/min (first step) and to 310 °C with a ramp of 40 °C/min (full parameters in chapter 3.2.3.2). These parameters ended in a runtime of 21 min. Figure 40 shows that the method could not separate the per-TMS derivatives of the hydroxy isomers.

Derivatization with MSTFA yielded the mono-TMS derivatives of these substances and the separation of 2αOHMT, 2βOHMT, and 4OHMT (Figure 39). Nevertheless, no separation of 2αOHMT and 6βOHMT was achieved.

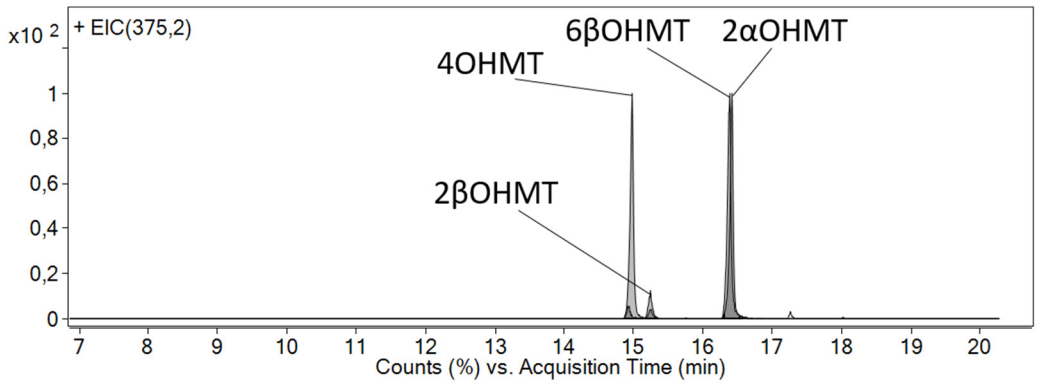

Figure 39: Overlay of EICs (m/z 375.2) from the mono-TMS derivatives of 2αOHTM, 2βOHMT, 4OHMT, and 6βOHMT obtained for method f)

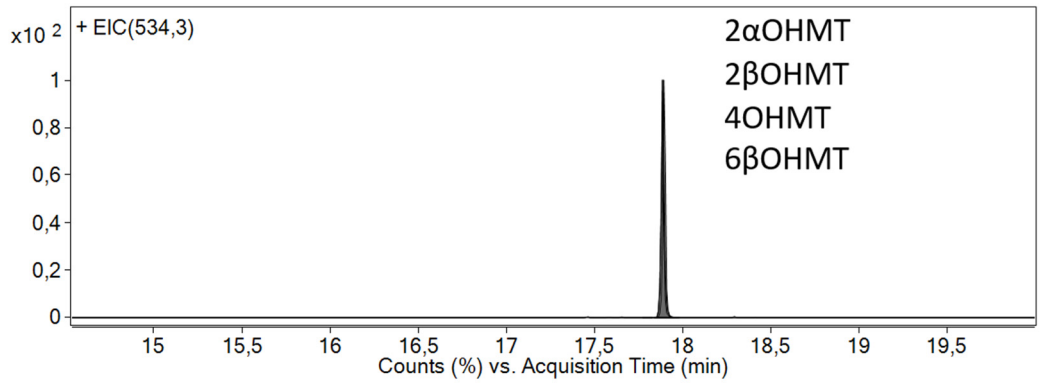

Figure 40: Overlay of EICs (m/z 534.3) from the per-TMS derivatives of 2αOHTM, 2βOHMT, 4OHMT, and 6βOHMT obtained for method f)

The method was used for monitoring the synthesis of 2ξOHMT and 4OHMT together with the LC method b). TMIS contamination in the liner of the GC injector partially led to per-TMS derivatization when the mono-TMS samples were injected directly from MSTFA. Therefore, MSTFA was evaporated under nitrogen flow, and the resulting residue was dissolved in ethyl acetate to avoid the unwanted per-TMS derivatives.

A steeper first ramp of 50 °C/min (150 °C to 240 °C), and a flatter second ramp of 3 °C/min (to 266 °C) were used in method g) (full parameters in chapter 3.2.3.2). These parameters ended in a much faster runtime but showed no other advantages over method f) for the separation of per-TMS derivatives. Method g) was also unable to fully separate the per-TMS derivatives of the MT reference standards (Figure 41). With similar parameters, Joseph separated 6α/βOHAED from 4OHAED and 2α/αOHAED [4].

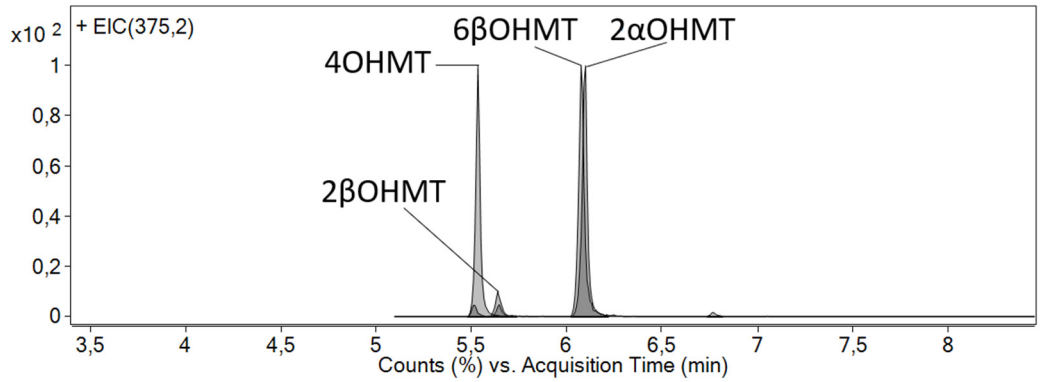

Figure 41: Overlay of EICs (m/z 375.2) from the mono-TMS derivatives of 2αOHTM, 2βOHMT, 4OHMT, and 6βOHMT obtained for method g)

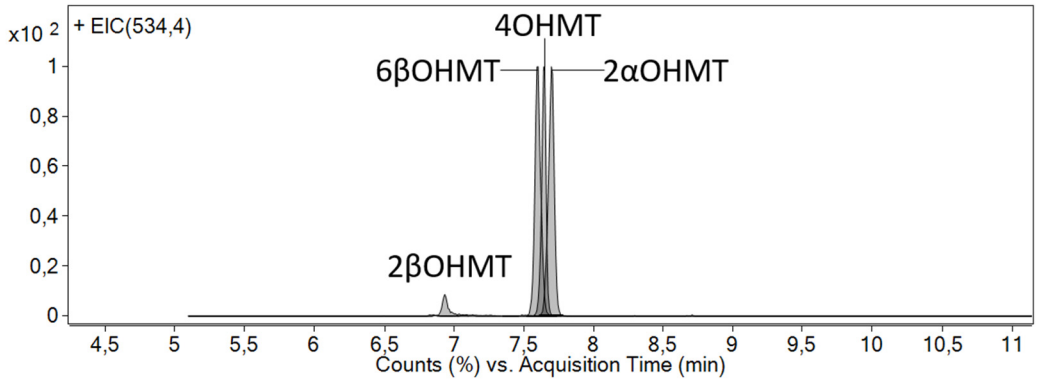

Figure 42: Overlay of EICs (m/z 534.4) from the per-TMS derivatives of 2αOHTM, 2βOHMT, 4OHMT, and 6βOHMT obtained for method g)

The chromatogram of the mono-TMS derivatives showed a similar separation as method f) (mono-TMS derivatives, Figure 42). The RTs for the different substances for method f) and method g) are shown in Table 18. The separation in both GC-EI-MS methods was not good enough to separate the isomers.

As the differentiation of the 2ξOHMT and 4OHMT was also not possible with the fragmentation obtained from the MS spectra, optimization of the GC-EI-MS methods was not followed up. EI ionization was used for the structure verification via the fragmentation pattern of the cleaned synthesis products.

Method h) was used to measure accurate masses of the synthesis products (2ξOHMT and 4OHMT). It used a long gradient (ramp 1 °C/min) starting at 200 °C. All four hydroxy metabolites as per-TMS derivative were separated from each other (Figure 43). Nevertheless, the method struggled in the baseline separation of 4OHMT and 2αOHMT (calculated resulting peak resolution 0.63), and the total run time was about 48 minutes.

GC-MS methods struggle to separate 4-hydroxy metabolites from 2-hydroxy metabolites (as per-TMS, [47]). This result was also confirmed in my research project. Martinez-Brito *et al.* only recently developed a GC-MS method for separating 2-, 4- and 6-OHMT, using a long temperature gradient (>20 min) and multiple reaction monitoring (MRM) [47].

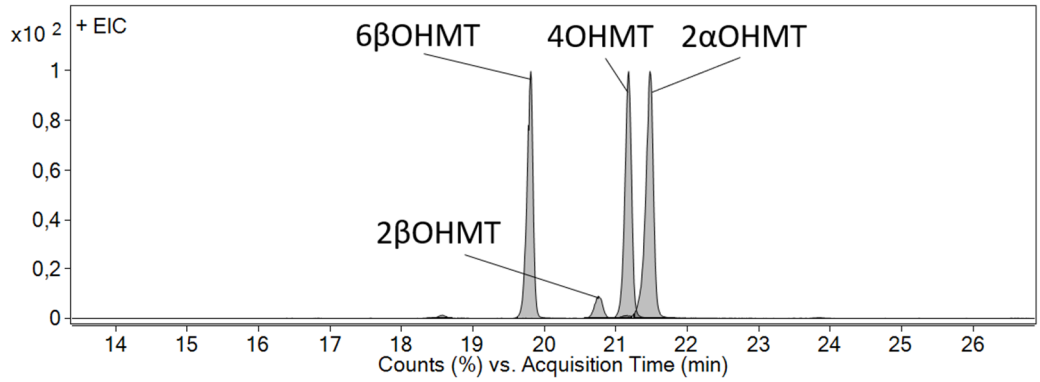

Figure 43: Overlay of EICs (m/z 534.4) from the per-TMS derivatives of 2αOHTM, 2βOHMT, 4OHMT, and 6βOHMT obtained for method h)

The disadvantages of GC-MS methods are the long run time and the time-consuming step of derivatization as described in 1.3. Furthermore, the artefactual building of 6-hydroxy metabolites in the derivatization process and the missing discrimination between 6α- and 6β-hydroxy isomers after derivatization to per-TMS derivatives are discussed and might influence the results in GC-MS analysis [47, 75].

Method h) was the only GC-MS method capable of separating the per-TMS derivatives of the four isomers. Due to the long runtime of the methods, poor separation, the additional sample preparation step (advantages and disadvantages explained in section 1.3), and the missing discrimination between 6α- and 6β-hydroxylated steroids, GC-MS methods were discarded for measuring the *in vitro* and *in vivo* studies.

Table 18: RTs of mono- and per-TMS derivatives of 2αOHMT, 2βOHMT, 4OHMT, and 6βOHMT for method f) and method g)

Substance	**Retention Time [min]**			
	Method f		**Method g**	
	mono-TMS	per-TMS	mono-TMS	per-TMS
2αOHMT	16.420	17.885	6.098	7.698
2βOHMT	15.250	17.885	5.664	6.934
4OHMT	14.979	17.885	5.533	7.651
6βOHMT	16.388	17.885	6.074	7.595

4.4.2 LC-MS methods

Three LC-MS methods were developed using two different starting points. The first method used an achiral reversed phase C18 column (Agilent ZORBAX Eclipse Plus RP C18 [1.8 µm, 2.1 x 100 mm], method b) shown in 3.2.1.2). The second and third method used a chiral phased column (Agilent Poroshell 120 Chrial-V [2.7 µm, 2.1 x 100 mm], method c) shown in 3.2.1.3).

Method b) used a single quadrupole MS as detector. As all hydroxy isomers have the same mass, differentiation of the isomers requires chromatographic separation. The method used a gradient from 5% to 95% ACN (solvent b) containing 0.1% formic acid in ten minutes (solvent a: water + 0.1% FoOH). It separated the 2ξOHMT isomers from 4OHMT but struggled in the separation of 2ξOHMT and 6OHMT (Figure 44). The RTs of the four isomers for this method are displayed in Table 19. As this method could not separate all hydroxy isomers, it was only used for synthesis control.

To achieve a better separation of all isomers, a LC-MS method was developed using a chiral phase column (Agilent Poroshell Chiral-V) and an ESI-QQQ-MS detector. The optimized method could separate the 2ξOHMT isomers and 4OHMT but failed in the base line separation of 6βOHMT and 2βOHMT (calculated resulting peak resolution 0.83). An example of the separation is shown in Figure 45.

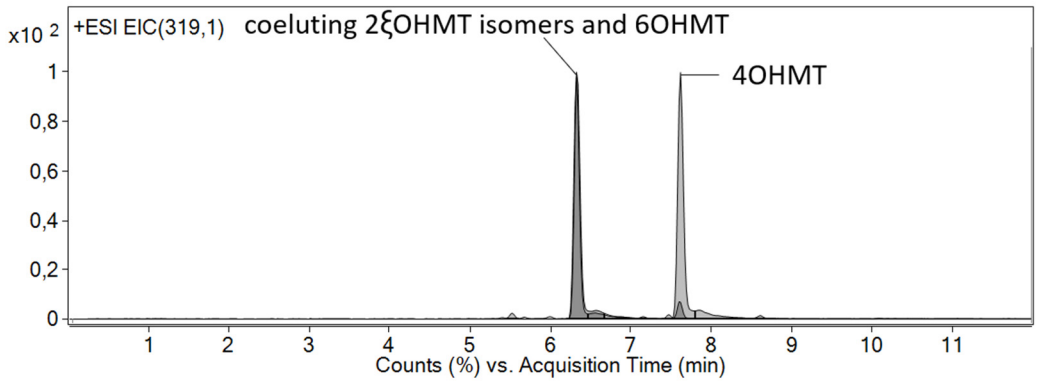

Figure 44: Overlay of EICs ([M+H]⁺ 319.1) of the reference substances using method b); showing the coeluting 6βOHMT (RT 7.775 min) and 2ξOHMT (RT 8.715 min), and 4OHMT (RT 10.193 min)

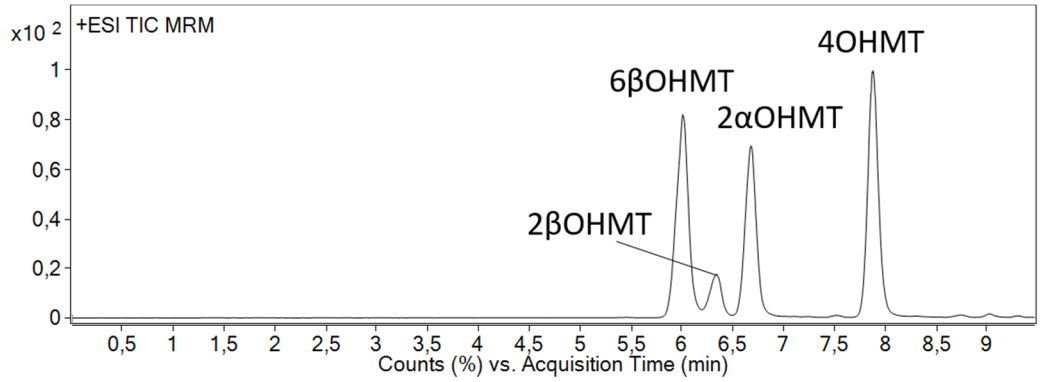

Figure 45: LC-ESI-QQQ-MS TIC chromatogram of the reference substances; 6βOHMT (RT 6.008 min), 2ξOHMT (RT 6.677 min [2αOHMT] and 6.333 min [2βOHMT]) and 4OHMT (RT 7.879 min)

The method used water (+0.1% FoOH) as solvent a, ACN (+0.1% FoOH) as solvent b, and the same gradient as method c) (3.2.1.3). Table 19 shows the RT for all substances of interest obtained with this method. Even though MS/MS in MRM mode was utilized, the method could not detect the low concentrations of the hydroxy metabolites found in the enzyme incubations, as the ionization of the molecules was too low. Figure 85 (annex) shows chromatograms of the sample HLM_1 in LC-ESI-QQQ-MS analysis compared to the results of the final SFC-ESI-QQQ method. The peak area was used to compare the sensitivity of the methods. The finally developed method (shown in 3.2.2.1 and discussed in 4.4.3) was more than ten times more sensitive than the LC method. Therefore, no further optimization of this LC-ESI-QQQ-MS method was performed.

Table 19: Retention times of the reference standards 2αOHMT, 2βOHMT, 4OHMT, and 6βOHMT for the three LC-MS methods (LC-ESI-MS/LC-ESI-QQQ-MS/LC-ESI-QTOF-MS)

Substance	**Retention Time [min]**		
	LC-ESI-MS method b)	LC-ESI-QQQ-MS	LC-ESI-QTOF-MS method c)
2αOHMT	6.324	6.667	8.715
2βOHMT	6.324	6.333	8.160
4OHMT	7.618	7.879	10.193
6βOHMT	6.324	6.008	7.775

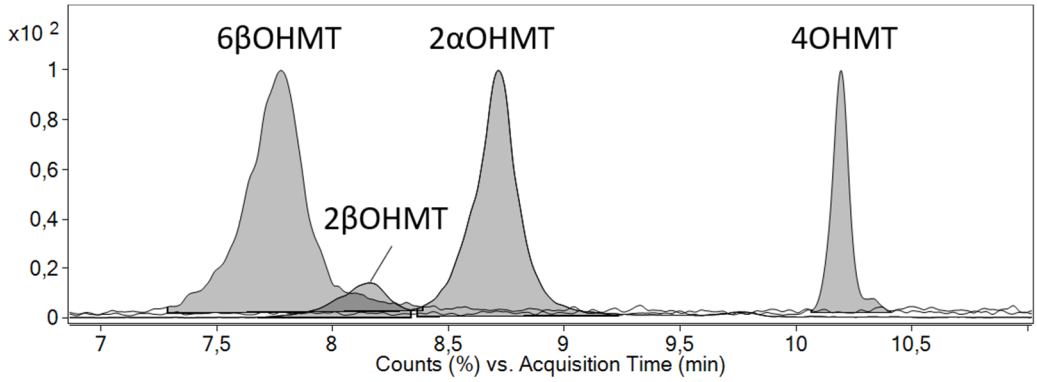

Figure 46: Overlay of EICs ([M+H]⁺ 319.2268) of the reference substances using method c); 6βOHMT (RT 7.775 min), 2ξOHMT(RT 8.715 min and 8.160 min) and 4OHMT (RT 10.193 min)

To increase the ionization for method c) (shown in 3.2.1.3) compared to the previously described LC-ESI-QQQ-MS method, 1 mM NH_4F was added to both solvents as an additive. To dissolve NH_4F in solvent b, 2.5% water was included in the solvent mixture. The method used the same gradient as the LC-ESI-QQQ-MS method and is depicted in section 3.2.1.3. Nevertheless, this method also struggled to separate 2βOHMT and 6βOHMT (Figure 46).

Instead of an ESI-QQQ-MS, the LC system was coupled to an ESI-QTOF-MS and therefore was used to obtain the accurate masses of underivatized reference material (2ξOHMT and 4OHMT). For this purpose, pure fractions of the synthesis products were used.

Most LC-MS methods have problems separating 6-hydroxy metabolites from 2-hydroxy metabolites. Nevertheless, only recently, Escobar-Wilches *et al.* managed to develop a UHPLC-MS method to separate, identify, and quantify seven hydroxylated T metabolites, including 6β- and 2β-hydroxytestosterone [52].

Nonetheless, as the GC-MS methods, also the LC-MS methods of this project struggled in the complete separation of the isomers and therefore were discarded for the measurements of the *in vivo* and *in vitro* studies.

4.4.3 SFC-MS methods

SFC, as an orthogonal technique to HPLC and GC-MS, together with MRM, was used to separate all metabolites of interest. Several chiral stationary phases were tested. Figure 47 compares three chiral stationary phases using a sample that contained both 2OHMT metabolites, as this was the critical resolution pair in SFC. Using a teicoplanin-based column (Agilent Poroshell Chiral-T; 2.7 µm, 4.6 x 100 mm), the two 2-hydroxy isomers of MT were not separated. However, the ChiralPak IB-U column (Chiral Technologies Europe; 1.6 µm, 3.0 x 100 mm) separated the isomers but showed a bad peak shape for both isomers. Agilent's Poroshell Chiral-V (vancomycin-based; 2.7 µm, 4.6 x 100 mm) gave a satisfactory resolution between 2αOHMT and 2βOHMT. Gradient optimization was performed to increase the critical resolution (calculated resulting peak resolution for 2αOHMT/2βOHMT in the final method was 1.24) and optimize the run time.

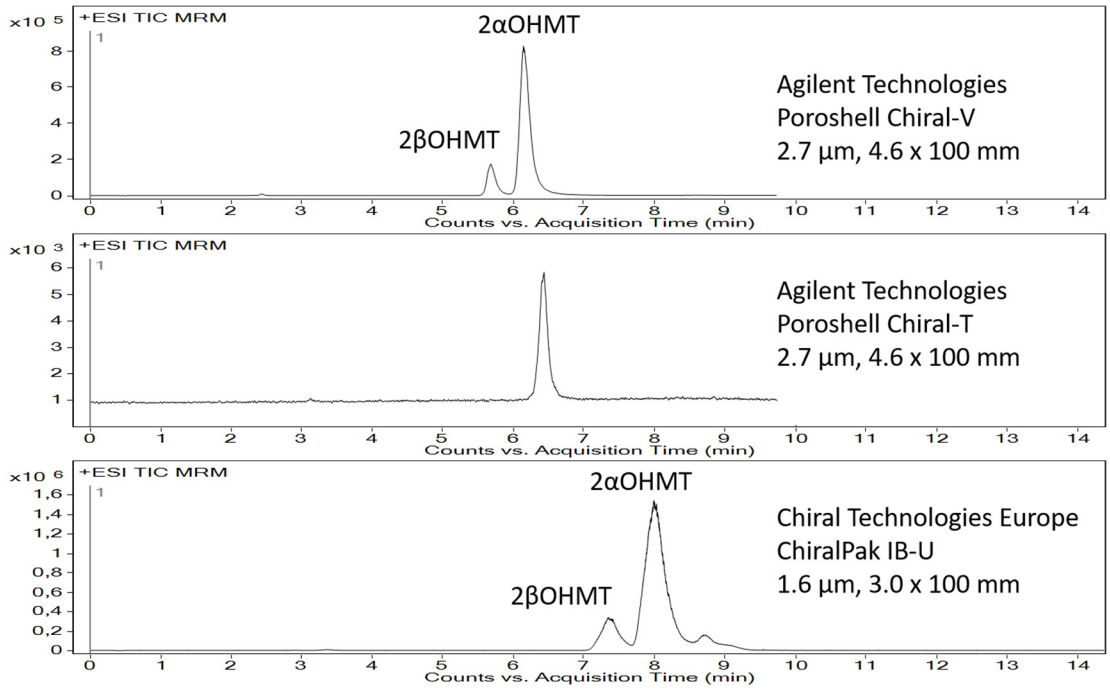

Figure 47: Comparison of the three chiral phased columns (Agilent Poroshell Chiral-V, Agilent Poroshell Chiral-T, and Chiral Chrialpak IB-U); ESI TIC MRM chromatograms of a sample containing 2αOHMT and 2βOHMT in a ~5:1 ratio

The makeup solvent composition was changed from pure methanol containing 0.1% formic acid to a mixture of methanol and water (97.5/2.5; v/v; 1 mM NH_4F, 0.1% FoOH) following the composition described by Parr *et al.* [76]. The new makeup solvent increased the sensitivity by a factor of ~two compared to the first makeup solvent mixture.

The ion source parameters were optimized with Agilent's source optimizer software V10.0 to maximize the sensitivity. For this purpose, the capillary and nozzle voltage, the sheeth and drying gas temperature and flow, and the nebulizer pressure were modified and compared with the settings of the first method (displayed as 100% in Figure 50). The results of this optimization are displayed in Figure 50. Section 3.2.2.1 shows the final SFC-ESI-QQQ-MS method parameters used to analyze the *in vitro* and *in vivo* studies.

Additional experiments with an atmospheric pressure chemical ionization (APCI) source were performed. The intention was to test if APCI yields a better ionization of the steroids. Different makeup solvents containing 10-100 mM NH_4F were used for method optimization. However, the APCI source showed no advantages, rather disadvantages over the ESI source. Figure 49 shows APCI and ESI results for a sample of 2ξOHMT (concentration 1 µg/mL). The sensitivity obtained from ESI was roughly 100 times higher than with APCI. The results were similar to the results described by Parr *et al.* for other steroids [76].

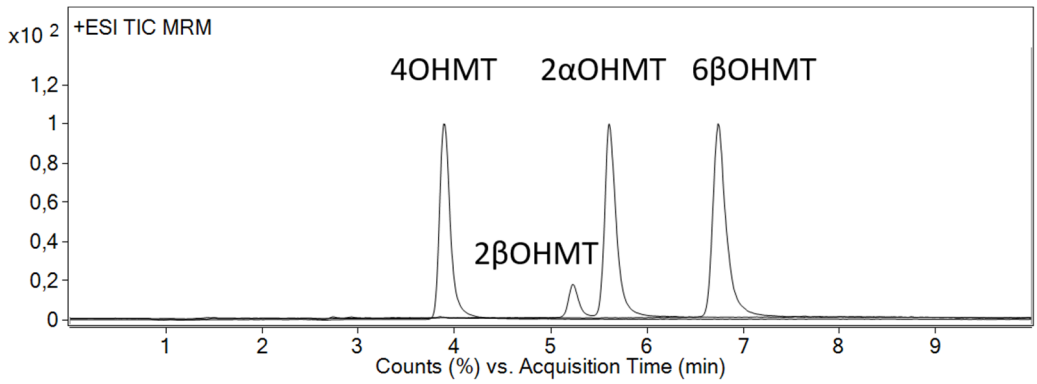

Figure 48: Overlay of the normalized MRM chromatograms of reference materials; 4OHMT (RT 3.842 min) 2ξOHMT (RT 5.188 min [2βOHMT] and 5.565 min [2αOHMT]), and 6βOHMT (RT 6.774 min)

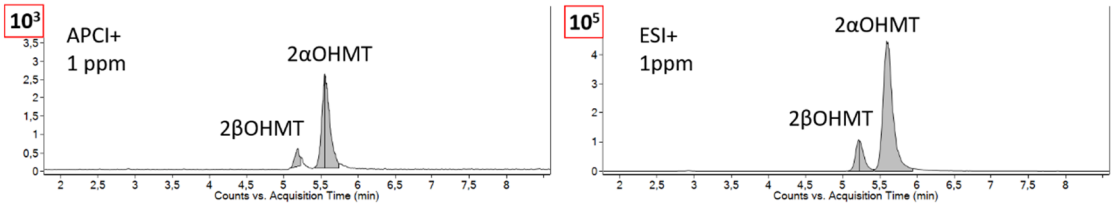

Figure 49: Comparison of APCI and ESI in positive mode, showing a ~100 (10^3 vs. 10^5; red boxes) times higher sensitivity for ESI; sample contained 1 ppm 2ξOHMT in a 1:5 ratio

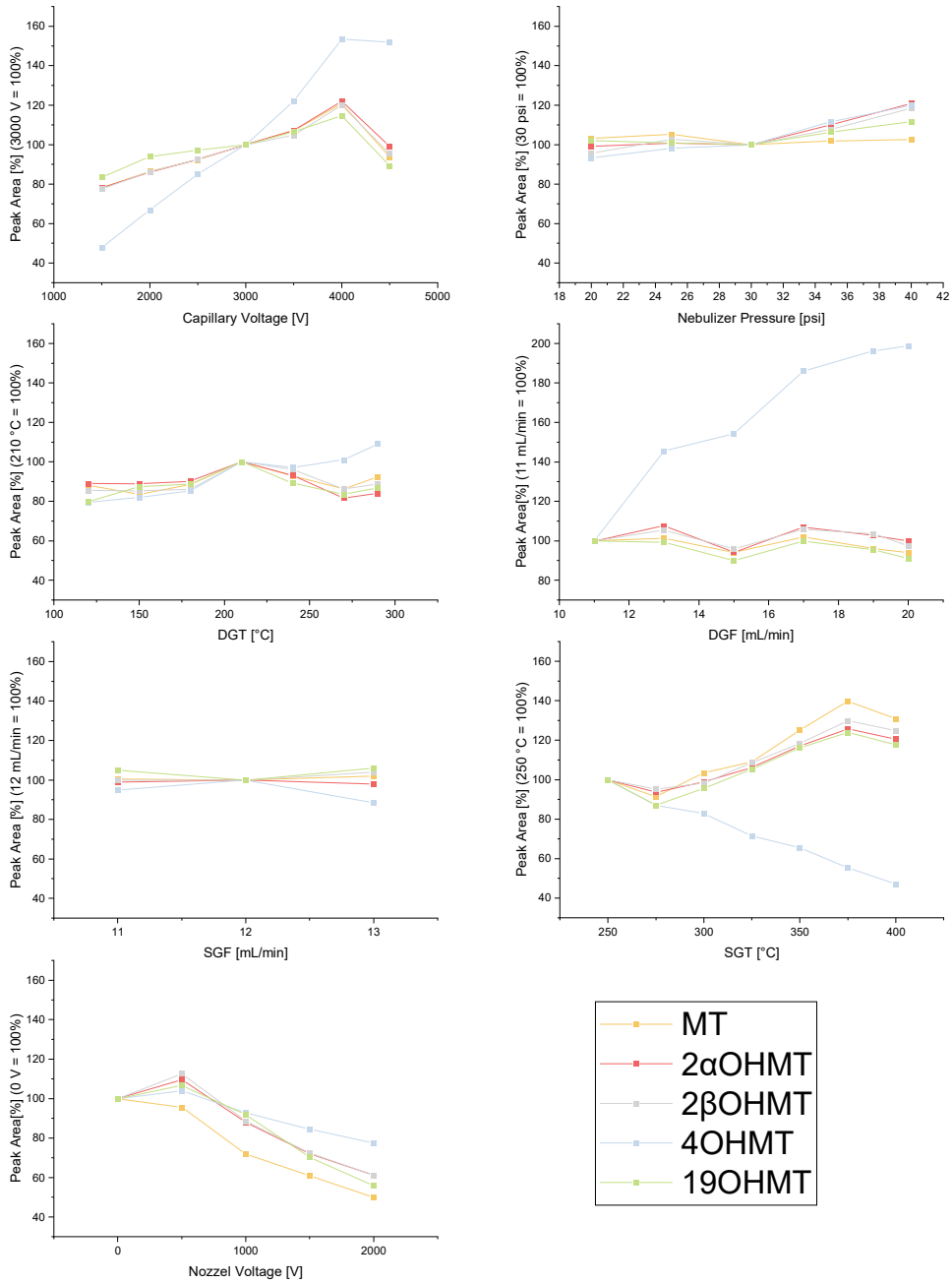

Figure 50: Plotted results of the source optimization for method e). The peak area related to the starting point before the optimization [%] is plotted against the tested values for the capillary voltage, nebulizer pressure, drying gas flow (DGF), drying gas temperature (DGT), sheath gas flow (SGF), sheath gas temperature (SGT), and nozzle voltage

4.5 *In vitro* Hydroxylation of MT

In vitro studies with pooled human liver microsomes (HLM) or different isolated CYP enzymes (CYP19A1, CYP2C19, CYP1A2, and CYP1B1) were performed to investigate the formation of the hydroxy metabolites of MT. Therefore, enzyme incubations were performed as described in 3.2.6. Test incubations with different substrate concentrations (100 µg/mL, 50 µg/mL, and 10 µg/mL) were performed to exclude potential enzyme saturation. In most cases, the formation of hydroxylated metabolites was very low. The final substrate concentration used for *in vitro* studies was 100 µg/mL; possible enzyme saturation was only detectable for HLM and CYP19A1 (HLM_1 [substrate concentration 10 µg/mL] and CYP19A1_1 [substrate concentration 10 µg/mL]).

The enzyme incubation results are presented in the following sections 4.5.1-4.5.3 and compared to literature data of structurally related AAS. Those studies aimed to investigate the impact of hydroxy metabolites in the metabolization of MT [method d)]. The primary metabolites of MT in humans, 5βTHMT, and 5αTHMT, are poorly detectable in electrospray ionization [45, 77] and will not be considered in these studies. AED incubations were performed as positive control to show similarities and differences. Formestane (4-hydroxyandrost-4-ene-3,17-dione) was not available as standard when the studies were performed. Therefore, 2α-hydroxyandrost-4-ene-3,17-dione, 2β-hydroxyandrost-4-ene-3,17-dione, 6β-hydroxyandrost-4-ene-3,17-dione, and 19-hydroxyandrost-4-ene-3,17-dione were monitored besides AED as substrate in the control experiments [method e)].

4.5.1 Biotransformation of MT with HLM

HLM are commonly used for studies of AAS metabolism [19, 21, 22, 30]. The cytochrome P450 isoform 3A4 (CYP3A4) is the most abundant enzyme in human liver metabolism [20, 32]. Wang *et al.* separated and characterized six different CYP450 isozymes from HLM in 1983 [78]. The HLM used for this study specifies ten different CYP450 isoforms.

Because of the wide variety of enzymes, HLM studies can give a good overview of possible metabolites that may be expected in humans. The MRM chromatograms of MT, 2αOHMT, 2βOHMT 4OHMT, 6βOHMT, and 19OHMT after 24-hour incubation of MT are displayed in Figure 87 (sample HLM_1; sample HLM_2 Figure 88; annex). Biotransformation with HLM resulted in the formation of all five hydroxy metabolites in both samples. In comparison, the negative control sample (Figure 98) showed low amount of three autoxidation products (2αOHMT, 2βOHMT, and 6βOHMT) besides the substrate. The relative peak area (peak area of the substance in correlation to the complete peak area of all detected substances [MT, 2αOHMT, 2βOHMT 4OHMT, 6βOHMT, and 19OHMT]) after correction with the internal standard (MD) was used to compare the results. Table 20 represents the comparison of the two HLM incubations to the negative control. It shows the corrected areas (absolute and relative [%]) of the substrate and its five hydroxy metabolites. The relative results are also illustrated in Figure 51. All five hydroxy metabolites of MT were formed in a higher amount compared to the negative control.

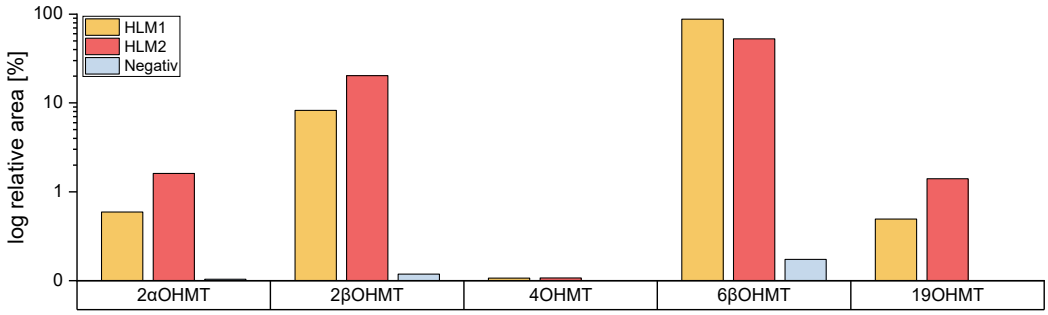

Figure 51: Plotted results of 2αOHMT, 2βOHMT, 4OHMT, 6βOHMT, and 19OHMT of the two HLM incubation studies compared to the negative control sample

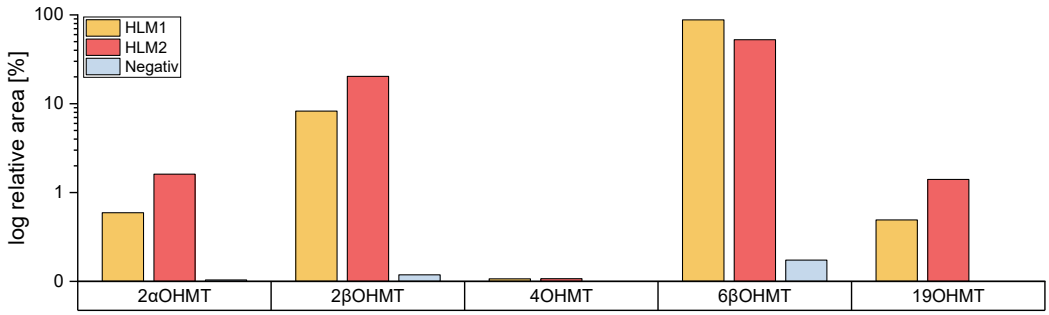

Figure 52: Comparison of the relative area of hydroxylated metabolites after HLM incubation of MT and AED, showing predominant hydroxylation in position 2β and 6β in both substrates

In the sample HLM_1, the substrate concentration was lowered to 10 µg/mL. Thus, the absolute areas were lower than in HLM_2 (100 µg/mL substrate), but relative areas were closer to previous literature results. 6βOHMT (RT 6.75 min) represents the main metabolite. After 24 hours of incubation, 6βOHMT showed a relative area of 87% (57% in HLM_2). The formation of 2βOHMT after 24 hours was 8.28% (relative area, HLM_2 20.29%). 2αOHMT and 19OHMT was found in both incubations but only in minor amounts (2αOHMT 0.77% [HLM_1]/1.61% [HLM_2], 19OHMT 0.69% [HLM_1]/1.40% [HLM_2]) and 4OHMT was only detected with 0.03% (relative area) in both incubations. Incubation with AED showed similar results (Figure 52). Therefore, the impact of HLM on the formation of 4OHMT might be negligible.

The formation rate of 6βOHMT matches the rates of 6β-hydroxytestosterone formation after testosterone incubation reported in literature [19, 21, 22]. CYP3A4 is associated as the central enzyme in the oxidation process in position six [19, 23, 26, 52]. Rendic *et al.* suggested that the 3-oxo-4-ene-electron effects contribute to the 6β-hydroxy formation [26]. Nevertheless, oxidation in 2β position is also described in literature as one major pathway in HLM studies [21, 22]. The results of Waxmann *et al.* [21] (~10% formation of 2β-hydroxy-testosterone) are similar to the results of HLM_1 (8.28% 2βOHMT). HLM_2 showed a lower 6βOHMT/2βOHMT ratio than HLM_1 (~2.5 compared to ~10). The HLM *in vitro* studies with MT and AED showed similar results and matched previous work results with different AAS [19-22].

6βOHMT and 2βOHMT were identified as major metabolites of MT's hydroxylation reaction in HLM incubations. Escobar-Wilches *et al.* reported similar results for the excretion of hydroxylated T metabolites in human urine [52].

*Table 20: Comparison of the absolute and relative (%) peak area of MT, 2αOHMT, 2βOHMT, 4OHMT, 6βOHMT and 19OHMT after HLM incubation (HLM_1, and HLM_2) and the negative control sample; * sample HLM_1 had a substrate concentration of only 10 µg/mL*

	HLM_1* [Area]	[%]	HLM_2 [Area]	[%]	negativ control [Area]	[%]
MT	971661	2.42	10454008	24.08	61367672	99.67
2αOHMT	309458	0.77	698489	1.61	10156	0.02
2βOHMT	3319583	8.28	8806061	20.29	45281	0.07
4OHMT	10810	0.03	13024	0.03	-	-
6βOHMT	35217895	87.81	22825049	52.59	147678	0.24
19OHMT	277373	0.69	608652	1.40	-	-

4.5.2 Biotransformation of MT with CYP2C19

The intention of the *in vitro* studies with CYP2C19 was to evaluate if MT behaves similarly to testosterone in the formation of 6β- and 2β hydroxy metabolites [19].

The biotransformation of MT with CYP2C19 resulted in the formation of three different hydroxylated metabolites. As expected, the MRM chromatograms after 24 hours of incubation showed the formation of 2αOHMT, 2βOHMT, and 6βOHMT (Figure 90, Figure 91, and Figure 92; annex). 6βOHMT was predicted to be the major hydroxy metabolite after CYP2C19 incubation, based on the literature results [19]. Interestingly 2βOHMT instead of the expected 6βOHMT was formed as the major metabolite. About 5% of MT was hydroxylated in position 2β, where only ~1% in position 6β. 2αOHMT was formed in only minor amounts (~0.1%). Table 21 and Figure 53 illustrate the results of the three incubations, which all showed similar outcomes. The results differ from the control samples, where AED was incubated with CYP2C19. In these samples, only 2βOHAED and 6βOHAED were detected besides the substrate, and the concentrations of these metabolites were similar to the amount formed in the negative control sample of AED. Therefore, no enzymatic hydroxylation reaction with CYP2C19 was observed for AED. Figure 54 depicts the results of MT and AED incubation for comparison. The 2β-hydroxy and 6β-hydroxy metabolite formation was significantly higher for MT than AED (p=0.05).

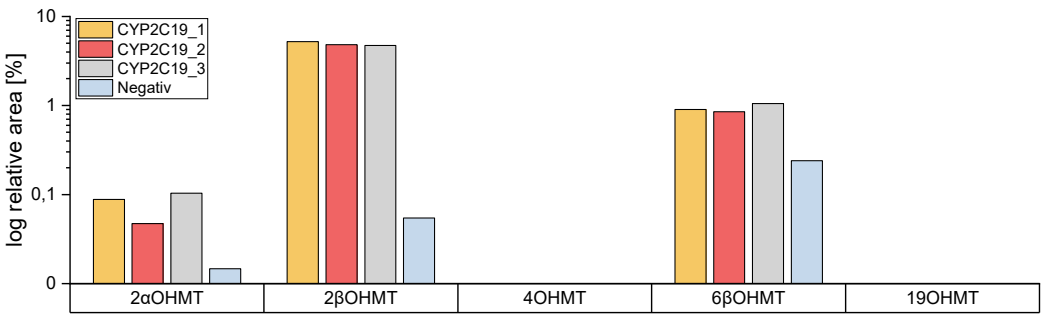

Figure 53: Plotted results of 2αOHMT, 2βOHMT, 4OHMT, 6βOHMT, and 19OHMT of the three CYP2C19 incubation studies of MT compared to the negative control sample

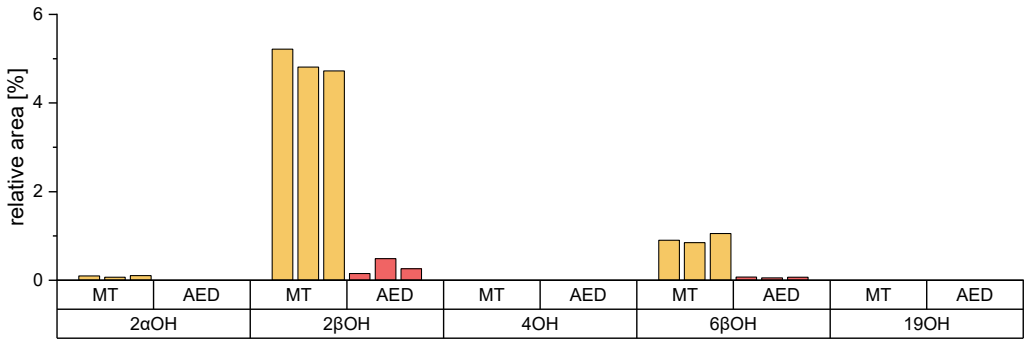

Figure 54: Comparison of the relative area of hydroxylated metabolites of MT and AED, showing MT hydroxylation in position 2β and 6β

The results might indicate that C17 hast to be sp^3 hybridized to be hydroxylated in position 2β. Yamazaki *et al.* published that CYP2C19 plays an essential role in the oxidation of steroids. AED formation after T incubation and hydroxylation reactions of T and progesterone in position 2β and 6β after incubation with CYP2C19 were described [19].

Incubations of T with human liver microsomes showed comparable results to CYP2C19 incubations [19]. The results of these studies differ from incubations of MT reported by Yamazaki *et al.*, where the formation of 6β-hydroxytestosterone is ten times higher than 2β-hydroxytestosterone [19]. Further comparison with CYP3A4 as the predominant enzyme for hydroxylation reactions in steroid metabolism may give a more in-depth insight into the role of CYP2C19 in the metabolization process of MT. Based on the presented results, CYP2C19 may be the predominant enzyme to form 2βOHMT.

Table 21: Comparison of the relative and absolute (%) peak area of MT, 2αOHMT, 2βOHMT, 4OHMT, 6βOHMT, and 19OHMT after HLM incubation (CYP2C19_1, CYP2C19_2, and CYP2C19_3) to the negative control sample

	CYP2C19_1 [Area] [%]	CYP2C19_2 [Area] [%]	CYP2C19_3 [Area] [%]	negativ control [Area] [%]
MT	56119175 93.79	35052797 94.27	41111191 94.12	61367672 99.67
2αOHMT	56631 0.09	25059 0.07	45282 0.10	10156 0.02
2βOHMT	3122766 5.22	1789081 4.81	2064023 4.73	45281 0.07
4OHMT	- -	- -	- -	- -
6βOHMT	539282 0.90	316486 0.85	460641 1.05	147678 0.24
19OHMT	- -	- -	- -	- -

4.5.3 Biotransformation of MT with CYP1A2 and CYP1B1

Because the results of the *in vitro* study of CYP1A2 and CYP1B1 incubations were nearly similar, they are displayed and discussed together. These two enzyme studies aimed to investigate if MT shows the same or comparable metabolization pattern as reported for estrogens [30]. The hypothesis was that CYP1A2 incubations lead to the formation of 2βOHMT and 4OHMT with preference for 2βOHMT and CYP1B1 incubations vice versa.

Biotransformation with CYP1A2 resulted in three hydroxylated metabolites of MT. The results of all three incubations (MRM chromatograms Figure 93 [CYP1A2_1], Figure 94 [CYP1A2_2], and Figure 95 [CYP1A2_3]) showed similar results. Over 99% of MT was not metabolized to hydroxylated compounds. 6βOHMT was found as the main metabolite with an average of 0.7% (relative area). The two 2-hydroxy isomers were found in small amounts (2αOHMT 0.02%, 2βOHMT ~0.1%), comparable to the amount found in the negative control sample. The amount of 6βOHMT was increased by a factor of ~ three during incubation with CYP1A2 compared to incubations without enzyme. Therefore, only 6βOHMT formation could be assigned to the biotransformation of MT

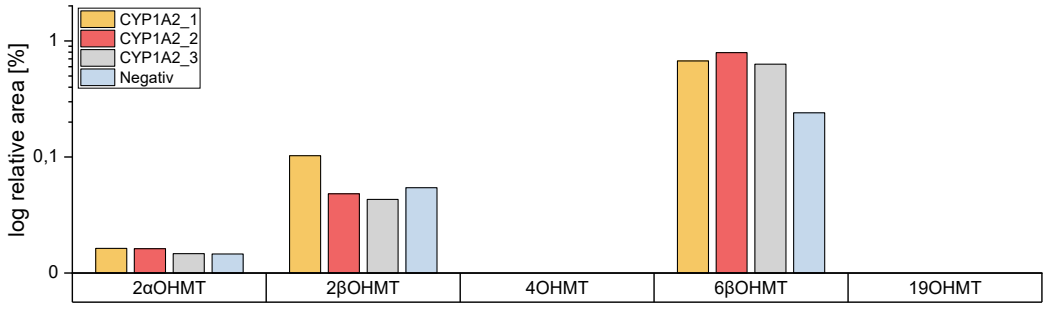

Figure 55: Plotted results of 2αOHMT, 2βOHMT, 4OHMT, 6βOHMT, and 19OHMT of the three CYP1A2 incubation studies compared to the negative control sample

with CYP1A2. The absolute and relative areas of MT and its metabolites are shown in Table 22 and plotted in Figure 55. To exclude enzyme saturation, incubations with lower substrate concentrations (50 µg/mL and 10 µg/mL) were performed but could barely be analyzed because the concentrations of the metabolites were too low to be detected. The results show that CYP1A2 influences the metabolization of MT to 6βOHMT but shows no remarkable influence on forming the 2-hydroxy isomers. As only a small amount of the parent compound was metabolized in these enzyme incubations, the impact of CYP1A2 on the metabolism of MT to hydroxylated metabolites can be seen as negligible.

Incubations with CYP1B1 showed similar results to the incubation of MT with CYP1A2. As illustrated in Figure 56 and shown in Table 23, the metabolization rate of MT was meager (over 99% MT was not metabolized to hydroxylated metabolites). Only 6βOHMT with an average of 0.7% for the two incubations was built in a higher amount than in the negative sample. The formation of both 2-hydroxy isomers (2αOHMT 0.02%, 2βOHMT ~0.1%) was comparable to the amount formed in the negative control sample.

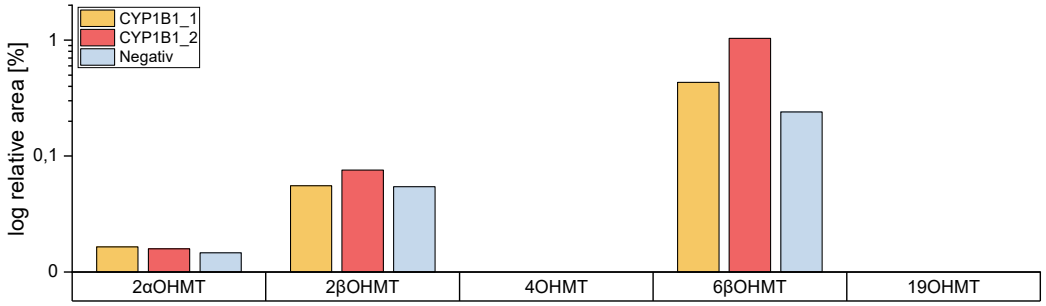

Figure 56: Plotted results of 2αOHMT, 2βOHMT, 4OHMT, 6βOHMT, and 19OHMT of the two CYP1B1 incubation studies compared to the negative control sample

Figure 96 shows the MRM chromatograms of the sample CYP1B1_1 and the absence of 4OHMT and 19OHMT (sample CYP1B1_2 Figure 97; annex). As for CYP1A2, the impact of CYP1B1 on the metabolism of MT can be seen as negligible.

As discussed before, literature already describes 6β-hydroxy metabolites as autoxidation products [47]. The *in vitro* studies of MT suggest that the formation of small amounts of 2α- and 2β-hydroxy metabolites also show a correlation to autoxidation. Therefore, incubations with AED (positive control) were used to verify this prediction.

CYP1A2 and CYP1B1 incubations of AED showed comparable results to the MT incubations. 6βOHAED and 2βOHAED were formed in the enzyme incubations and also the negative control sample. Therefore, these results might indicate minor amounts of 2βOHMT (~1.5 ng/mL) as an autoxidation product of MT.

Cheng *et al.* and Lee *et al.* published that both enzymes play an essential role in A-ring oxidation of estrogens [30, 79]. CYP1A2 was reported to build mainly the 2-hydroxy metabolites, where CYP1B1 had a higher impact on the catechol building in position 4 (4-hydroxyestrogens). The hypothesis that MT behaves like estrogens in CYP1A2 and CYP1B1 incubations was not verified.

Table 22: Comparison of the relative and absolute (%) peak area of MT, 2αOHMT, 2βOHMT, 4OHMT, 6βOHMT and 19OHMT after HLM incubation (CYP1A2_1, CYP1A2_2, and CYP1A2_3) to the negative control sample

	CYP1A2_1 [Area] [%]	CYP1A2_2 [Area] [%]	CYP1A2_3 [Area] [%]	negativ control [Area] [%]
MT	43841755 99.20	60239644 99.12	56967588 99.29	61367672 99.67
2αOHMT	9424 0.02	12738 0.02	9547 0.02	10156 0.02
2βOHMT	45297 0.10	41518 0.07	36459 0.06	45281 0.07
4OHMT	- -	- -	- -	- -
6βOHMT	297023 0.67	481588 0.79	361300 0.63	147678 0.24
19OHMT	- -	- -	- -	- -

Table 23: Comparison of the relative and absolute (%) peak area of MT, 2αOHMT, 2βOHMT, 4OHMT, 6βOHMT, and 19OHMT after HLM incubation (CYP1B1_1 and CYP1B1_2) to the negative control sample

	CYP1B1_1 [Area] [%]	CYP1B1_2 [Area] [%]	negativ control [Area] [%]
MT	50992595 99.47	60570508 98.86	61367672 99.67
2αOHMT	11095 0.02	12253 0.02	10156 0.02
2βOHMT	38098 0.07	53907 0.09	45281 0.07
4OHMT	- -	- -	- -
6βOHMT	221481 0.43	634784 1.04	147678 0.24
19OHMT	- -	- -	- -

4.5.4 Biotransformation of MT with CYP19A1

The *in vitro* study with CYP19A1 aimed to investigate the formation of 2βOHMT and 19OHMT in the aromatization process of MT to 17α-methyltestosterone. Both substances may be hypothesized as intermediate products in the formation of 2β,19-dihydroxy-17α-methyltestosterone. Monitoring of 17α-methyltestosterone as product of the aromatization of MT was not included in this project but will be a part of the following projects. Like the HLM incubations, the first sample (CYP19A1_1) was incubated with a lower substrate concentration of only 10 µg/mL. The MRM chromatograms of the sample CYP19A1_1 are shown in Figure 98. The incubation led to the formation of four hydroxylated compounds. As hypothesized, 2βOHMT (10%) and 19OHMT (29%) were found as main hydroxylated metabolites. Besides these two metabolites, also 6βOHMT was found in a relatively high amount (5%). As seen in the other incubation studies, 2αOHMT was formed, but only in a minor amount (0.4%).

Instead of 10 µg/mL in CYP19A1_1, for the samples CYP19A1_2 and CYP19A1_3, a substrate concentration of 100 µg/mL was used (similar to the negative control sample). For these two incubations, 2βOHMT (1.3%) and 19OHMT (8.3%) represented the main hydroxylated products but in lower relative amounts than the sample CYP19A1_1. Similar to the sample CYP19A1_1, also 6βOHMT (1%) and 2αOHMT (0.05%) were found. The corrected absolute areas of the 2-hydroxy isomers were equal in all three replicates of incubations.

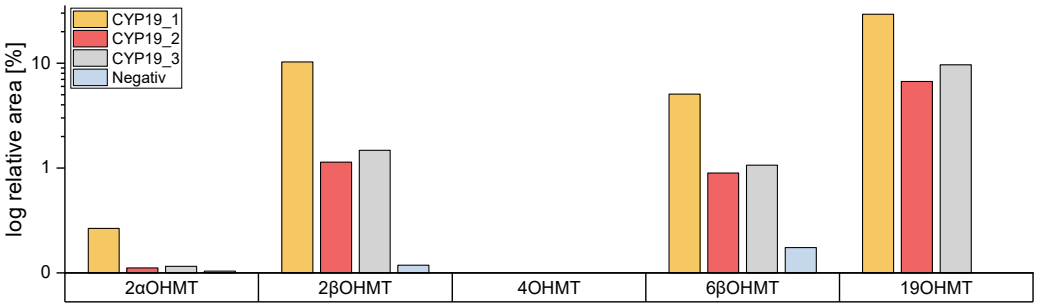

Figure 57: Plotted results of 2αOHMT, 2βOHMT, 4OHMT, 6βOHMT, and 19OHMT of the three aromatase incubation studies compared to the negative control sample

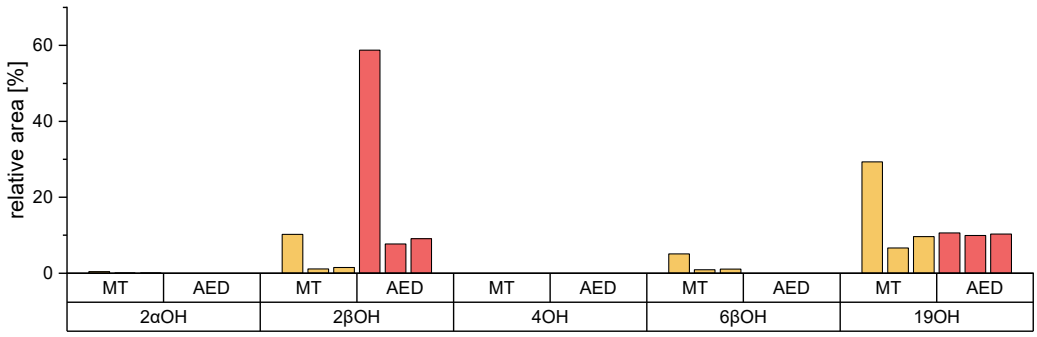

Figure 58: Comparison of the relative area of hydroxylated metabolites of MT and AED, showing hydroxylation in position 2β and 19 for both substrates

These results for 2ξOHMT may indicate a saturation of the enzyme. However, the absolute areas of 6βOHMT and 19OHMT in the samples with 100 µg/mL substrate concentration (CYP19A1_2 [Figure 99] and CYP19A1_3 [Figure 100]) showed an increase compared to sample with lower substrate concentration (10 µg/mL, sample CYP19A1_1). The overall metabolization rate for the study with 10 µg/mL substrate concentration was about 50% (CYP19A1_1) and 10% for the incubations with higher substrate concentrations (CYP19A1_2 and CYP19A1_3). The corresponding peak areas are illustrated in Figure 57 and displayed in Table 24.

The A-ring aromatization process is already discussed in the literature but not completely clarified [31, 34, 80]. Several mechanisms of the last step in the aromatization are discussed. One prediction is hydroxylation at C2 and C19 (2β,19-hydroxy-17α-methyltestosterone; as discussed in 1.2.1), leading to the loss of water and formic acid [31, 34]. The main metabolite of the considered substances in all three incubations with aromatase was 19OHMT, with 29% / 8.3% (relative area). As described for other endogenous steroids, the hydroxylation in position 19 showed the major pathway in aromatization that leads to 17α-methylestradiol. Therefore, the finding of 19OHMT was expected as one of the main metabolites because it represents the first step of the aromatization. The formation of 2βOHMT was much lower (10%, respectively ~1,3%) than 19OHMT.

Nevertheless, the formation of 2βOHMT as one of the intermediate products in the aromatization of MT was verified with these results. The results of AED incubation with CYP19A1 strengthen this statement. Figure 58 shows the results of both incubation studies (MT and AED as positive control). The oxidation of C2 in the aromatization process for MT and AED preferred the 2β position. For future work, 2β,19-dihydroxy-17α-methyltestosterone has to be synthesized, and time-depending incubations with CYP19A1 will be performed to get a better overview of the last step in the aromatization of androgens and confirmation of the postulated mechanism. Also, incubations of 2βOHMT and 19OHMT as substrate with aromatase will give a better understanding of the aromatization process in the metabolism of MT.

*Table 24: Comparison of the relative and absolute (%) peak area of MT, 2αOHMT, 2βOHMT, 4OHMT, 6βOHMT, and 19OHMT after HLM incubation (CYP19A1_1, CYP19A1_2, and CYP19A1_3) to the negative control sample; * sample CYP19A1_1 had a substrate concentration of only 10 µg/mL*

	CYP19A1_1 * [Area] [%]	CYP19A1_2 [Area] [%]	CYP19A1_3 [Area] [%]	negativ control [Area] [%]
MT	222788 54.95	34494137 91.19	26366207 87.77	61367672 99.67
2αOHMT	17185 0.42	17808 0.05	18962 0.06	10156 0.02
2βOHMT	415356 10.24	429395 1.14	442550 1.47	45281 0.07
4OHMT	- -	- -	- -	- -
6βOHMT	205717 5.07	359972 0.95	319863 1.06	147678 0.24
19OHMT	1188101 29.31	2526343 6.68	2893369 9.93	- -

4.5.5 Conclusion of the Biotransformation Studies of MT

The *in vitro* studies with MT showed different outcomes. The only hydroxylated compound found in all incubations was 6βOHMT, which is consistent with literature data [19, 22, 23, 26, 32]. 2βOHMT was found as the major metabolite of CYP2C19 incubations. It was also found in the incubations with HLM, CYP19A1, and in small amounts in CYP1A2 and CYP1B1 (comparable to the negative sample concentrations).

The finding of 2βOHMT in the CYP19A1 incubations showed its influence in the aromatization process of androgens. 2αOHMT was found in every incubation but only in small amounts. 4OHMT was only detected in the HLM incubations. Several aspects may explain these findings. First, the extraction of 4-hydroxy-3-oxo-4-ene steroids is highly influenced by the pH [68]. Therefore, 4OHMT may not be extracted correctly. Second, the ionization efficiency of 4OHMT is not as good as 2ξOHMT (about 1:5). Furthermore, the formation of 4OHMT in the metabolism of MT might be so low that its influence is negligible.

The results of CYP1A2 and CYP1B1 incubations (only 6βOHMT in minimal amount) indicate that the role of these enzymes in the metabolism of MT is negligible.

As expected, 19OHMT was found after incubations with aromatase, as the hydroxylation of C19 is well described in the aromatization process of androgens [34].

The negative control sample showed 2βOHMT and 6βOHMT as autoxidation products. These results were confirmed by *in vivo* studies with AED yielding similar results.

Table 25 illustrates the overview of the biotransformation studies of MT.

Table 25: Overview of the results of the in vivo studies of MT; ✓showing the finding of the metabolite in the specific incubation; (✓) showing the finding in a small amount, comparable to the negative control sample

	2αOHMT	2βOHMT	4OHMT	6βOHMT	19OHMT
HLM	✓	✓	✓	✓	✓
CYP2C19	✓	✓		✓	
CYP1A2	(✓)	(✓)		✓	
CYP1B1	(✓)	(✓)		✓	
CYp19A1	✓	✓		✓	✓
Negative	✓	✓		✓	

4.6 *In vivo* Hydroxylation of MT

An *in vivo* study was performed to investigate the human metabolism of MT. Urine samples were obtained before and 130 hours after administering 10 mg MT as a tablet (Metadren®) to a healthy volunteer (male, 50 years, 80 kg). The recommendations described in the Helsinki Declaration were fulfilled for this study [81]. Preparation of the samples followed the protocol described in 3.2.7. β-Glucuronidase was used to cleave the glucuronidated phase-II-metabolites. Testosterone-*d3*-glucuronide was added as an internal standard to confirm the enzyme activity of the β-glucuronidase in each sample. The resulting liberated testosterone-d3 has a RT of 4.5 min (example peak in the MRM chromatogram of 2βOHMT in Figure 59) and is dominant in all samples. The enzyme activity was monitored only in qualitative way and not in quantitative way.

The focus was set to the formation of 2βOHMT, 4OHMT, and 6βOHMT, as no signal for the transition for 19OHMT at the corresponding RT was detected, and the qualifier transitions did not identify 2αOHMT in the urine samples. Figure 59 depicts the MRM chromatograms of the blank urine (MT00). MT was identified in a minimal amount, which might correlate to carry over problems of the method itself. Nevertheless, as the amount was nearly not detectable, it was assumed that there was no influence on the other samples. The blank urine showed the absence of hydroxylated metabolites (2βOHMT, 4OHMT, 6βOHMT). However, the transition m/z 319→183 of 4OHMT showed a peak (also in all other samples) with a small RT shift towards a shorter RT (RT 3.72 min). 6βOHMT (RT 6.75 min) showed similar problems as 4OHMT. The transition of m/z 319→283 showed an artifact peak in the blank (also in all other samples) with a small retention time shift towards a smaller RT (6.58 min).

The results of the sample 5.5 hours after administration (MT02) are shown in Figure 60. This sample was used as an example because it contains the parent compound and all three hydroxy metabolites. The most abundant metabolite found in this sample was 2βOHMT. 4OHMT was also detected in the sample. However, the transition problem of 4OHMT, described for the blank urine, challanges its identification. The quantifier

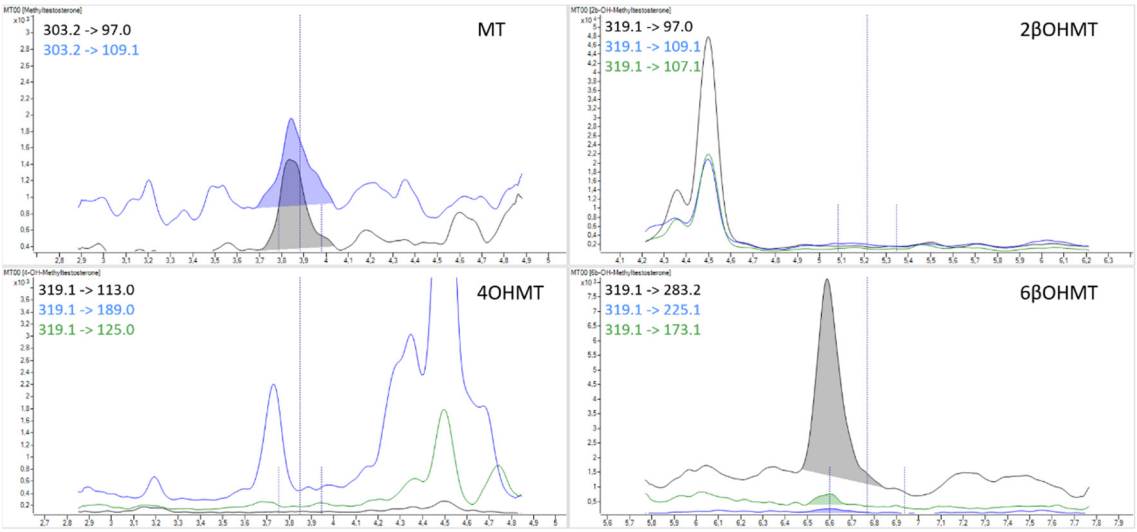

Figure 59: MRM chromatograms of the blank sample MT00 showing MRM of MT, 2βOHMT, 4OHMT, and 6βOHMT

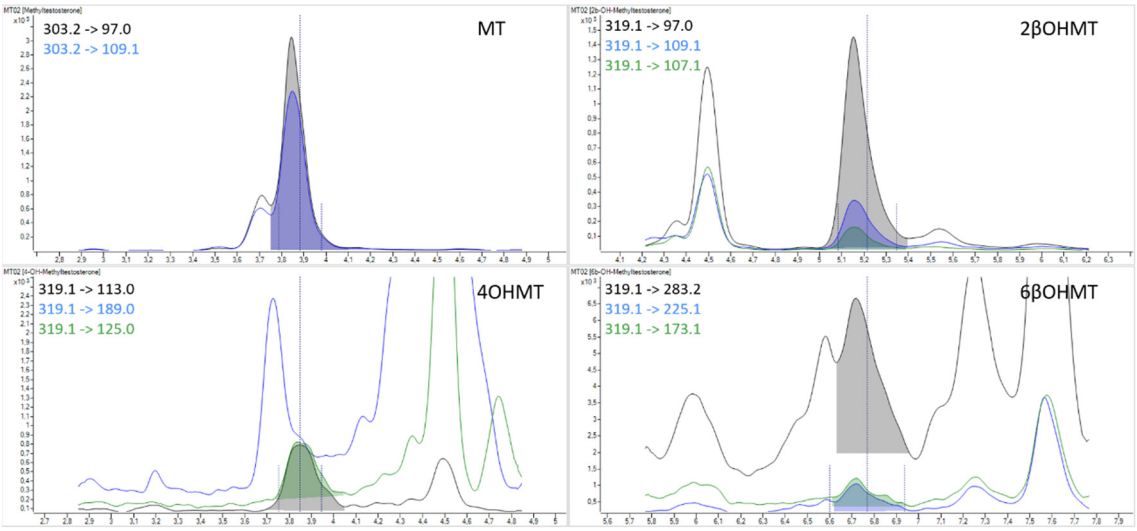

Figure 60: MRM chromatograms of the sample MT02 (5.5 hours after administration) showing MRM of MT, 2βOHMT, 4OHMT, and 6βOHMT

(m/z 319→113) and one of the qualifiers (m/z 319→125) are detectable. A shoulder building at the artifact peak from the qualifier transition m/z 319→183 was visible. Therefore, the exact integration of this shoulder was not possible. This problem was found in all samples where a quantifier peak (m/z 319 → 183) for 4OHMT was detected. Therefore, only the qualifier m/z 319 → 125 was used to identify 4OHMT in the urine samples. Similar to this, a shoulder building was also present for 6βOHMT but, different from 4OHMT, in the quantifier transition (m/z 319 → 283). Therefore, integration of the quantifier peak of 6βOHMT was performed manually. Overall, only minor amounts of

hydroxylated metabolites were found compared to relatively high amounts of unmetabolized MT. The excretion pattern of the three hydroxy metabolites is depicted in Figure 61. 2βOHMT as the main metabolite was detected from the 5.5 hours urine to the 14.5 hours urine after the MT administration. 6βOHMT was only found in the first two samples (5.5 and 8 hours after the administration) and at a much lower concentration than 2βOHMT. The concentration was visualized as peak area because this *in vivo* study intends to gain information about the qualitative and not the quantitative extend of metabolite formation in men. 4OHMT was found in the urine after 5.5 hours and until 22 hours after administration in very low concentrations.

As already described in the literature, the two reduced metabolites of MT, 5αTHMT and 5βTHMT, are the main metabolites found in the human metabolism of MT (see 1.2.3). Joseph found 2βOHAED as the main hydroxy metabolite after AED administration. He also considered investigating if 2β-hydroxylation might give long term metabolites [4]. Incubation of MT with HLM (4.5.1) showed a high percentage of 2βOHMT formed after 24 hours of incubation (3.2.6). After these results, 2βOHMT was expected to be found in the urine.

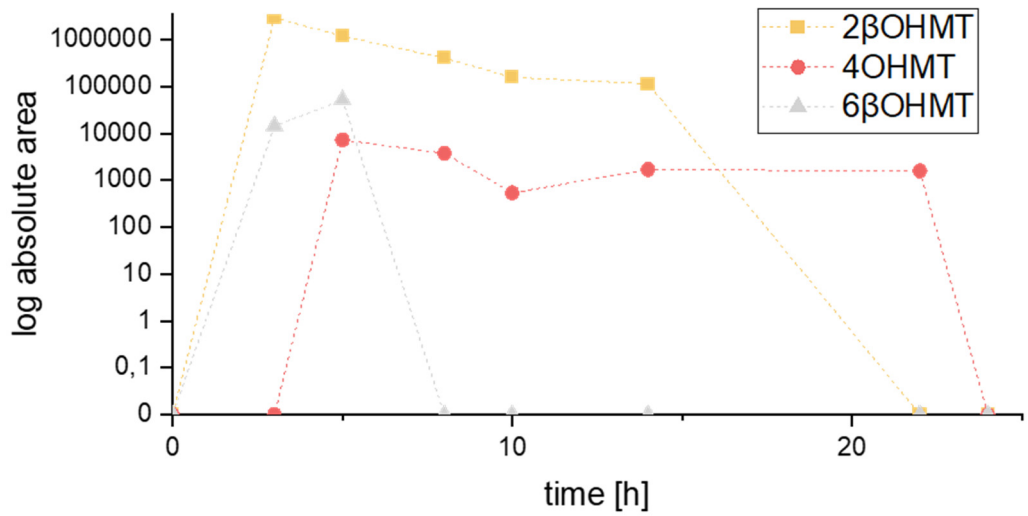

Figure 61: Urinary excretion of 2βOHMT, 4OHMT, and 6βOHMT in the first 24 hours after administration of 10 mg MT to one healthy man (samples MT00 to MT06)

4OHMT seemed to have no significant influence on the metabolism of MT in *in vitro* studies. Nevertheless, as the WADA prohibits oxymesterone, it was also investigated in the obtained samples. Because CYP3A4 is the main enzyme in human metabolism, 6βOHMT was expected to be found in the urine.

Unlike Martinez-Brito *et al.*, 4OHMT was found only in small amounts (peak area) compared to 2βOHMT [47]. The concentration might vary because the pH strongly influences the extraction rate of 4-hydroxy metabolites [68]. Also, the ionization of 4OHMT was about five times lower than the ionization of the 2-hydroxy isomers. The ionization is exemplified in Figure 62, showing the MRM chromatograms of 4OHMT and 2ξOHMT (concentration 10 ng/mL both; 2αOHMT ~8.5 ng/mL, 2βOHTM ~1.5 ng/mL). Martinez-Brito *et al.* described a coeluting artifact of 6βOHMT, which might be formed in the derivatization reaction [47]. The SFC measurement results of the *in vivo* samples showed similarities to that even without derivatization. These results show that the formation of the artifact is not related to the derivatization reaction rather than possibly being part of the urine sample itself or the process of liberating the phase-II-metabolites.

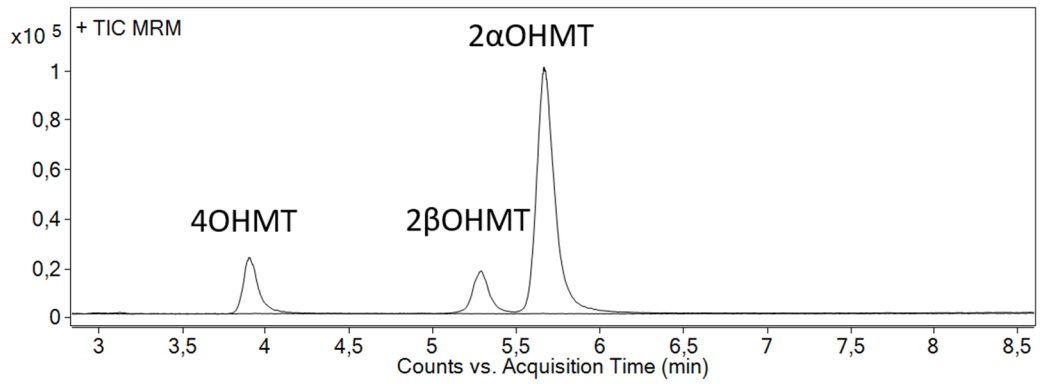

Figure 62: Overlay of MRM chromatograms of 2αOHMT (concentration ~8.5 ng/mL accordingly to the ratio of 2ξOHMT determined by ^{1}H-NMR [section 4.1 - NMR part]), 2βOHMT (concentration ~1.5 ng/mL accordingly to the ratio of 2ξOHMT determined by ^{1}H-NMR [section 4.1 - NMR part]) and 4OHMT (concentration 10 ng/mL)

Compared to the results of Escobar-Wilches *et al.* [52], the excretion of MT showed similarities for 2β and 6β hydroxylation as the main hydroxylated metabolites for T/MT in men. However, Escobar-Wilches *et al.* [52] found 6β-hydroxytestosterone to be the main metabolite excreted by men, which intraindividual differences might explain.

Overall, the *in vivo* study showed that the hydroxylated metabolites 2βOHMT, 4OHMT, and 6βOHMT were detected in urine after MT administration. The hypothesis of 2βOHMT as a long-term marker for MT abuse could not be confirmed (max 14.5 hours), as the well-described reduced metabolites 5αTHMT and 5βTHMT can be detected up to 103 hours after administration by GC-QQQ-MS in the same urine samples [47] (urine samples for the *in vivo* study was obtained from Martinez-Brito *et al.*).

Further investigations of the matrix effect's impact on the analysis of human urine samples have to be performed to optimize the developed SFC-MS/MS method. Therefore, optimization of the ionization of the steroids will be performed. New source techniques like UniSpray ionization might be the key to optimize the limit of detection/quantification [82]. A second approach will be the optimization of sample preparation.

5 Summary and Outlook

Anabolic androgenic steroids (AAS) are commonly used as performance-enhancing drugs (PEDs) in sports because of their anabolic effects. Nearly half of the adverse analytical findings (AAF) in 2019 are correlated to AAS misuse [83]. The metabolization process plays an essential role in the analysis of endogenous and exogenous steroids. Therefore, investigations on drug metabolizing and steroidogenic CYP enzymes are important in antidoping research. The most common reaction catalyzed by CYP enzymes in phase-I-metabolism is the introduction of a hydroxy group.

Currently, analysis of AAS is mostly performed using GC-MS systems. These methods usually correlate with laborious sample preparation and extended run times compared to LC-MS(/MS) methods. On the other hand, LC-MS(/MS) methods have a lower separation efficiency than GC-MS systems. SFC, as an orthogonal analytical approach, was used to separate the hydroxy metabolites of MT.

This project aimed to get a more in-depth look at the metabolization and analysis of MT, an AAS prohibited as PED in sport by the WADA [1], focusing on hydroxylated metabolites and the aromatization process. Therefore, reference material of 2αOHMT, 2βOHMT, and 4OHMT was synthesized and characterized by HRMS and NMR. *In vitro* studies with HLM, CYP2C19, CYP1A2, CYP1B1, and CYP19A1 and an *in vivo* study with one healthy male volunteer were conducted to investigate the formation of hydroxylated MT metabolites. Because existing and developed GC-MS(/MS) and LC-MS(/MS) methods could not separate the hydroxylated metabolites of interest, an SFC-MS/MS method was developed, which gave a good separation. SFC showed its orthogonality by means of the elution order 4OHMT>2βOHMT>2αOHMT>6βOHMT, which differed from GC (2βOHTM>6βOHMT>4OHTM>2αOHMT, as per-TMS) and LC (6βOHMT>2βOHMT>2αOHMT>4OHMT).

Finally, the formation of 2βOHMT in HLM and CYP2C19 incubation were verified with synthesized reference material, where CYP2C19 may show the predominant way in its formation. Additionally, the presence of 2βOHMT after CYP19A1 incubation shows its influence in the aromatization of MT.

Investigation of urine samples after MT administration showed the formation of 2βOHMT, 6βOHMT, and 4OHMT. However, all three metabolites were only detected to a maximum of 22 hours after the administration and in very low concentrations.

Thus, hydroxylated metabolites of MT cannot be seen as superior metabolites over the classical MT metabolites 5αTHMT and 5βTHMT [45].

Future work may focus on developing an SFC-HRMS method to investigate the formation of unknown hydroxy metabolites. As only recently described by Savill *et al.*, incubation studies with different cell lines may be a good alternative for *in vivo* studies with steroids [84]. Further, the synthesis and characterization of possible metabolite structures will be the next step in investigating the hydroxylated metabolome. Boldenone is the AAS with the majority of reported AAF according to the WADA Testing Figures [83]. Therefore, boldenone, or its corresponding 17-methyl analog metandienone, might be an interesting substance for this kind of study.

In addition, further experiments on the aromatization of MT with 2βOHMT and 19OHMT as substrate, and the identification of 2β,19-dihydroxymethyltestosterone as intermediate with synthesized reference material are needed.

6 Zusammenfassung und Ausblick

Anabol androgene Steroide (AAS) werden aufgrund ihrer anabolen Wirkung häufig als leistungssteigernde Mittel (PEDs) im Sport eingesetzt. Fast die Hälfte der unerwünschten analytischen Befunde (AAF) im Jahr 2019 korreliert mit dem Missbrauch von AAS [83]. Eine wesentliche Rolle bei der Detektion von endogenen und exogenen Steroiden in Urinproben spielt die Metabolisierung. Daher sind Untersuchungen zu arzneimittelmetabolisierenden und steroidogenen CYP-Enzymen in der Antidopingforschung wichtig. Die häufigste Reaktion, die von CYP-Enzymen im Phase-I-Metabolismus katalysiert wird, ist die Einführung einer Hydroxygruppe.

Die Analyse von AAS wird derzeit meist mit GC-MS-Systemen durchgeführt. Diese Methoden sind in der Regel mit einer aufwendigen Probenvorbereitung und längeren Laufzeiten im Vergleich zu LC-MS(/MS)-Methoden verbunden. Auf der anderen Seite haben LC-MS(/MS)-Methoden eine geringere Trenneffizienz im Vergleich zu GC-MS-Systemen. Die SFC als orthogonaler analytischer Ansatz wurde zur Trennung der Hydroxymetaboliten von MT verwendet.

Ziel dieses Projektes war es, die Metabolisierung und Analyse von MT, einem von der WADA als PED im Sport verbotenen AAS [1], genauer zu untersuchen, wobei der Fokus auf hydroxylierte Metabolite und die Aromatisierung lag. Dazu wurde Referenzmaterial von 2αOHMT, 2βOHMT und 4OHMT synthetisiert und mittels HRMS und NMR charakterisiert. *In vitro* Versuche mit HLM, CYP2C19, CYP1A2, CYP1B1 und CYP19A1 sowie ein *in vivo* Versuch mit einem gesunden männlichen Probanden wurden durchgeführt, um die Entstehung von hydroxylierten MT-Metaboliten zu untersuchen. Da bestehende und entwickelte GC-MS(/MS)- und LC-MS(/MS)-Methoden nicht in der Lage waren, die hydroxylierten Metaboliten zu trennen, wurde eine SFC-MS/MS-Methode entwickelt, die eine gute Trennung ergab. Die SFC zeigte seine Orthogonalität an Hand der Elutionsfolge 4OHMT>2βOHMT>2αOHMT>6βOHMT, welche sich

grundlegend von der GC (2βOHTM>6βOHMT>4OHTM>2αOHMT, als per-TMS) und der LC (6βOHMT>2βOHMT>2αOHMT>4OHMT) unterschied.

Die Entstehung von 2βOHMT in HLM und CYP2C19 Inkubation mit wurde mit synthetisiertem Referenzmaterial verifiziert, wobei CYP2C19 offenbar den vorherrschenden Weg bei der Entstehung von 2βOHMT zeigt. Das Vorhandensein von 2βOHMT nach Inkubation mit CYP19A1 zeigt dessen Einfluss auf die Aromatisierung von MT.

Die Untersuchung von Urinproben nach Einnahme von MT zeigte die Entstehung von 2βOHMT, 6βOHMT und 4OHMT. Alle drei Metaboliten wurden jedoch nur bis maximal 22 Stunden nach der Verabreichung und in sehr geringen Konzentrationen nachgewiesen.

Somit können hydroxylierte Metabolite von MT gegenüber den klassischen MT Metaboliten 5αTHMT und 5βTHMT nicht als übergeordnet angesehen werden [45].

Zukünftige Arbeiten könnten sich auf die Entwicklung einer SFC-HRMS-Methode beschäftigen, um die Bildung von unbekannten hydroxylierten Metaboliten zu untersuchen. Wie erst kürzlich von Savill *et al.* beschrieben, können Inkubationsstudien mit verschiedenen Zelllinien eine gute Alternative für *in vivo* Studien mit Steroiden sein [84]. Die Synthese und Charakterisierung möglicher weiterer Metabolitstrukturen werden der nächste Schritt bei der Untersuchung des Phase-I-Metabolismus von MT sein. Boldenon ist das AAS mit den meisten berichteten AAF gemäß des WADA Testing Figures Report [83]. Daher könnte Boldenon oder sein entsprechendes 17-Methyl Analogon Metandienon eine interessante Substanz für diese Art von Studie sein.

Zudem sind weitere Versuche zu der Aromatisierung von MT mit 2βOHMT und 19OHMT als Substrat, und die Identifizierung von 2β,19-Dihydroxymethyltestosterone als Zwischenprodukt mit synthetisierter Referenzsubstanz nötig.

7 Curriculum Vitae

8 References

[1] World Anti-Doping Agency. Prohibited List 2021. (2020)

[2] Balthazart J. Steroid Metabolism and the Activation of Social Behavior. In: Balthazart J (Ed.) *Molecular and Cellular Basis of Social Behavior in Vertebrates*, Springer Berlin Heidelberg, Berlin, Heidelberg (1989) 105-159

[3] Miller WL, Auchus RJ. The molecular biology, biochemistry, and physiology of human steroidogenesis and its disorders. *Endocrine Reviews* 32 (2011) 81-151

[4] Joseph JF. Metabolism of androstane derivatives with focus on hydroxylation reactions. *Biology, Chemistry, Pharmacy,* Freie Universität Berlin (2016)

[5] Hanukoglu I. Steroidogenic enzymes: Structure, function, and role in regulation of steroid hormone biosynthesis. *The Journal of Steroid Biochemistry and Molecular Biology* 43 (1992) 779-804

[6] Gower DB. Analysis of Androgens and Their Derivatives. In: Makin HLJ, Gower DB (Eds.) *Steroid Analysis*, Springer Netherlands, Dordrecht (2010) 457-558

[7] Mutschler E, Schaible H-G, Vaupel P. *Anatomie Physiologie Pathophysiologie des Menschen*, Wissenschaftliche Verlagsgesellschaft mbH Stuttgart, Stuttgart (2007)

[8] Fukami M, Homma K, Hasegawa T, Ogata T. Backdoor pathway for dihydrotestosterone biosynthesis: implications for normal and abnormal human sex development. *Developmental Dynamics* 242 (2013) 320-329

[9] Rižner TL, Penning TM. Role of aldo-keto reductase family 1 (AKR1) enzymes in human steroid metabolism. *Steroids* 79 (2014) 49-63

[10] Longcope C. Estriol production and metabolism in normal women. *J Steroid Biochem* 20 (1984) 959-962

[11] Wilson JD, Griffin JE. The use and misuse of androgens. *Metabolism* 29 (1980) 1278-1295

[12] Rolf C, Knie U, Lemmnitz G, Nieschlag E. Interpersonal testosterone transfer after topical application of a newly developed testosterone gel preparation. *Clinical Endocrinology* 56 (2002) 637-641

[13] Jockenhövel F. Testosterone therapy - what, when and to whom? *The Aging Male* 7 (2004) 319-324

[14] Kicman AT. Pharmacology of anabolic steroids. *British Journal of Pharmacology* 154 (2008) 502-521

[15] Eacker SM, Agrawal N, Qian K, Dichek HNL, Gong E-Y, Lee K, Braun RE. Hormonal Regulation of Testicular Steroid and Cholesterol Homeostasis. *Molecular Endocrinology* 22 (2008) 623-635

[16] Payne AH, Hales DB. Overview of Steroidogenic Enzymes in the Pathway from Cholesterol to Active Steroid Hormones. *Endocrine Reviews* 25 (2004) 947-970

[17] Jancova P, Anzenbacher P, Anzenbacherova E. Phase II drug metabolizing enzymes. *Biomedical Papers of the Medical Faculty of the Univervity Palacky, Olomouc, Czech Republic* 154 (2010) 103-116

[18] Riddick DS, Ding X, Wolf CR, Porter TD, Pandey AV, Zhang QY, Gu J, Finn RD, Ronseaux S, Mclaughlin LA, Henderson CJ, Zou L, Fluck CE. NADPH-cytochrome P450 oxidoreductase: roles in physiology, pharmacology, and toxicology. *Drug Metabolism and Disposition* 41 (2013) 12-23

[19] Yamazaki H, Shimada T. Progesterone and testosterone hydroxylation by cytochromes P450 2C19, 2C9, and 3A4 in human liver microsomes. *Archives of Biochemestry and Biophysics* 346 (1997) 161-169

[20] Shimada T, Yamazaki H, Mimura M, Inui Y, Guengerich FP. Interindividual variations in human liver cytochrome P-450 enzymes involved in the oxidation of drugs, carcinogens and toxic chemicals: studies with liver microsomes of 30 Japanese and 30 Caucasians. *Journal of Pharmacology and Experimental Therapeutics* 270 (1994) 414-423

[21] Waxman DJ, Attisano C, Guengerich FP, Lapenson DP. Human liver microsomal steroid metabolism: Identification of the major microsomal steroid hormone 6β-hydroxylase cytochrome P-450 enzyme. *Archives of Biochemistry and Biophysics* 263 (1988) 424-436

[22] Usmani KA, Rose RL, Hodgson E. Inhibition and Activation of the Human Liver Microsomal and Human Cytochrome P450 3A4 Metabolism of Testosterone by Deployment-Related Chemicals. *Drug Metabolism and Disposition* 31 (2003) 384

[23] Mäenpää J, Pelkonen O, Cresteil T, Rane A. The role of cytochrome P450 3A (CYP3A) isoform(s) in oxidative metabolism of testosterone and benzphetamine in human adult and fetal liver. *The Journal of Steroid Biochemistry and Molecular Biology* 44 (1993) 61-67

[24] Choi MH, Skipper PL, Wishnok JS, Tannenbaum SR. Characterization of testosterone 11β-hydroxylation catalyzed by human liver microsomal cytochromes P450. *Drug Metabolism and Disposition* 33 (2005) 714

[25] Krauser JA, Voehler M, Tseng L-H, Schefer AB, Godejohann M, Guengerich FP. Testosterone 1β-hydroxylation by human cytochrome P450 3A4. *European Journal of Biochemistry* 271 (2004) 3962-3969

[26] Rendic S, Nolteernsting E, Schanzer W. Metabolism of anabolic steroids by recombinant human cytochrome P450 enzymes. Gas chromatographic-mass spectrometric determination of metabolites. *Journal of Chromatography B* 735 (1999) 73-83

[27] Rittle J, Green MT. Cytochrome P450 Compound I: Capture, Characterization, and C-H Bond Activation Kinetics. *Science* 330 (2010) 933-937

[28] Sevrioukova IF, Poulos TL. Understanding the mechanism of cytochrome P450 3A4: recent advances and remaining problems. *Dalton Trans* 42 (2013) 3116-3126

[29] Groves JT. Key elements of the chemistry of cytochrome P-450: The oxygen rebound mechanism. *Journal of Chemical Education* 62 (1985) 928

[30] Lee AJ, Cai MX, Thomas PE, Conney AH, Zhu BT. Characterization of the Oxidative Metabolites of 17β-Estradiol and Estrone Formed by 15 Selectively Expressed Human Cytochrome P450 Isoforms. *Endocrinology* 144 (2003) 3382-3398

[31] Hosoda H, Fishman J. Unusually facile aromatization of 2β-hydroxy-19-oxo-4-androstene-3,17-dione to estrone. Implications in estrogen biosynthesis. *Journal of the American Chemical Society* 96 (1974) 7325-7329

[32] Niwa T, Murayama N, Imagawa Y, Yamazaki H. Regioselective hydroxylation of steroid hormones by human cytochromes P450. *Drug Metabolism Reviews* 47 (2015) 89-110

[33] Sugimoto H, Shiro Y. Diversity and Substrate Specificity in the Structures of Steroidogenic Cytochrome P450 Enzymes. *Biological and Pharmaceutical Bulletin* 35 (2012) 818-823

[34] Yoshimoto FK, Guengerich FP. Mechanism of the third oxidative step in the conversion of androgens to estrogens by cytochrome P450 19A1 steroid aromatase. *Journal of the American Chemical Society* 136 (2014) 15016-15025

[35] Di Nardo G, Castrignanò S, Sadeghi SJ, Baravalle R, Gilardi G. Bioelectrochemistry as a tool for the study of aromatization of steroids by human aromatase. *Electrochemistry Communications* 52 (2015) 25-28

[36] Akhtar M, Calder MR, Corina DL, Wright JN. Mechanistic studies on C-19 demethylation in oestrogen biosynthesis. *Biochememical Journal* 201 (1982) 569-580

[37] Hahn EF, Fishman J. Immunological probe of estrogen biosynthesis. Evidence for the 2 beta-hydroxylative pathway in aromatization of androgens. *Journal of Biological Chemistry* 259 (1984) 1689-1694

[38] Dumasia MC. In vivo biotransformation of 17 alpha-methyltestosterone in the horse revisited: identification of 17-hydroxymethyl metabolites in equine urine by capillary gas chromatography/mass spectrometry. *Rapid Commun Mass Spectrometry* 17 (2003) 320-329

[39] Mckinney AR, Suann CJ, Stenhouse AM. A stereochemical examination of the equine metabolism of 17α-methyltestosterone. *Analytica Chimica Acta* 581 (2007) 377-387

[40] Biddle STB, O'Donnell A, Houghton E, Creaser C. Metabolism of methyltestosterone in the greyhound. *Rapid Communications in Mass Spectrometry* 23 (2009) 713-721

[41] Blokland MH, Rossum HJV, Herbold HA, Sterk SS, Stephany RW, Ginkel LaV. Metabolism of methyltestosterone, norethandrolone and methylboldenone in a heifer. *Analytica Chimica Acta* 529 (2005) 317-323

[42] Schoene C, Nedderman AN, Houghton E. Preliminary study of the metabolism of 17 alpha-methyltestosterone in horses utilizing gas chromatography-mass spectrometric techniques. *Analyst* 119 (1994) 2537-2542

[43] Yamada M, Aramaki S, Okayasu T, Hosoe T, Kurosawa M, Kijima-Suda I, Saito K, Nakazawa H. Identification and quantification of metabolites common to 17α-methyltestosterone and mestanolone in horse urine. *Journal of Pharmaceutical and Biomedical Analysis* 45 (2007) 125-133

[44] Williams TM, Kind AJ, Hyde WG, Hill DW. Characterization of urinary metabolites of testosterone, methyltestosterone, mibolerone and boldenone in greyhound dogs. *Journal of Veterinary Pharmacology and Therapeutics* 23 (2000) 121-129

[45] Pozo ÓJ, Van Eeno o P, Deventer K, Lootens L, Van Thuyne W, Parr MK, Schänzer W, Sancho JV, Hernández F, Meuleman P, Leroux-Roels G, Delbeke FT. Detection and Characterization of a New Metabolite of 17α-Methyltestosterone. *Drug Metabolism and Disposition* 37 (2009) 2153

[46] U.S. Anti Doping Agency. U.S. Cycling Athlete Barbara Gicquel Accepts Sanction for Anti-Doping Rule Violation. https://www.usada.org/sanction/barbara-gicquel-accepts-doping-sanction-2/. 13.12.2020 (2020)

[47] Martinez-Brito D, Iannone M, Tatangelo MA, Molaioni F, De La Torre X, Botrè F. A further insight into methyltestosterone metabolism: New evidences from in vitro and in vivo experiments. *Rapid Communications in Mass Spectrometry* 34 (2020) e8870

[48] Pope HG, Jr., Wood RI, Rogol A, Nyberg F, Bowers L, Bhasin S. Adverse Health Consequences of Performance-Enhancing Drugs: An Endocrine Society Scientific Statement. *Endocrine Reviews* 35 (2014) 341-375

[49] Parr MK, Schänzer W. Detection of the misuse of steroids in doping control. *The Journal of Steroid Biochemistry and Molecular Biology* 121 (2010) 528-537

[50] Thevis M, Kuuranne T, Geyer H, Schänzer W. Annual banned-substance review: analytical approaches in human sports drug testing. *Drug Testing and Analysis* 6 (2014) 164-184

[51] Thevis M, Schänzer W. Mass spectrometry in sports drug testing: Structure characterization and analytical assays. *Mass Spectrometry Reviews* 26 (2007) 79-107

[52] Escobar-Wilches DC, Ventura-Bahena A, De Lourdes López-González M, Torres-Sánchez L, Figueroa M, Sierra-Santoyo A. Analysis of testosterone-hydroxylated metabolites in human urine by ultra high performance liquid chromatography-Mass Spectrometry. *Analytical Biochemestry* 597 (2020) 113670

[53] Koal T, Schmiederer D, Pham-Tuan H, Röhring C, Rauh M. Standardized LC-MS/MS based steroid hormone profile-analysis. *The Journal of Steroid Biochemistry and Molecular Biology* 129 (2012) 129-138

[54] Caron P, Turcotte V, Guillemette C. A chromatography/tandem mass spectrometry method for the simultaneous profiling of ten endogenous steroids, including progesterone, adrenal precursors, androgens and estrogens, using low serum volume. *Steroids* 104 (2015) 16-24

[55] Gómez C, Pozo OJ, Marcos J, Segura J, Ventura R. Alternative long-term markers for the detection of methyltestosterone misuse. *Steroids* 78 (2013) 44-52

[56] Couchman L, Vincent RP, Ghataore L, Moniz CF, Taylor NF. Challenges and benefits of endogenous steroid analysis by LC–MS/MS. *Bioanalysis* 3 (2011) 2549-2572

[57] Boccard J, Badoud F, Jan N, Nicoli R, Schweizer C, Pralong F, Veuthey J-L, Baume N, Rudaz S, Saugy M. Untargeted profiling of urinary steroid metabolites after testosterone ingestion: opening new perspectives for antidoping testing. *Bioanalysis* 6 (2014) 2523-2536

[58] Donike M. N-Methyl-N-trimethylsilyl-trifluoracetamid, ein neues Silylierungsmittel aus der Reihe der silylierten Amide. *Journal of Chromatography A* 42 (1969) 103-104

[59] Geyer H, Schänzer W, Mareck-Engelke U, Nolteernsting E, G O. Screening procedure for anabolic steroids-control of hydrolysis with deuterated androsterone glucuronide and studies with direct hydrolysis. *W. Schänzer, H. Geyer, A. Gotzmann, U Mareck (eds.) Recent Advances in Doping Analysis, Sport und Buch Strauß, Köln* 5 (1998) 99-102

[60] Tomoeda M, Ishizaki M, Kobayashi H, Kanatomo S, Koga T, Inuzuka M, Furuta T. Studies on conformation and reactivity—I The polyphosphoric acid-catalyzed ring opening of 4,5-epoxy-3-oxo steroids—the synthesis of 4-ethylthiocholest-4-en-3-one and its analogs. *Tetrahedron* 21 (1965) 733-742

[61] Liao J, Fu L, Zeng J, Wei X, Zeng W, Liu Y. Method for preparation of methyltestosterone with 4-androstene-3,17-dione. in, Huazhong Pharmaceutical Co., Ltd., (2016)

[62] Kuuranne T, Pystynen K-H, Thevis M, Leinonen A, Schänzer W, Kostiainen R. Screening of In Vitro Synthesised Metabolites of 4,9,11-Trien-3-One Steroids by Liquid Chromatography-Mass Spectrometry. *European Journal of Mass Spectrometry* 14 (2008) 181-189

[63] Mareck U, Thevis M, Guddat S, A. Gotzmann, Bredehöft M, Geyer H, Schänzer W. Comprehensive Sample Preparation for Anabolic Steroids, Glucocorticosteroids, Beta-Receptor Blocking Agents, Selected Anabolic Androgenic Steroids and Buprenorphine in Human Urine. *W. Schänzer, H. Geyer, A. Gotzmann, U. Mareck (eds) Recent advances in doping analysis, Sport und Buch Strauß, Köln* 12 (2004) 65-68

[64] Burnett RD, Kirk DN. Some observations on the preparation of 2-hydroxy-steroid 4-en-3-ones. *Journal of the Chemical Society, Perkin Transactions 1* (1973) 1830-1836

[65] Rao PN, Axelrod LR. Synthesis of 2β-Hydroxytestosterone1. *Journal of the American Chemical Society* 82 (1960) 2830-2832

[66] Gleispach H. The use of different silylating agents for structure analyses of steroids. *Journal of Chromatography A* 91 (1974) 407-412

[67] Kollmeier AS, De La Torre X, Müller C, Botrè F, Parr MK. In-depth gas chromatography/tandem mass spectrometry fragmentation analysis of formestane and evaluation of mass spectral discrimination of isomeric 3-keto-4-ene hydroxy steroids. *Rapid Communications in Mass Spectrometry* 34 (2020) e8937

[68] Parr MK, Opfermann G, W S. Analytical Properties of 4-Hydroxysteroids and some Esters. *W. Schänzer, H. Geyer, A. Gotzmann, U Mareck (eds.) Recent Advances in Doping Analysis, Sport und Buch Strauß, Köln* 12 (2004) 129-139

[69] Vouros P, Harvey DJ, Odiorne TJ. Some Aspects of Intra- and Inter-Molecular Reactions of Siliconium Ions in the Vapor Phase. *Spectroscopy Letters* 6 (1973) 603-615

[70] Kirk DN, Toms HC, Douglas C, White KA, Smith KE, Latif S, Hubbard RWP. A survey of the high-field 1H NMR spectra of the steroid hormones, their hydroxylated derivatives, and related compounds. *Journal of the Chemical Society, Perkin Transactions 2* (1990)

[71] Kohler M. Metabolismus von 4-Hydroxyandrostendion und 4-Hydroxytestosteron. *Fachbereich Biochemie,* Universität zu Köln (2006)

[72] Loibner H, Zbiral E. Reaktionen mit phosphororganischen Verbindungen. XLII. Nucleophile Substitutionen an Hydroxysteroiden mit Hilfe von Triphenylphosphan/Azodicarbonsäureester. *Helvetica Chimica Acta* 60 (1977) 417-425

[73] Guezane Lakoud S, Djerourou A. Esterification and etherification of steroid and terpene under Mitsunobu conditions. *Arabian Journal of Chemistry* 9 (2016) 889-892

[74] Parr MK, Zöllner A, Fußhöller G, Opfermann G, Schlörer N, Zorio M, Bureik M, Schänzer W. Unexpected contribution of cytochrome P450 enzymes CYP11B2 and CYP21, as well as CYP3A4 in xenobiotic androgen elimination – Insights from metandienone metabolism. *Toxicology Letters* 213 (2012) 381-391

[75] Schänzer W, Horning S, Donike M. Metabolism of anabolic steroids in humans: Synthesis of 6β-hydroxy metabolites of 4-chloro-1,2-dehydro-17α-methyltestosterone, fluoxymesterone, and metandienone. *Steroids* 60 (1995) 353-366

[76] Parr MK, Wüst B, Teubel J, Joseph JF. Splitless hyphenation of SFC with MS by APCI, APPI, and ESI exemplified by steroids as model compounds. *Journal of Chromatography B* 1091 (2018) 67-78

[77] Schänzer W, Donike M. Metabolism of anabolic steroids in man: synthesis and use of reference substances for identification of anabolic steroid metabolites. *Analytica Chimica Acta* 275 (1993) 23-48

[78] Wang PP, Beaune P, Kaminsky LS, Dannan GA, Kadlubar FF, Larrey D, Guengerich FP. Purification and characterization of six cytochrome P-450 isozymes from human liver microsomes. *Biochemistry* 22 (1983) 5375-5383

[79] Cheng ZN, Shu Y, Liu ZQ, Wang LS, Ou-Yang DS, Zhou HH. Role of cytochrome P450 in estradiol metabolism in vitro. *Acta Pharmacol Sin* 22 (2001) 148-154

[80] Osawa Y, Higashiyama T, Fronckowiak M, Yoshida N, Yarborough C. Aromatase. *The Journal of Steroid Biochemistry and Molecular Biology* 27 (1987) 781-789

[81] Declaration of Helsinki (1964). *BMJ* 313 (1996) 1448-1449

[82] Bakusic J, De Nys S, Creta M, Godderis L, Duca RC. Study of temporal variability of salivary cortisol and cortisone by LC-MS/MS using a new atmospheric pressure ionization source. *Scientific Reports* 9 (2019) 19313

[83] World Anti-Doping Agency. Anti-Doping Testing Figures Report 2019. (2020)

[84] Savill R, Baues H, Voigt E, Zierau O, Thieme D, Keiler AM. Cell culture as a toolbox to generate phase I metabolites for anti-doping screening. *Drug Testing and Analysis* (2021)

9 List of figures

Figure 1: Numbering system of steroids exemplified with cholestane (I) and its spatial arrangement of 5α- (IIa) and 5β-configuration (IIb), adapted from [4] 1

Figure 2: Basic structures of pregnans (C21-steroids, III), androgens (C19-steroids, IV), and estranes (C18-steroids, V) 2

Figure 3: Essential biosynthetic pathways in the formation of pregnanes (pregnenolone), glucocorticoids (cortisol), gestagens (progesterone), androgens (androstenedione), mineralocorticoids (aldosterone), and estrogens (estrone) with involved CYP enzymes, starting from cholesterol; partially adapted from [4] and [6] 3

Figure 4: Biosynthetic pathways including the formation of dihydrotestosterone (front-door-pathway) and estrogens (including involved enzymes): pregnenolone (PREG), dehydroepiandrosterone (DHEA), 16-hydroxydehydroepiandrosterone (16OHDHEA), 16-hydroxyandrostendione (16OHAED), androstenedione (AED), 5α-androstanedione (5αAD), testosterone (T), 5α-dihydrotestosterone (5αDHT), estrone (E1), estradiol (E2), estriol (E3), hydroxysteroid dehydrogenase (HSD), aldo-keto reductase (AKR), SRD5A (5α-reductase); partially adapted from [8-10] 4

Figure 5: Typical modifications of T resulting in methyltestosterone, metandienone, dehydrochlormethyltestosterone (DHCMT), nandrolone, stanozolol.....5

Figure 6: Proposed mechanism of the hydroxylation of 3-oxo-4-ene-steroids with CYP, exemplified on the formation of 6β-hydroxymethyltestosterone; adapted from [26] 8

Figure 7: Aromatization process of testosterone; every hydroxylation consumes one oxygen and NADPH molecule; C19 methyl group is finally cleaved off as formic acid 9

Figure 8: The three discussed pathways for the third step in the aromatization process, described by Yoshimoto et al. (I + II) and Hosoda et al. (III) [31, 34] 10

Figure 9: Number of adverse analytical findings of MT from 2014 to 2019 reported by the WADA laboratories (Testing Figures Report 2014-2019)..... 13

Figure 10: In situ formation of TMIS from MSTFA/NH4I/ethanethiol (1000:2:3, v/w/v).....25

Figure 11: Reaction scheme of derivatization of 2βOHMT with TMIS; the resulting per-TMS derivatives 3,5-diene-2,3,17-triol tris-TMS (A) and 2,4-diene-2,3,17-triol tris-TMS (B) from the reaction of 2β-hydroxy-17α-methyltestosterone 26

Figure 12: Reaction scheme of derivatization of 2βOHMT with MSTFA; the resulting mono-TMS derivative 4-ene-2,17-diol-2-TMS (C) from the reaction of 2β-hydroxy-17α-methyltestosterone 26

Figure 13: Chemical structures of the educt 17α-methyltestosterone (1) and the three desired products 2β-hydroxy-17α-methyltestosterone (4), 2α-hydroxy-17α-methyltestosterone (5) and 4-hydroxy-17α-methyltestosterone [oxymesterone] (6) 29

Figure 14:Chemical structures of 19-hydroxyandrost-4-ene-3,17-dione (left) and the expected product 19-hydroxy-17α-methyltestosterone (right) 30

Figure 15: Incubation protocol for the in vivo studies adapted from [62] 32

Figure 16: Protocol for the sample preparation of urine analysis 33

Figure 17: Two-step synthesis of the three hydroxylated metabolites 2α-hydroxy-17α-methyltestosterone (5) 2β-hydroxy-17α-methyltestosterone (4) and 4-hydroxy-17α-methyltestosterone (6) starting from 17α methyltestosterone (1) 34

Figure 18: GC-EI-MS total ion current (TIC) chromatogram of underivatized 4β,5β-epoxy-17α-methyltestosterone (2) and 4α,5α-epoxy-17α-methyltestosterone (3) 35

Figure 19: GC-EI-MS spectra of 4β,5β-epoxy-17α-methyltestosterone at 70 eV $[M]^{\bullet+}$= 318.2 35

Figure 20: GC-EI-MS spectra of 4α,5α-epoxy-17α-methyltestosterone at 70 eV $[M]^{\bullet+}$= 318.2 35

Figure 21: The predicted chemical reaction of the ring-opening in acid conditions exemplified by 4β,5β-epoxy-17α-methyltestosterone (2) to 2α-hydroxy-17α-methyltestosterone (5) and 2β-hydroxy-17α-methyltestosterone (4) 36

Figure 22: LC-ESI-MS total ion chromatogram of the product mixture showing 2OHMT, 4OHMT, 6OHMT, and unidentified byproducts 37

Figure 23: Structures of 2αOHMT (left) and 2βOHMT (right), showing the tension in the A-ring of 2βOHMT 37

Figure 24: GC-EI-QTOF-MS chromatogram (TIC) of per-TMS derivatives of 2α-hydroxy-17α-methyltestosterone and 2β-hydroxy-17α-methyltestosterone, method h) 38

Figure 25: GC-EI-QTOF-MS spectra of 2α-hydroxy-17α-methyltestosterone as per-TMS derivative $[M]^{\bullet+}$=534.3383 38

Figure 26: GC-EI-QTOF-MS spectra of 2β-hydroxy-17α-methyltestosterone as per-TMS derivative $[M]^{\bullet+}$=534.3379 39

Figure 27: ^{1}H-NMR spectrum of 2ξ-hydroxy-17α-methyltestosterone enantiomers in $CDCl_3$, insert shows zoom at 4.00 - 4.50 ppm 42

Figure 28: ^{13}C-NMR DEPTQ spectrum of 2ξ-hydroxy-17α-methyltestosterone enantiomers in $CDCl_3$ 43

Figure 29: ^{1}H,^{13}C-HSQC spectrum of 2ξ-hydroxy-17α-methyltestosterone in $CDCl_3$, zoomed area of 0.75 - 2.5 ppm and 5 - 60 ppm 44

Figure 30: GC-EI-QTOF-MS spectra of 4-hydroxy-17α-methyltestosterone as per-TMS derivative $[M]^{\bullet+}$= 534.3382 46

Figure 31: ^{1}H-NMR spectrum of 4-hydroxy-17α-methyltestosterone in DMSO-d_6 48

Figure 32: ^{13}C-NMR spectrum of 4-hydroxy-17α-methyltestosterone in DMSO-d_6 49

Figure 33: ^{1}H,^{13}C-HSQC spectrum of 4-hydroxy-17α-methyltestosterone in DMSO-d_6 50

Figure 34: Steps of the chemical synthesis of 19-hydroxy-17α-methyltestosterone (10) using 19-hydroxyandrost-4-en-3,17-dione (7) as educt; first intermediate product (8) after the protection of position 3 and second intermediate product (9) after Grignard reaction and hydrolysis with water 52

Figure 35: Anticipated reaction mechanism of C19 ester with CH_3MgBr to give the unprotected hydroxy group 53

Figure 36: GC-MS chromatogram after TMIS derivatization showing 6 main products unidentified byproduct 1 (m/z 444, RT 11.6), unidentified byproduct 2 (m/z 460, RT 13.1 min), unidentified byproduct 3 (m/z 460, RT 13.8 min), unidentified byproduct 4 (m/z 446, RT 15.0) min, 19OHAED (m/z 518, RT 16.3 min, educt) and 19OHMT (m/z 534, RT 17.3, product) 53

Figure 37: GC-EI-MS spectra of 19OHMT as per TMS derivative at 70 eV $[M]^{\bullet+}$= 534.3 54

Figure 38: SFC-QQQ-MS chromatogram of the steroid mix (4OHMT, MT, 2βOHMT, 2αOHMT, 19OHMT [including two unidentified byproducts]) using method d) 55

Figure 39: Overlay of EICs (m/z 375.2) from the mono-TMS derivatives of 2αOHTM, 2βOHMT, 4OHMT, and 6βOHMT obtained for method f) 57

Figure 40: Overlay of EICs (m/z 534.3) from the per-TMS derivatives of 2αOHTM, 2βOHMT, 4OHMT, and 6βOHMT obtained for method f) 58

Figure 41: Overlay of EICs (m/z 375.2) from the mono-TMS derivatives of 2αOHTM, 2βOHMT, 4OHMT, and 6βOHMT obtained for method g) 58

Figure 42: Overlay of EICs (m/z 534.4) from the per-TMS derivatives of 2αOHTM, 2βOHMT, 4OHMT, and 6βOHMT obtained for method g) 59

Figure 43: Overlay of EICs (m/z 534.4) from the per-TMS derivatives of 2αOHTM, 2βOHMT, 4OHMT, and 6βOHMT obtained for method h) 60

Figure 44: Overlay of EICs ($[M+H]^+$ 319.1) of the reference substances using method b); showing the coeluting 6βOHMT (RT 7.775 min) and 2ξOHMT (RT 8.715 min), and 4OHMT (RT 10.193 min) 61

Figure 45: LC-ESI-QQQ-MS TIC chromatogram of the reference substances; 6βOHMT (RT 6.008 min), 2ξOHMT (RT 6.677 min [2αOHMT] and 6.333 min [2βOHMT]) and 4OHMT (RT 7.879 min) 62

Figure 46: Overlay of EICs ($[M+H]^+$ 319.2268) of the reference substances using method c); 6βOHMT (RT 7.775 min), 2ξOHMT(RT 8.715 min and 8.160 min) and 4OHMT (RT 10.193 min) 63

Figure 47: Comparison of the three chiral phased columns (Agilent Poroshell Chiral-V, Agilent Poroshell Chiral-T, and Chiral Chrialpak IB-U); ESI TIC MRM chromatograms of a sample containing 2αOHMT and 2βOHMT in a ~5:1 ratio 64

Figure 48: Overlay of the normalized MRM chromatograms of reference materials; 4OHMT (RT 3.842 min) 2ξOHMT (RT 5.188 min [2βOHMT] and 5.565 min [2αOHMT]), and 6βOHMT (RT 6.774 min) 65

Figure 49: Comparison of APCI and ESI in positive mode, showing a ~100 (10^3 vs. 10^5; red boxes) times higher sensitivity for ESI; sample contained 1 ppm 2ξOHMT in a 1:5 ratio 66

Figure 50: Plotted results of the source optimization for method e). The peak area related to the starting point before the optimization [%] is plotted against the tested values for the capillary voltage, nebulizer pressure, drying gas flow (DGF), drying gas temperature (DGT), sheath gas flow (SGF), sheath gas temperature (SGT), and nozzle voltage 66

Figure 51: Plotted results of 2αOHMT, 2βOHMT, 4OHMT, 6βOHMT, and 19OHMT of the two HLM incubation studies compared to the negative control sample 68

Figure 52: Comparison of the relative area of hydroxylated metabolites after HLM incubation of MT and AED, showing predominant hydroxylation in position 2β and 6β in both substrates 69

Figure 53: Plotted results of 2αOHMT, 2βOHMT, 4OHMT, 6βOHMT, and 19OHMT of the three CYP2C19 incubation studies of MT compared to the negative control sample 71

Figure 54: Comparison of the relative area of hydroxylated metabolites of MT and AED, showing MT hydroxylation in position 2β and 6β.....72

Figure 55: Plotted results of 2αOHMT, 2βOHMT, 4OHMT, 6βOHMT, and 19OHMT of the three CYP1A2 incubation studies compared to the negative control sample..... 74

Figure 56: Plotted results of 2αOHMT, 2βOHMT, 4OHMT, 6βOHMT, and 19OHMT of the two CYP1B1 incubation studies compared to the negative control sample.....74

Figure 57: Plotted results of 2αOHMT, 2βOHMT, 4OHMT, 6βOHMT, and 19OHMT of the three aromatase incubation studies compared to the negative control sample 77

Figure 58: Comparison of the relative area of hydroxylated metabolites of MT and AED, showing hydroxylation in position 2β and 19 for both substrates.....78

Figure 59: MRM chromatograms of the blank sample MT00 showing MRM of MT, 2βOHMT, 4OHMT, and 6βOHMT..... 82

Figure 60: MRM chromatograms of the sample MT02 (5.5 hours after administration) showing MRM of MT, 2βOHMT, 4OHMT, and 6βOHMT..... 82

Figure 61: Urinary excretion of 2βOHMT, 4OHMT, and 6βOHMT in the first 24 hours after administration of 10 mg MT to one healthy man (samples MT00 to MT06) 83

Figure 62: Overlay of MRM chromatograms of 2αOHMT (concentration ~8.5 ng/mL accordingly to the ratio of 2ξOHMT determined by ^{1}H-NMR [section 4.1 - NMR part]), 2βOHMT (concentration ~1.5 ng/mL accordingly to the ratio of 2ξOHMT determined by ^{1}H-NMR [section 4.1 - NMR part]) and 4OHMT (concentration 10 ng/mL) 84

Figure 63: GC-EI-MS chromatogram (EIC) of 2αOHMT (RT 6.130 min) and 2βOHMT (RT 5.684 min) as mono-TMS derivative 111

Figure 64:GC-EI-MS chromatogram (EIC) of 4OHMT as mono-TMS derivative (RT 5.565 min) 111

Figure 65: GC-EI-MS chromatogram (TIC) of 4OHMT as per-TMS derivative (RT 5.565 min) 111

Figure 66: GC-EI-MS spectra of 2αOHMT as mono TMS derivative at 70 eV $[M-15]^{\bullet+}$= 375.2 112

Figure 67: GC-EI-MS spectra of 2βOHMT as mono TMS derivative at 70 eV $[M-15]^{\bullet+}$= 375.2 112

Figure 68:GC-EI-MS spectra of 4OHMT as mono TMS derivative at 70 eV $[M-15]^{\bullet+}$= 375.3 112

Figure 69: GC-EI-MS spectra of 2αOHMT as per TMS derivative at 70 eV $[M]^{\bullet+}$= 534.4 113

Figure 70: GC-EI-MS spectra of 2βOHMT as per TMS derivative at 70 eV $[M]^{\bullet+}$= 534.4 113

Figure 71: GC-EI-MS spectra of 4OHMT as per TMS derivative at 70 eV $[M]^{\bullet+}$= 534.4 113

Figure 72: HRMS ESI spectrum, accurate mass of 2α-hydroxy-17α-methyltestosterone $[M+H]^+$ = 319.2265 114

Figure 73: HRMS ESI spectrum, accurate mass of 2β-hydroxy-17α-methyltestosterone $[M+H]^+$ = 319.2267 114

Figure 74: HRMS ESI spectrum, accurate mass of 4-hydroxy-17α-methyltestosterone $[M+H]^+$ = 319.2268 114

Figure 75: ^{13}C NMR spectrum of 2ξ-hydroxy-17α-methyltestosterone 115

Figure 76: $^{1}H,^{1}H$-COSY spectrum of 2ξ-hydroxy-17α-methyltestosterone, inserts show zoom areas of 4.1 – 4.35 ppm and 4.0 – 4.5 ppm / 4.1 - 4.4 ppm and 2.2 – 2.6 ppm 115

Figure 77: $^{1}H,^{13}C$-HMBC spectrum of 2ξ-hydroxy-17α-methyltestosterone 116

Figure 78: $^{1}H,^{1}H$-COSY spectrum of 4-hydroxy-17α-methyltestosterone 116

Figure 79: $^{1}H,^{13}C$-HMBC spectrum of 4-hydroxy-17α-methyltestosterone 117

Figure 80:GC-EI-MS spectra of 19OHAED as per-TMS derivative at 70 eV $[M]^{\bullet+}$= 518.3 117

Figure 81: GC-EI-MS spectra of byproduct 1 of 19OHMT synthesis after TMIS derivatization at 70 eV $[M]^{\bullet+}$= 444.3 117

Figure 82: GC-EI-MS spectra of byproduct 2 of 19OHMT synthesis after TMIS derivatization at 70 eV $[M]^{\bullet+}$= 460.3 118

Figure 83: GC-EI-MS spectra of byproduct 3 of 19OHMT synthesis after TMIS derivatization at 70 eV $[M]^{\bullet+}$= 460.2 118

Figure 84: GC-EI-MS spectra of byproduct 4 of 19OHMT synthesis after TMIS derivatization at 70 eV $[M]^{\bullet+}$= 446.3 118

Figure 85: LC (upper chromatogram) vs. SFC (lower chromatogram) method; comparison exemplified with sample HLM_1 with 6βOHMT (area 15923065 vs. 990511) and 2βOHMT (area 2443467 vs. 47775) 119

Figure 86: Chromatograms MRM (MT, 2αOHMT, 2βOHMT,4OHMT, 6βOHMT, 19OHMT) of the negative control of in vitro metabolization 119

Figure 87: Chromatograms MRM of MT, 2αOHMT, 2βOHMT 4OHMT, 6βOHMT and 19OHMT after 24-hour incubation of MT with pooled human liver microsomes (sample HLM_1) 119

Figure 88: Chromatograms MRM of MT, 2αOHMT, 2βOHMT 4OHMT, 6βOHMT and 19OHMT after 24-hour incubation of MT with pooled human liver microsomes (sample HLM_2) 120

Figure 89: Chromatograms MRM; MT incubation studies methanol blank 1; carryover of MT visible.....120

Figure 90: Chromatograms MRM of MT, 2αOHMT, 2βOHMT 4OHMT, 6βOHMT and 19OHMT after 24-hour incubation of MT with CYP2C19 (sample (CYP2C19_1)..... 121

Figure 91: Chromatograms MRM of MT, 2αOHMT, 2βOHMT 4OHMT, 6βOHMT and 19OHMT after 24-hour incubation of MT with CYP2C19 (sample CYP2C19_2)..... 121

Figure 92: Chromatograms MRM of MT, 2αOHMT, 2βOHMT 4OHMT, 6βOHMT and 19OHMT after 24-hour incubation of MT with CYP2C19 (sample CYP2C19_3)..... 122

Figure 93: Chromatograms MRM of MT, 2αOHMT, 2βOHMT 4OHMT, 6βOHMT and 19OHMT after 24-hour incubation of MT with CYP1A2 (sample CYP1A2_1) 122

Figure 94: Chromatograms MRM of MT, 2αOHMT, 2βOHMT 4OHMT, 6βOHMT, and 19OHMT after 24-hour incubation of MT with CYP1A2 (sample CYP1A2_2)..... 123

Figure 95: Chromatograms MRM of MT, 2αOHMT, 2βOHMT 4OHMT, 6βOHMT and 19OHMT after 24-hour incubation of MT with CYP1A2 (sample CYP1A2_3)..... 123

Figure 96: Chromatograms MRM of MT, 2αOHMT, 2βOHMT 4OHMT, 6βOHMT and 19OHMT after 24-hour incubation of MT with CYP1B1 (sample CYP1B1_1) 124

Figure 97: Chromatograms MRM of MT, 2αOHMT, 2βOHMT 4OHMT, 6βOHMT and 19OHMT after 24-hour incubation of MT with CYP1B1 (sample CYP1B1_2)..... 124

Figure 98: Chromatograms MRM of MT, 2αOHMT, 2βOHMT 4OHMT, 6βOHMT and 19OHMT after 24-hour incubation of MT with aromatase (sample CYP19_1) 125

Figure 99: Chromatograms MRM of MT, 2αOHMT, 2βOHMT 4OHMT, 6βOHMT and 19OHMT after 24-hour incubation of MT with aromatase (sample CYP19_2)..... 125

Figure 100: Chromatograms MRM of MT, 2αOHMT, 2βOHMT 4OHMT, 6βOHMT and 19OHMT after 24-hour incubation of MT with aromatase (sample CYP19_3)..... 126

10 List of tables

Table 1: Steroids and reference material 15

Table 2: Solvents, reagents, and materials 16

Table 3: Overview of the used methods, showing the used instruments, their field of application in this thesis, and the method shortcut 18

Table 4: Parameters for LC purification method a) 19

Table 5: HPLC-ESI-MS parameters for method b) 20

Table 6: HPLC-ESI-QTOF-MS parameters for method c) 21

Table 7: SFC-ESI-QQQ-MS parameters, method d) + e) 22

Table 8: Precursor and product ions of 17α-methyltestosterone, its hydroxy metabolites and internal standards for MRM experiments, method d) 23

Table 9: Precursor and product ions of androst-4-ene-3,17-dione, its hydroxy metabolites, and the internal standard MD for MRM experiments; method e) .. 24

Table 10: GC-EI-MS parameters applied in method f) 27

Table 11: GC-EI-MS parameters applied in method g) 28

Table 12: GC-EI-QTOF-MS parameters applied in method h) 28

Table 13: Postulated fragments, their exact mass, accurate mass, and the resulting mass errors for tris-TMS derivatives of 2α-hydroxy-17α-methyltestosterone (GC-QTOF-MS) 41

Table 14: Postulated fragments, their exact mass, accurate mass, and the resulting mass differences for tris-TMS derivatives of 2β-hydroxy-17α-methyltestosterone (GC-QTOF-MS) 41

Table 15: Chemical shifts of 2ξ-hydroxy-17α-methyltestosterone (^{1}H-NMR and ^{13}C-NMR) in comparison to predicted values and chemical shifts of 2ξ-hydroxytestosterone from literature [70, 71]; *value for 4-hydroxytestosterone [71] 45

Table 16: Postulated fragments, their exact mass, accurate mass, and the resulting mass differences for 4-hydroxy-17α-methyltestosterone, GC-QTOF-MS of per-TMS derivative 47

Table 17: Chemical shifts of 4-hydroxy-17α-methyltestosterone (^{1}H-NMR and ^{13}C-NMR) in comparison to predicted values and chemical shifts of 4-hydroxyandrost-4-ene-3,17-dione from literature [70, 71], *value for 4-hydroxytestosterone [71] ... 51

Table 18: RTs of mono- and per-TMS derivatives of 2αOHMT, 2βOHMT, 4OHMT, and 6βOHMT for method f) and method g) 60

Table 19: Retention times of the reference standards 2αOHMT, 2βOHMT, 4OHMT, and 6βOHMT for the three LC-MS methods (LC-ESI-MS/LC-ESI-QQQ-MS/LC-ESI-QTOF-MS) 62

Table 20: Comparison of the absolute and relative (%) peak area of MT, 2αOHMT, 2βOHMT, 4OHMT, 6βOHMT and 19OHMT after HLM incubation (HLM_1, and HLM_2) and the negative control sample; * sample HLM_1 had a substrate concentration of only 10 µg/mL 70

Table 21: Comparison of the relative and absolute (%) peak area of MT, 2αOHMT, 2βOHMT, 4OHMT, 6βOHMT, and 19OHMT after HLM incubation (CYP2C19_1, CYP2C19_2, and CYP2C19_3) to the negative control sample 73

Table 22: Comparison of the relative and absolute (%) peak area of MT, 2αOHMT, 2βOHMT, 4OHMT, 6βOHMT and 19OHMT after HLM incubation (CYP1A2_1, CYP1A2_2, and CYP1A2_3) to the negative control sample 76

Table 23: Comparison of the relative and absolute (%) peak area of MT, 2αOHMT, 2βOHMT, 4OHMT, 6βOHMT, and 19OHMT after HLM incubation (CYP1B1_1 and CYP1B1_2) to the negative control sample 76

Table 24: Comparison of the relative and absolute (%) peak area of MT, 2αOHMT, 2βOHMT, 4OHMT, 6βOHMT, and 19OHMT after HLM incubation (CYP19A1_1, CYP19A1_2, and CYP19A1_3) to the negative control sample; * sample CYP19A1_1 had a substrate concentration of only 10 µg/mL 79

Table 25: Overview of the results of the in vivo studies of MT; ✓ showing the finding of the metabolite in the specific incubation; (✓) showing the finding in a small amount, comparable to the negative control sample 80

11 Annex

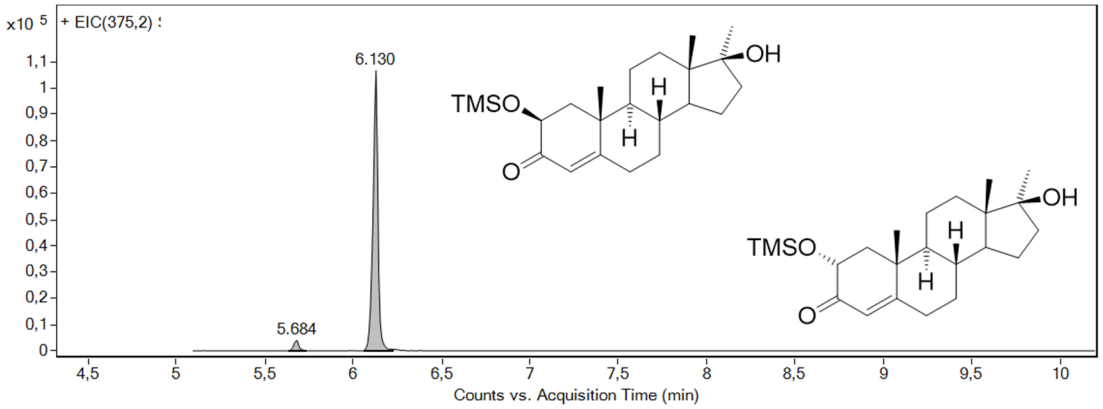

Figure 63: GC-EI-MS chromatogram (EIC) of 2αOHMT (RT 6.130 min) and 2βOHMT (RT 5.684 min) as mono-TMS derivative

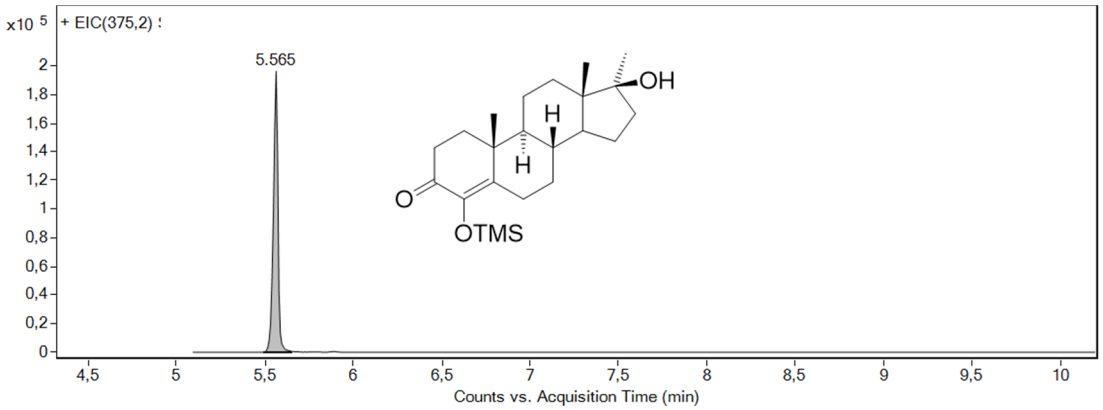

Figure 64:GC-EI-MS chromatogram (EIC) of 4OHMT as mono-TMS derivative (RT 5.565 min)

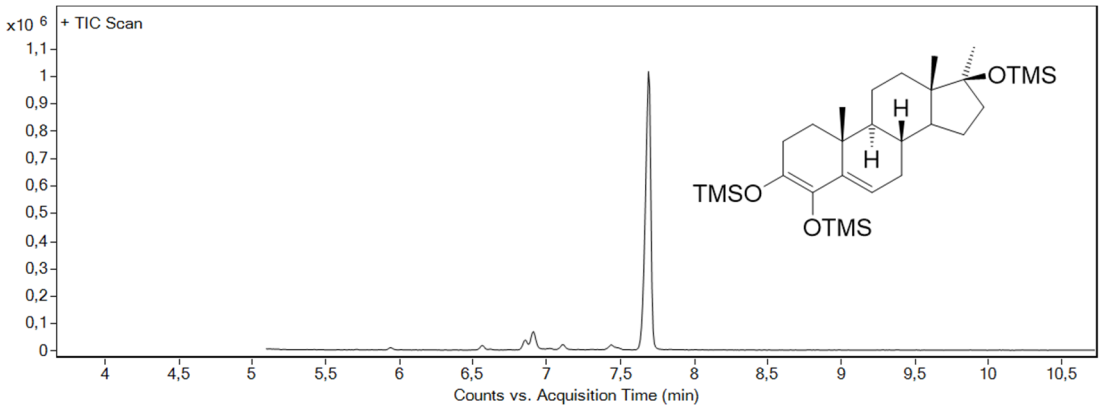

Figure 65: GC-EI-MS chromatogram (TIC) of 4OHMT as per-TMS derivative (RT 5.565 min)

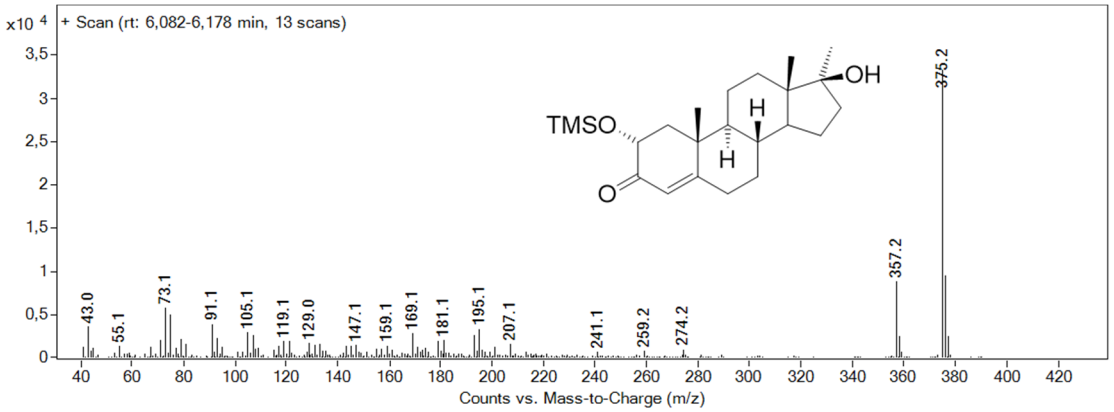

Figure 66: GC-EI-MS spectra of 2αOHMT as mono TMS derivative at 70 eV [M-15]$^{\bullet+}$= 375.2

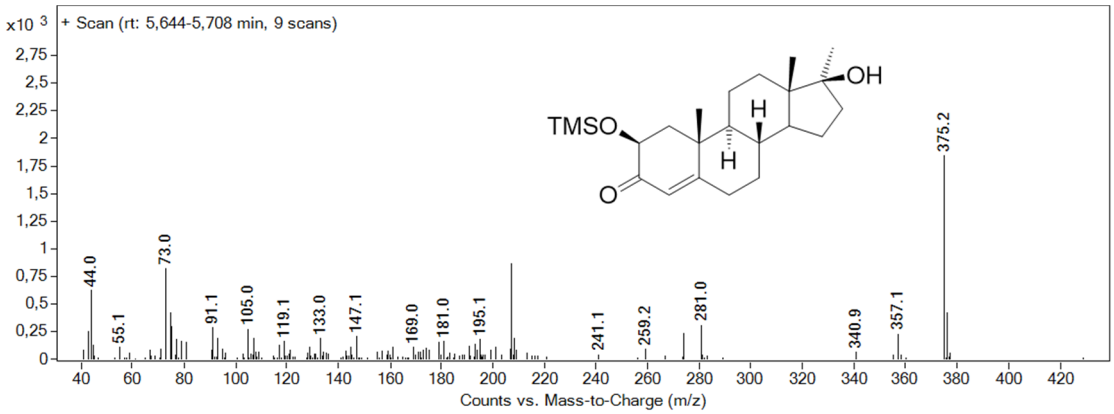

Figure 67: GC-EI-MS spectra of 2βOHMT as mono TMS derivative at 70 eV [M-15]$^{\bullet+}$= 375.2

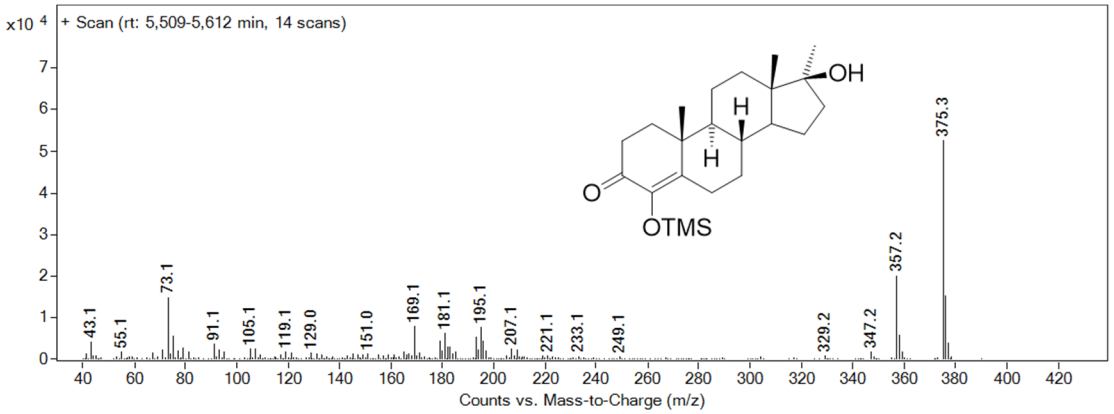

Figure 68:GC-EI-MS spectra of 4OHMT as mono TMS derivative at 70 eV [M-15]$^{\bullet+}$= 375.3

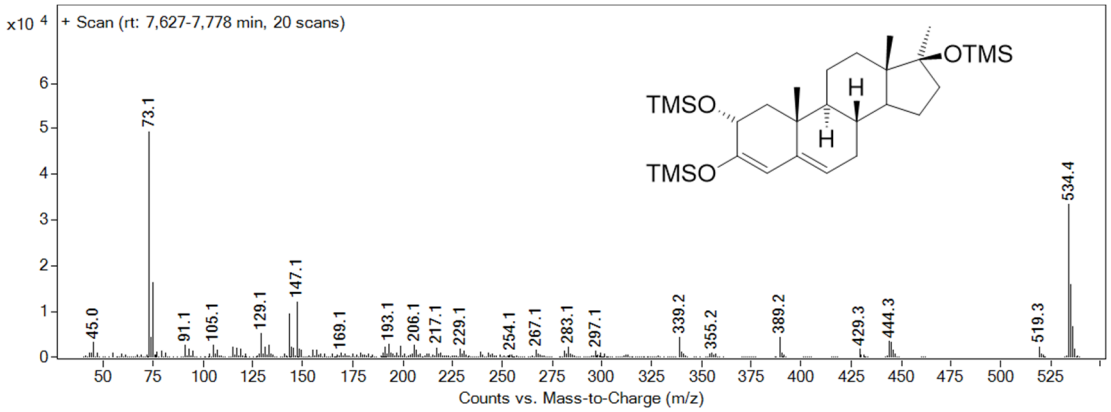

Figure 69: GC-EI-MS spectra of 2αOHMT as per TMS derivative at 70 eV $[M]^{\bullet+}$= 534.4

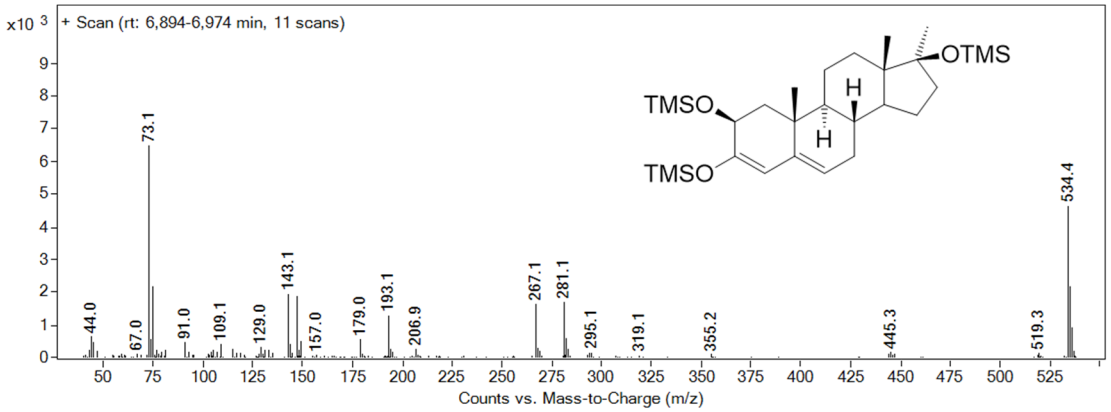

Figure 70: GC-EI-MS spectra of 2βOHMT as per TMS derivative at 70 eV $[M]^{\bullet+}$= 534.4

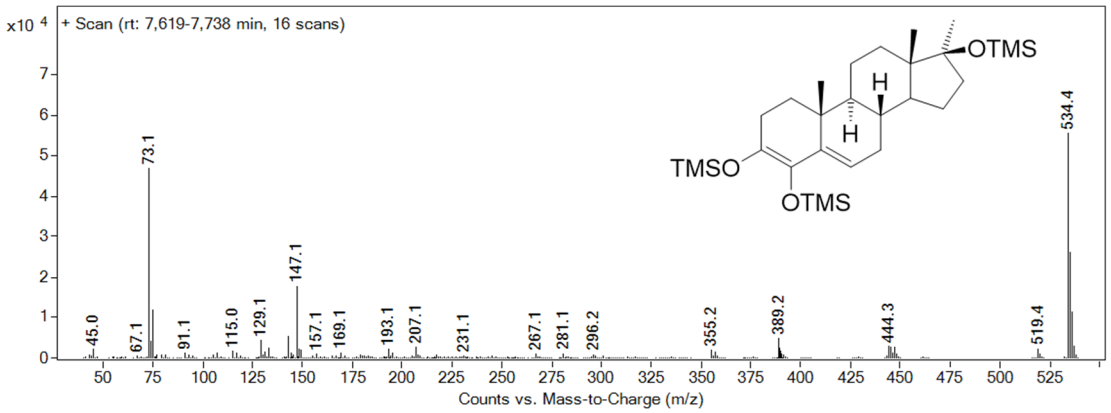

Figure 71: GC-EI-MS spectra of 4OHMT as per TMS derivative at 70 eV $[M]^{\bullet+}$= 534.4

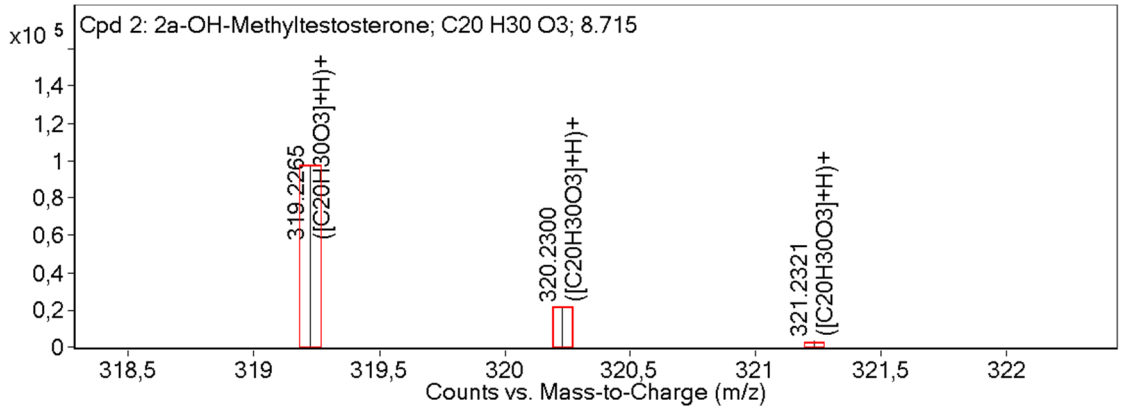

Figure 72: HRMS ESI spectrum, accurate mass of 2α-hydroxy-17α-methyltestosterone $[M+H]^+$ = 319.2265

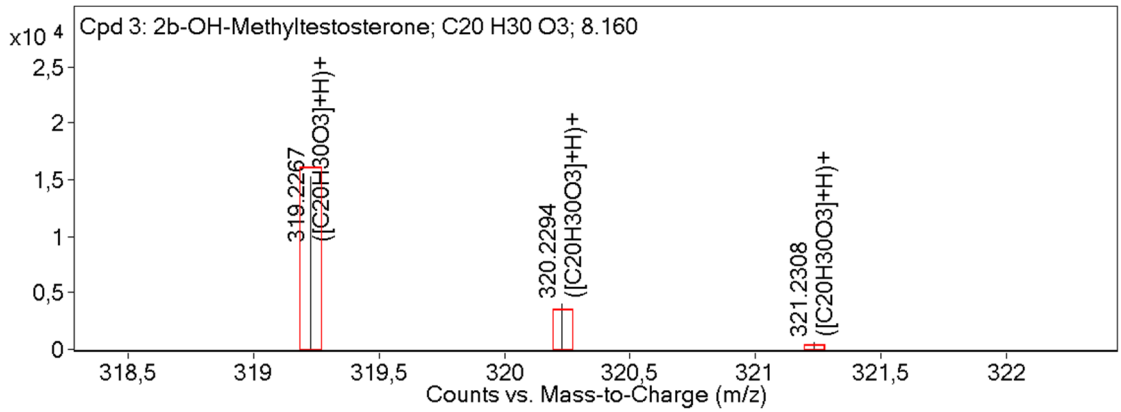

Figure 73: HRMS ESI spectrum, accurate mass of 2β-hydroxy-17α-methyltestosterone $[M+H]^+$ = 319.2267

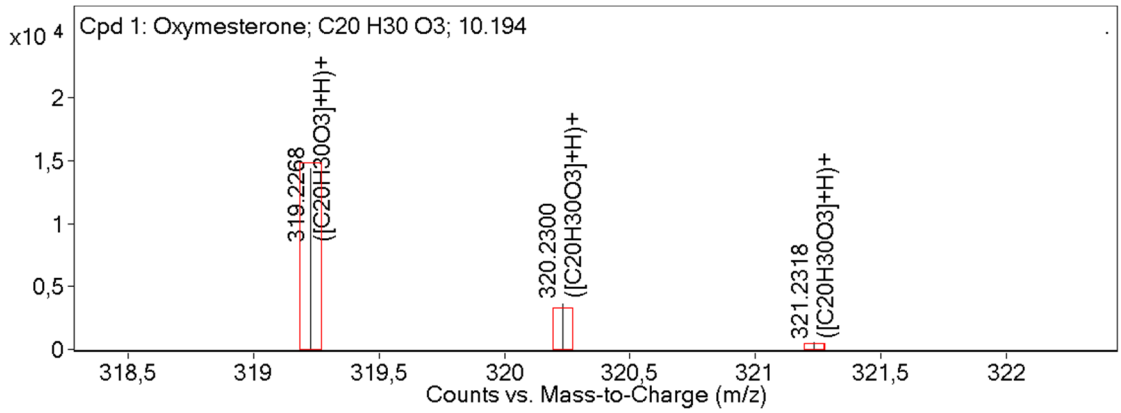

Figure 74: HRMS ESI spectrum, accurate mass of 4-hydroxy-17α-methyltestosterone $[M+H]^+$ = 319.2268

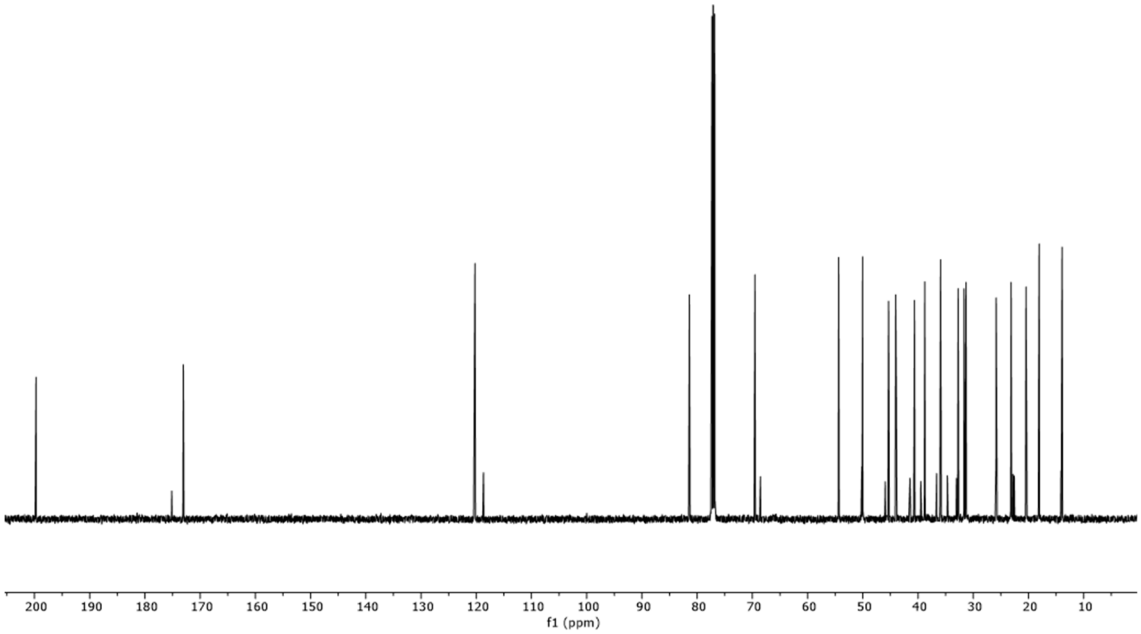

Figure 75: ^{13}C NMR spectrum of 2ξ-hydroxy-17α-methyltestosterone

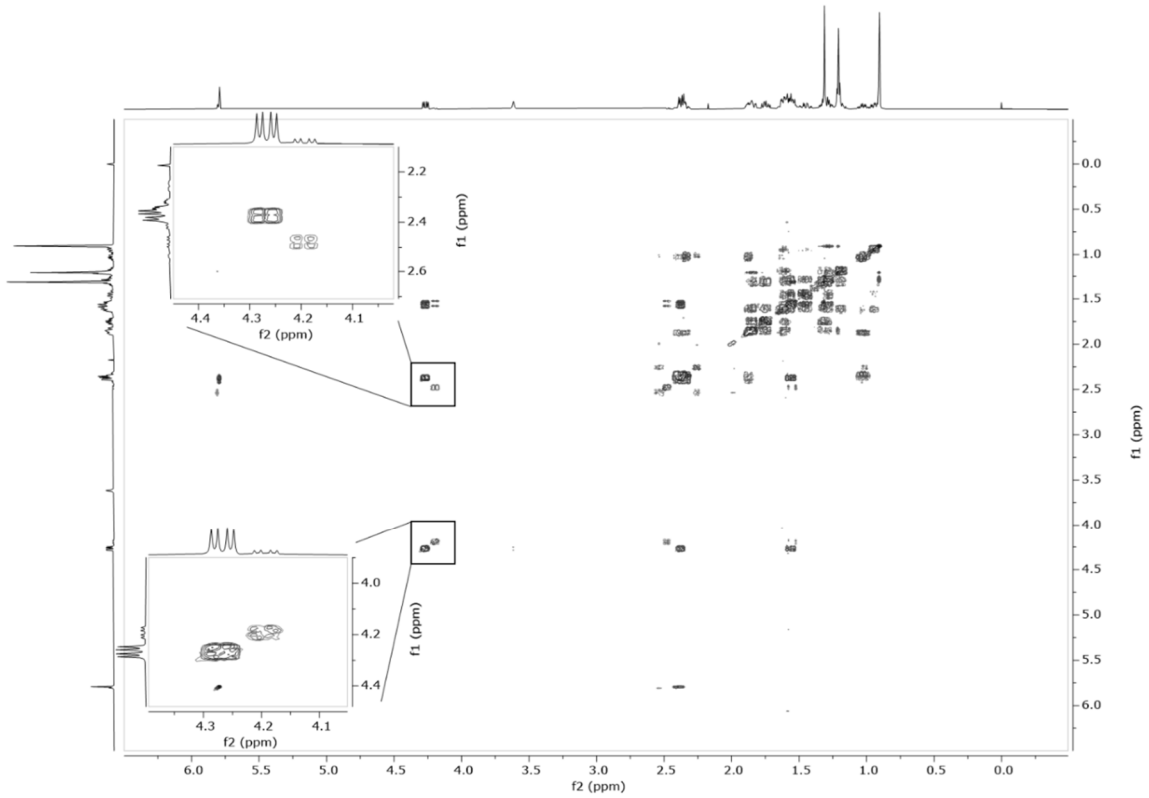

Figure 76: $^{1}H,^{1}H$-COSY spectrum of 2ξ-hydroxy-17α-methyltestosterone, inserts show zoom areas of 4.1 – 4.35 ppm and 4.0 – 4.5 ppm / 4.1 - 4.4 ppm and 2.2 – 2.6 ppm

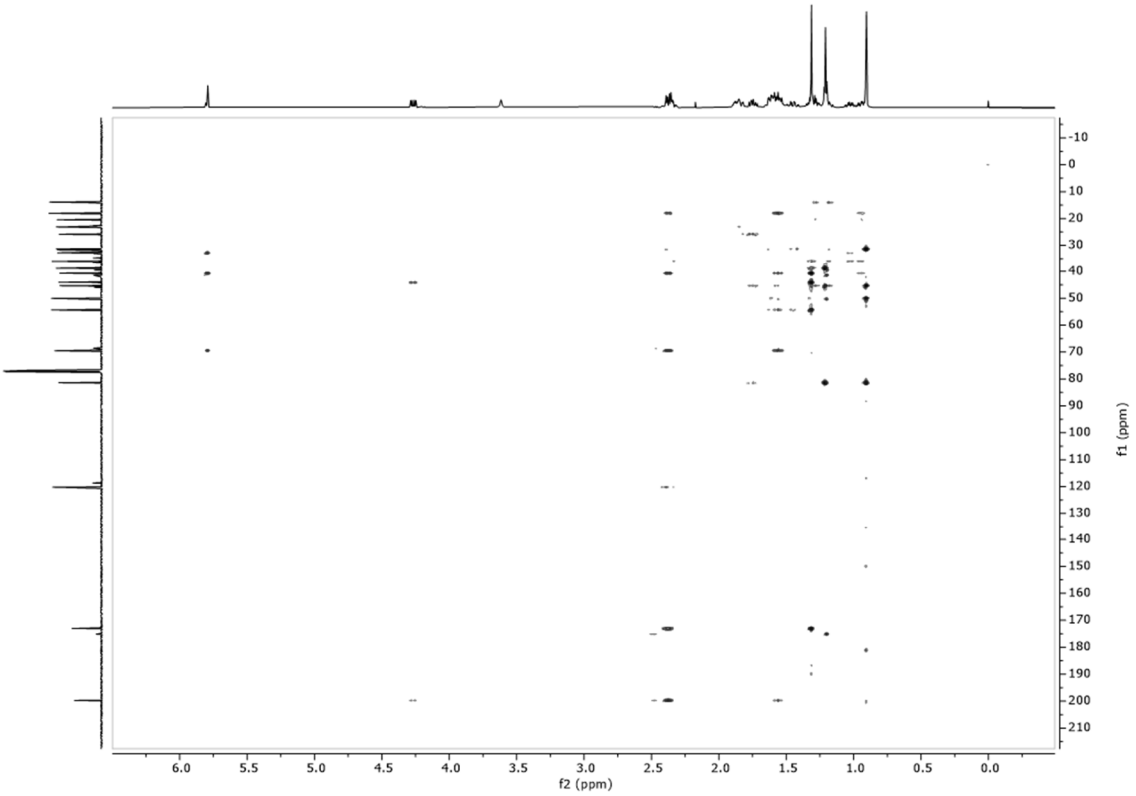

Figure 77: $^{1}H,^{13}C$-HMBC spectrum of 2ξ-hydroxy-17α-methyltestosterone

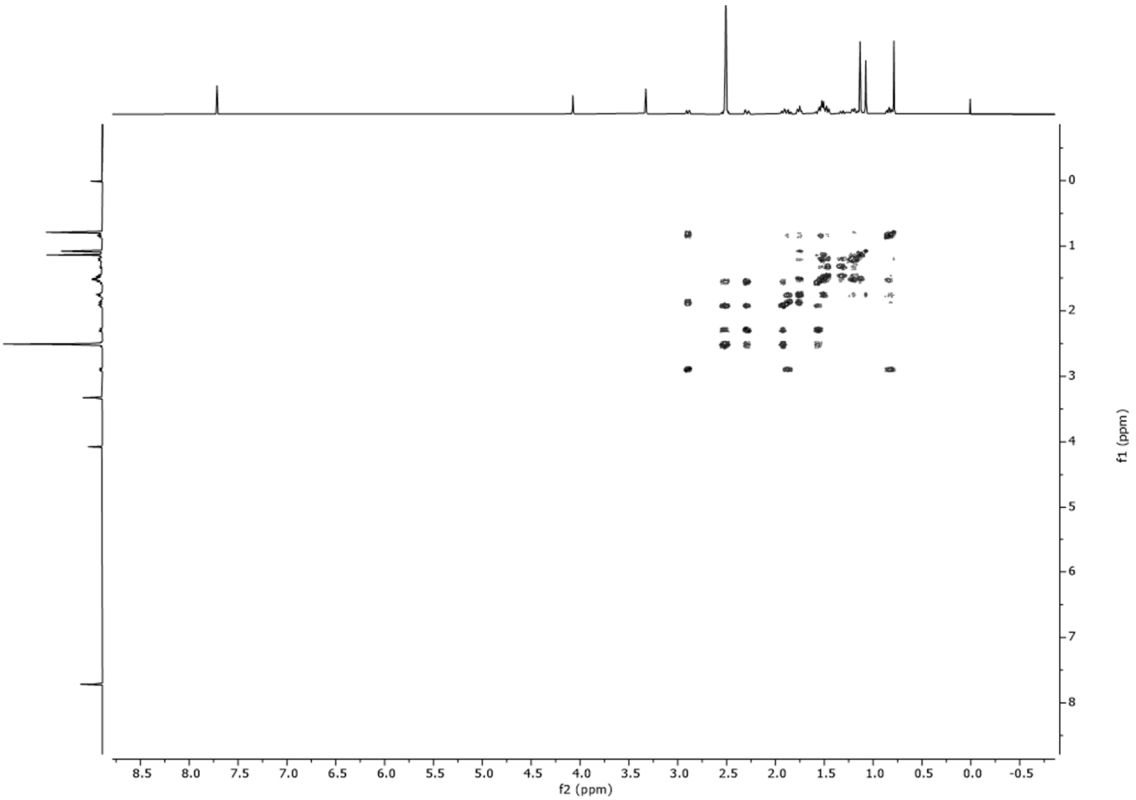

Figure 78: $^{1}H,^{1}H$-COSY spectrum of 4-hydroxy-17α-methyltestosterone

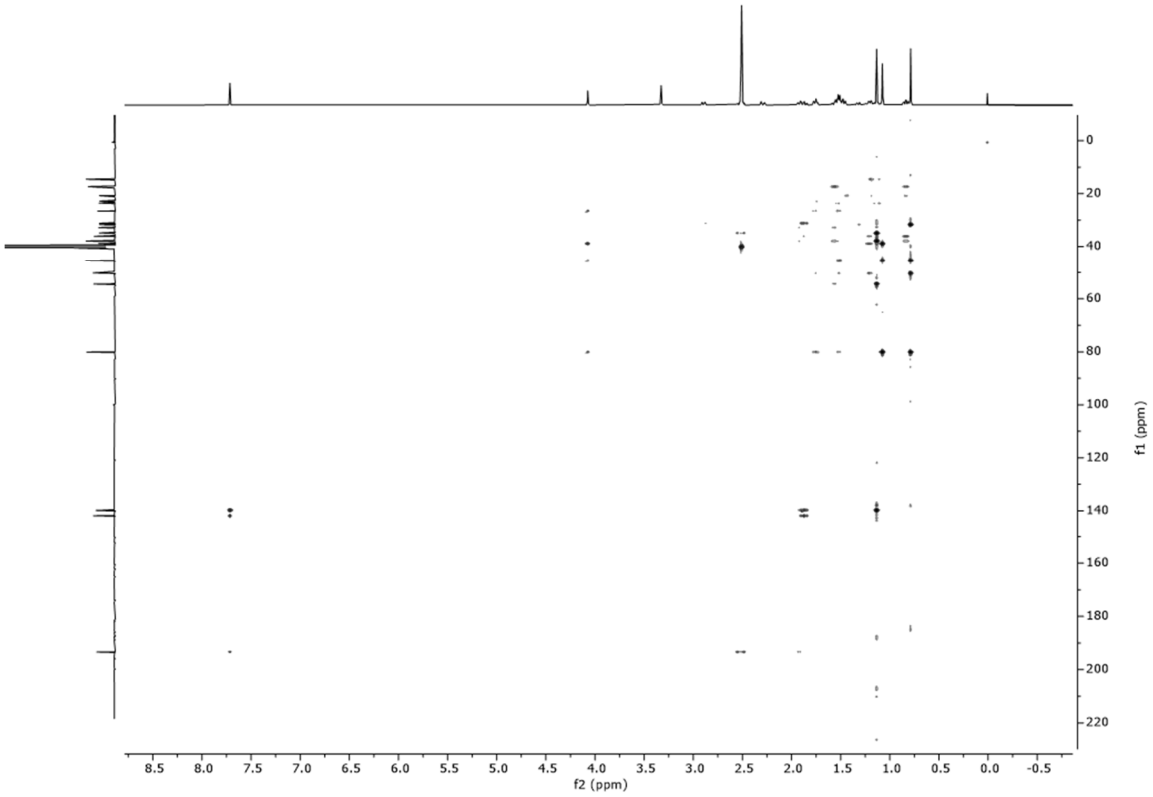

Figure 79: $^{1}H,^{13}C$-HMBC spectrum of 4-hydroxy-17α-methyltestosterone

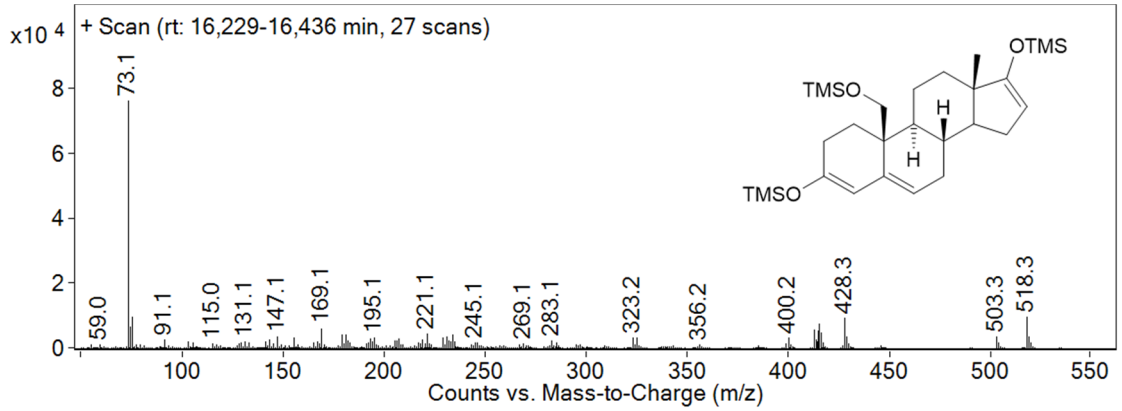

Figure 80:GC-EI-MS spectra of 19OHAED as per-TMS derivative at 70 eV $[M]^{\bullet+}$= 518.3

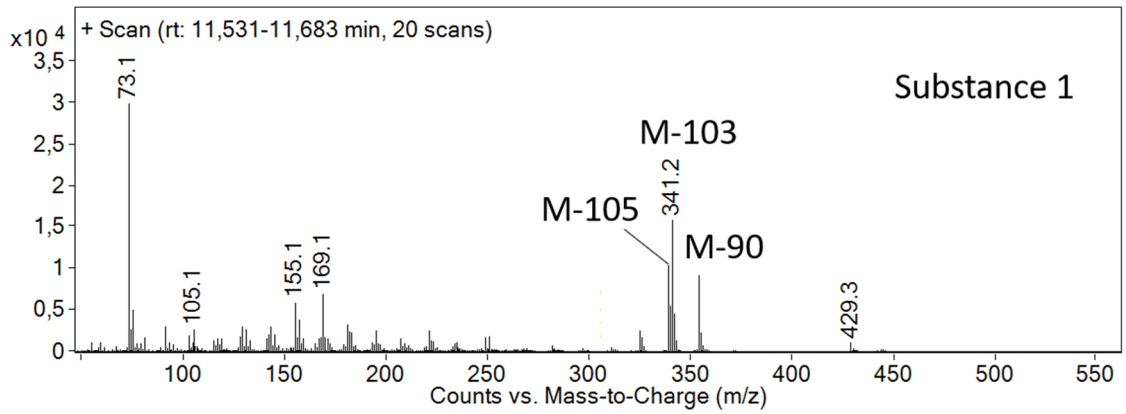

Figure 81: GC-EI-MS spectra of byproduct 1 of 19OHMT synthesis after TMIS derivatization at 70 eV $[M]^{\bullet+}$= 444.3

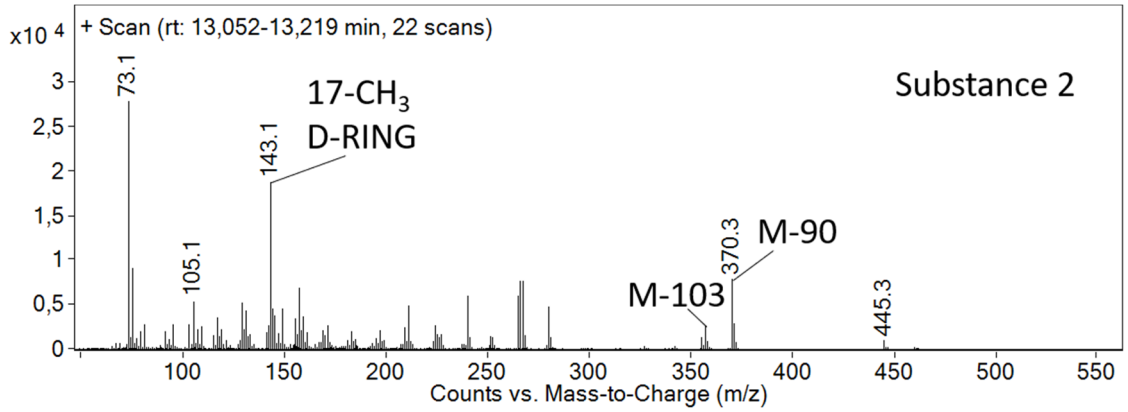

Figure 82: GC-EI-MS spectra of byproduct 2 of 19OHMT synthesis after TMIS derivatization at 70 eV [M]•+= 460.3

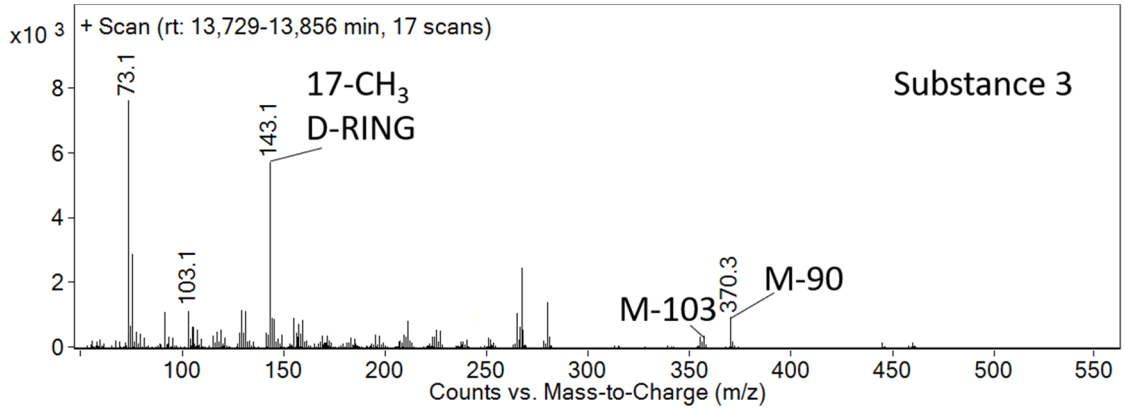

Figure 83: GC-EI-MS spectra of byproduct 3 of 19OHMT synthesis after TMIS derivatization at 70 eV [M]•+= 460.2

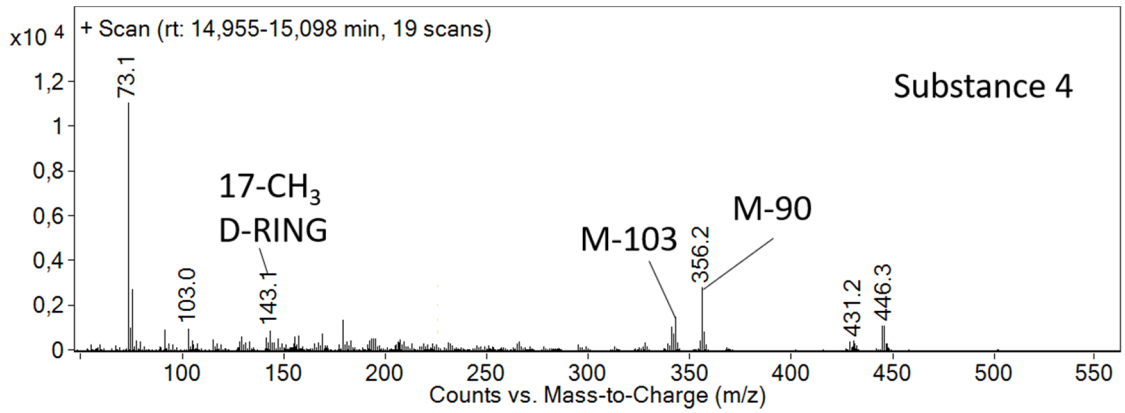

Figure 84: GC-EI-MS spectra of byproduct 4 of 19OHMT synthesis after TMIS derivatization at 70 eV [M]•+= 446.3

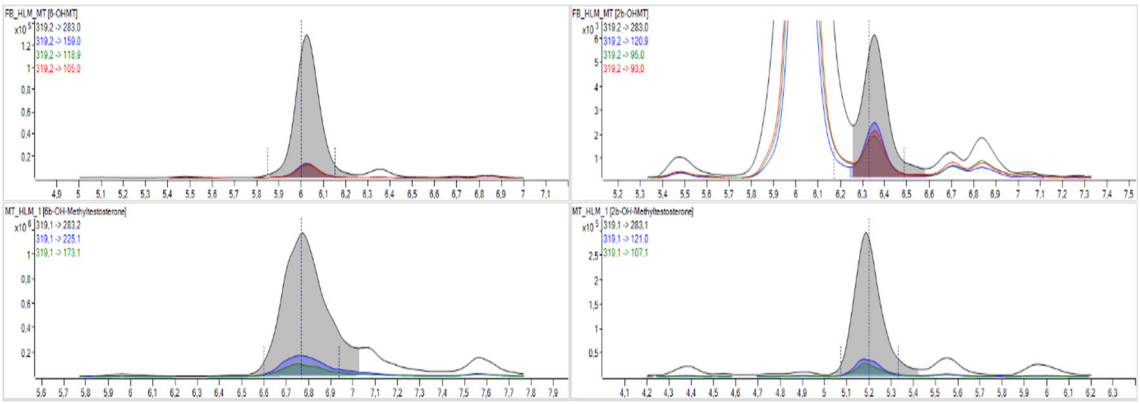

Figure 85: LC (upper chromatogram) vs. SFC (lower chromatogram) method; comparison exemplified with sample HLM_1 with 6βOHMT (area 15923065 vs. 990511) and 2βOHMT (area 2443467 vs. 47775)

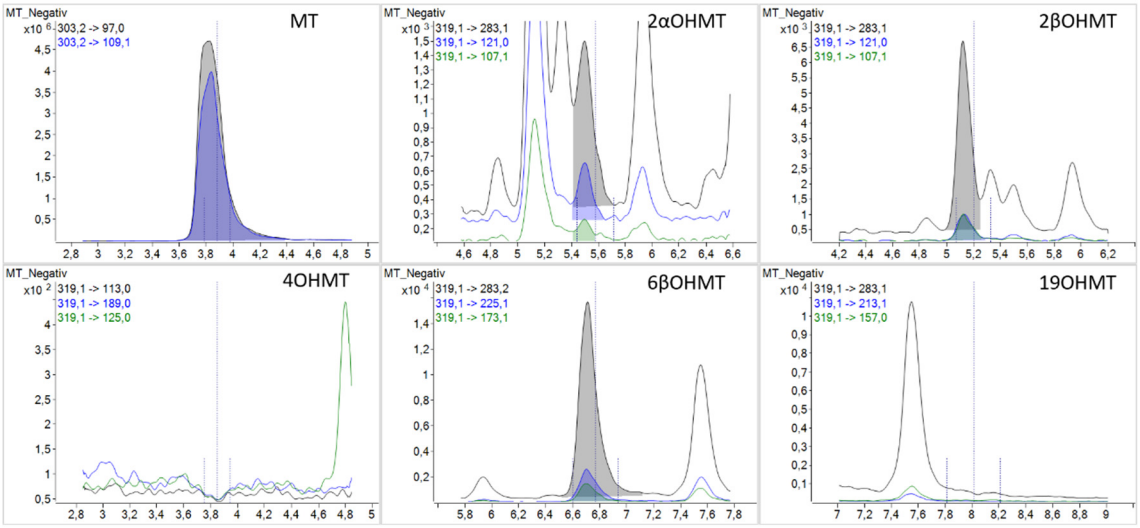

Figure 86: Chromatograms MRM (MT, 2αOHMT, 2βOHMT,4OHMT, 6βOHMT, 19OHMT) of the negative control of in vitro metabolization

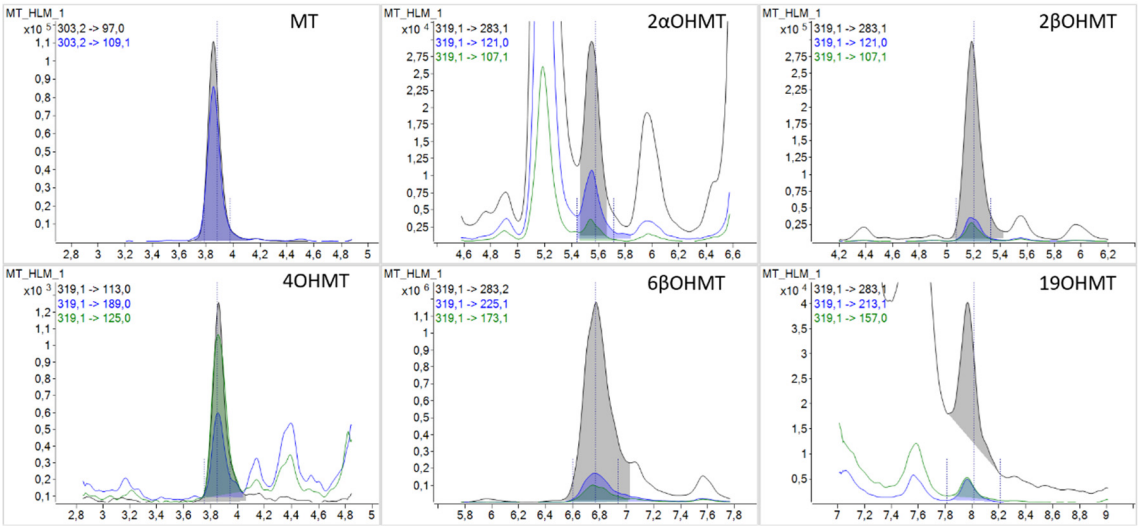

Figure 87: Chromatograms MRM of MT, 2αOHMT, 2βOHMT 4OHMT, 6βOHMT and 19OHMT after 24-hour incubation of MT with pooled human liver microsomes (sample HLM_1)

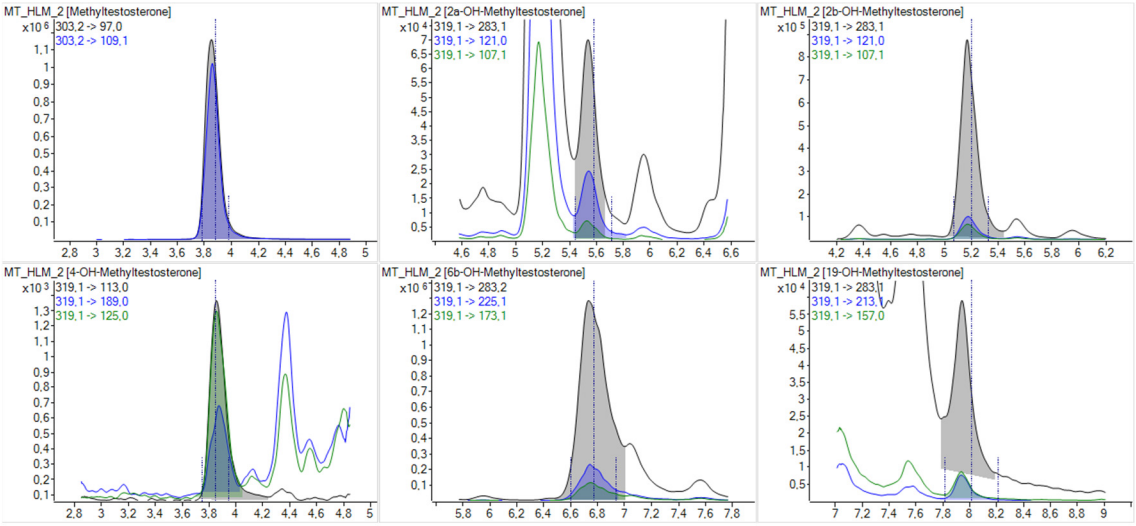

Figure 88: Chromatograms MRM of MT, 2αOHMT, 2βOHMT 4OHMT, 6βOHMT and 19OHMT after 24-hour incubation of MT with pooled human liver microsomes (sample HLM_2)

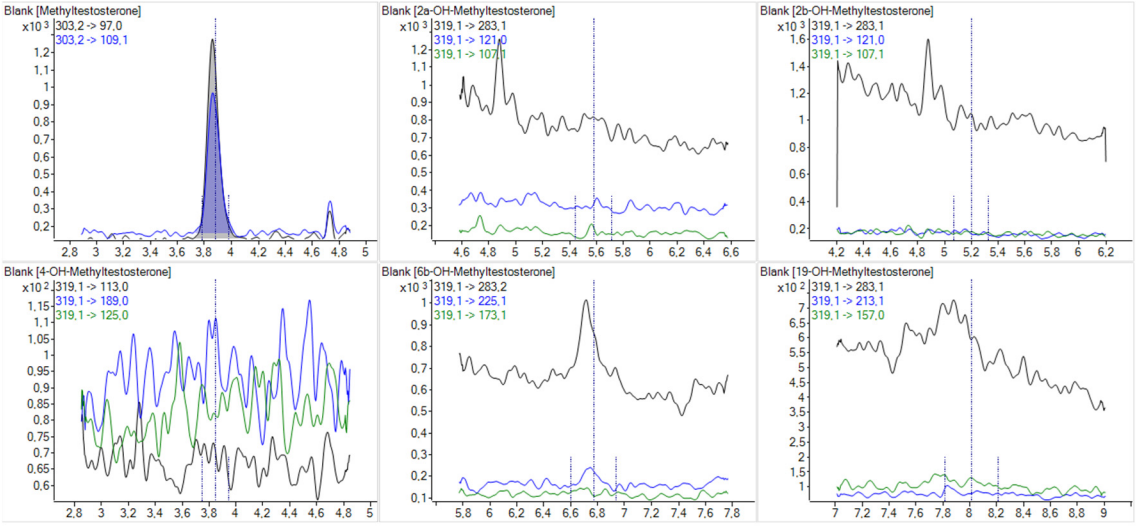

Figure 89: Chromatograms MRM; MT incubation studies methanol blank 1; carryover of MT visible

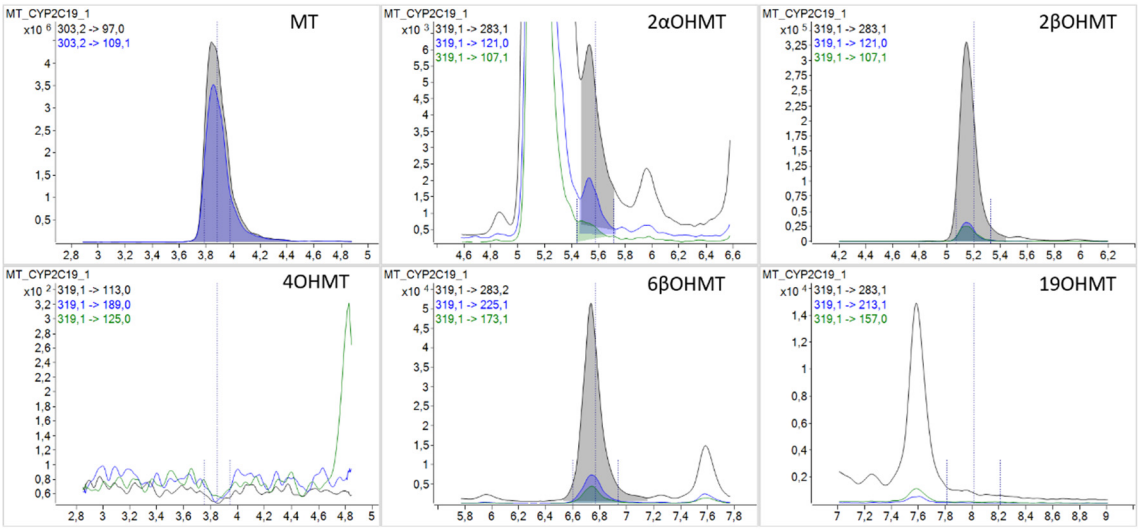

Figure 90: Chromatograms MRM of MT, 2αOHMT, 2βOHMT 4OHMT, 6βOHMT and 19OHMT after 24-hour incubation of MT with CYP2C19 (sample (CYP2C19_1)

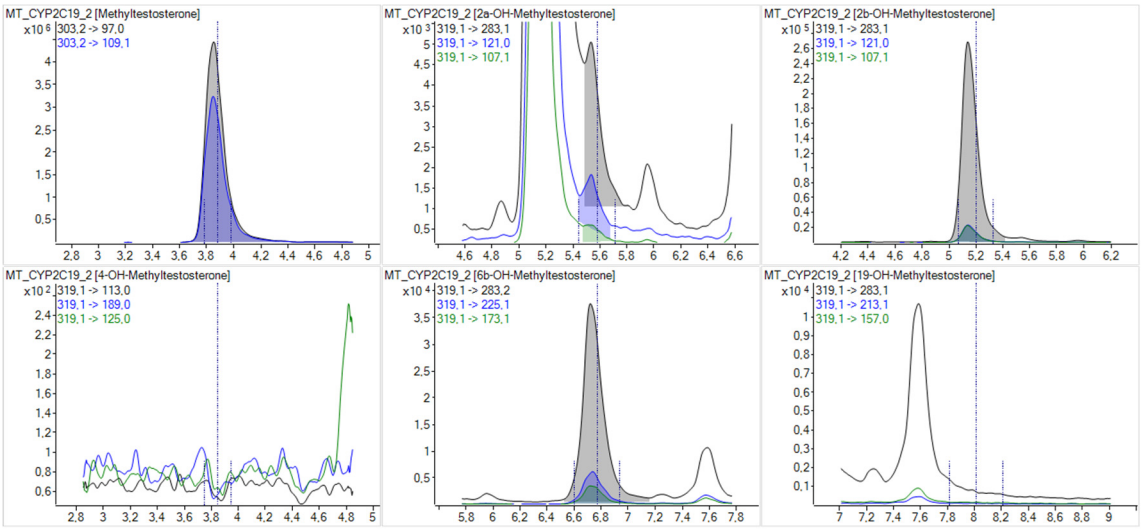

Figure 91: Chromatograms MRM of MT, 2αOHMT, 2βOHMT 4OHMT, 6βOHMT and 19OHMT after 24-hour incubation of MT with CYP2C19 (sample CYP2C19_2)

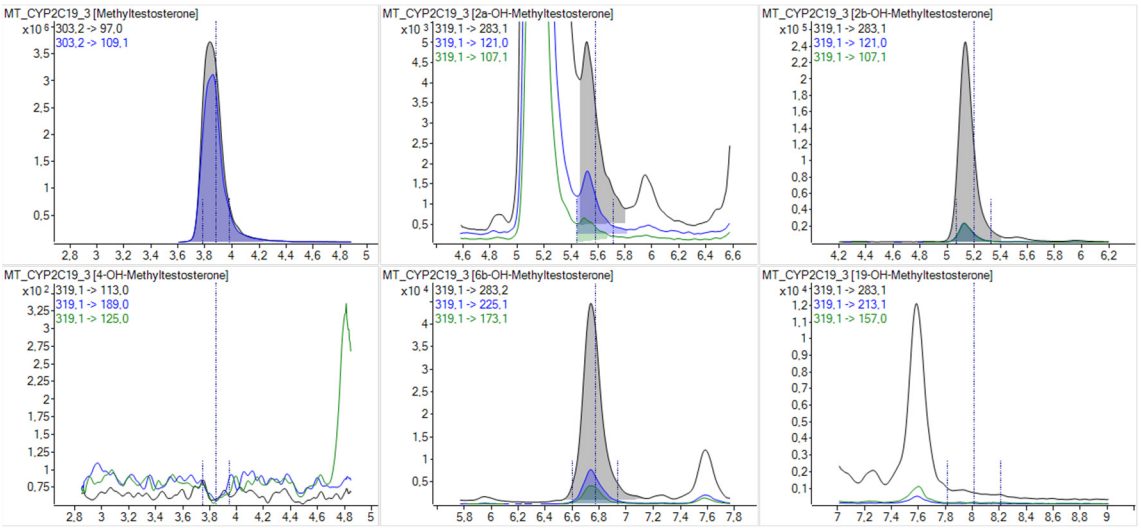

Figure 92: Chromatograms MRM of MT, 2αOHMT, 2βOHMT 4OHMT, 6βOHMT and 19OHMT after 24-hour incubation of MT with CYP2C19 (sample CYP2C19_3)

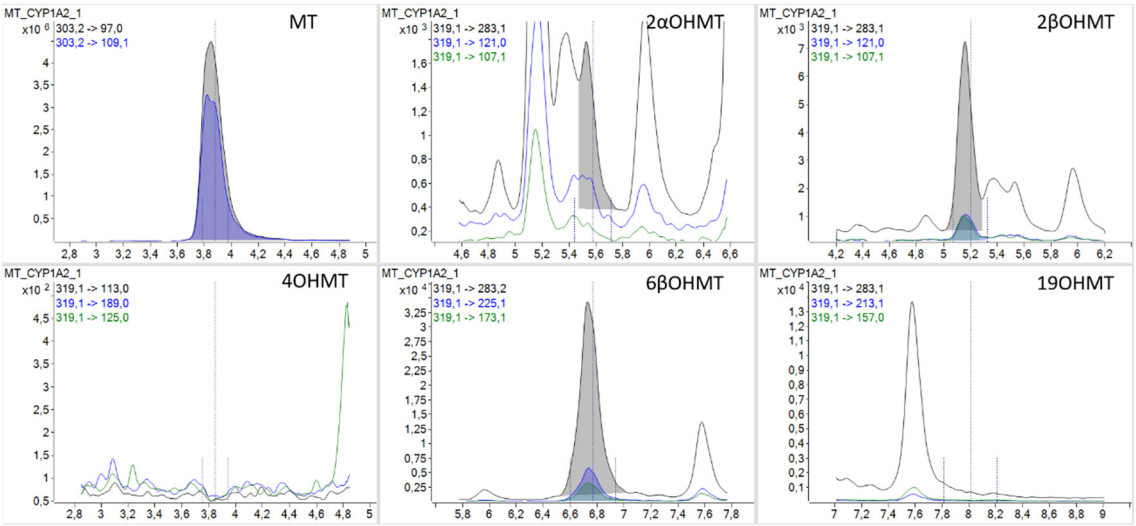

Figure 93: Chromatograms MRM of MT, 2αOHMT, 2βOHMT 4OHMT, 6βOHMT and 19OHMT after 24-hour incubation of MT with CYP1A2 (sample CYP1A2_1)

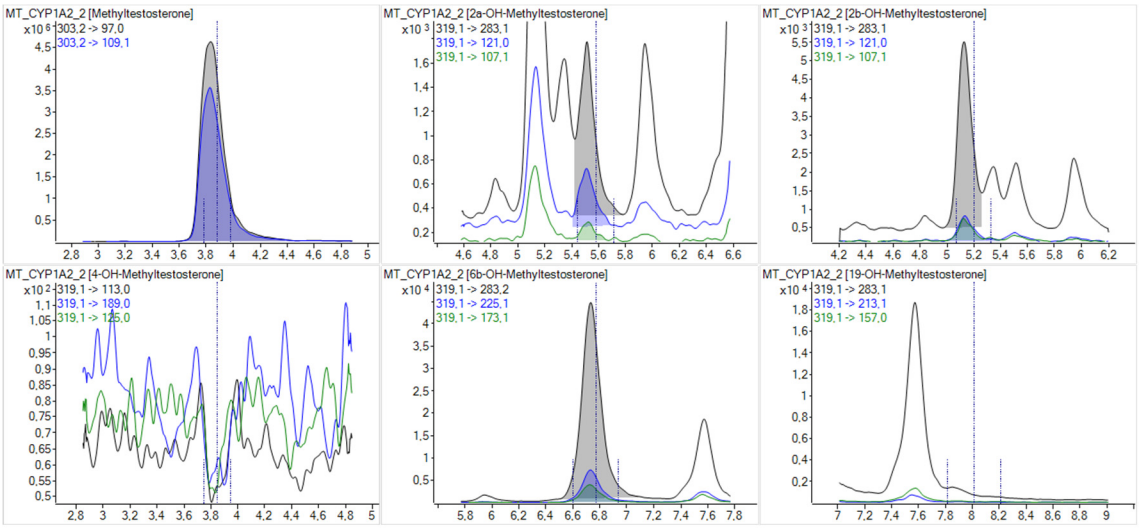

Figure 94: Chromatograms MRM of MT, 2αOHMT, 2βOHMT 4OHMT, 6βOHMT, and 19OHMT after 24-hour incubation of MT with CYP1A2 (sample CYP1A2_2)

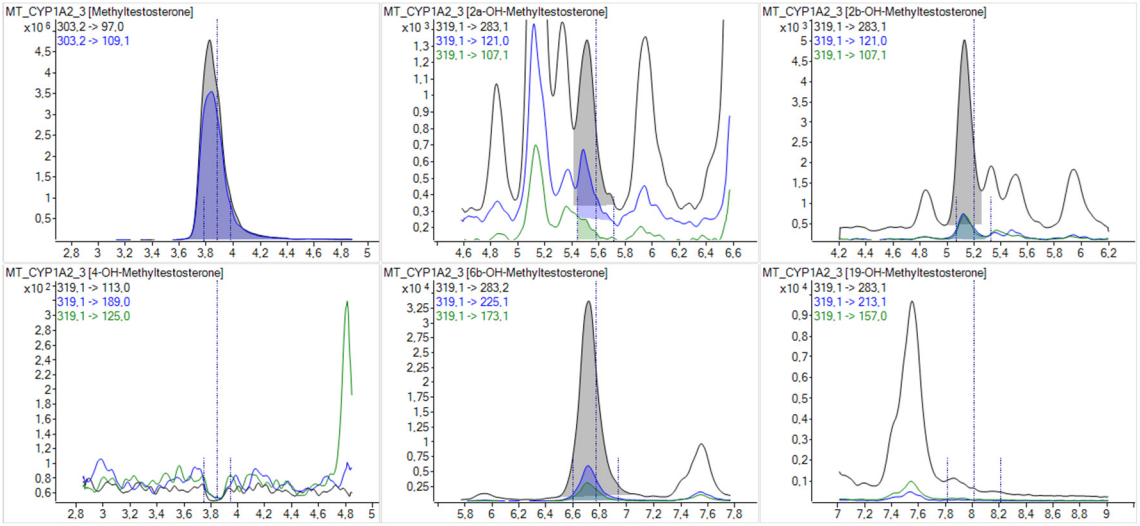

Figure 95: Chromatograms MRM of MT, 2αOHMT, 2βOHMT 4OHMT, 6βOHMT and 19OHMT after 24-hour incubation of MT with CYP1A2 (sample CYP1A2_3)

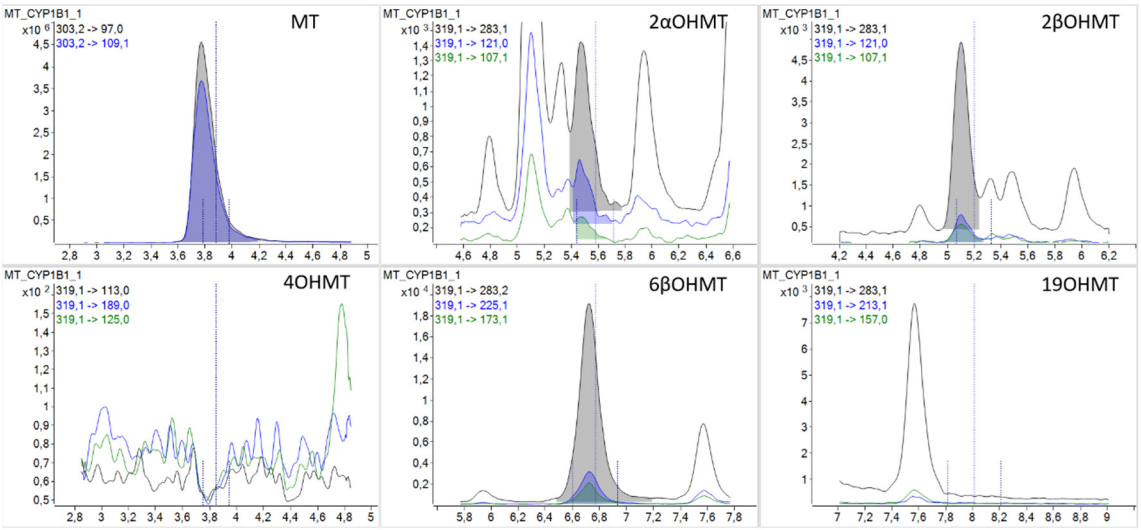

Figure 96: Chromatograms MRM of MT, 2αOHMT, 2βOHMT 4OHMT, 6βOHMT and 19OHMT after 24-hour incubation of MT with CYP1B1 (sample CYP1B1_1)

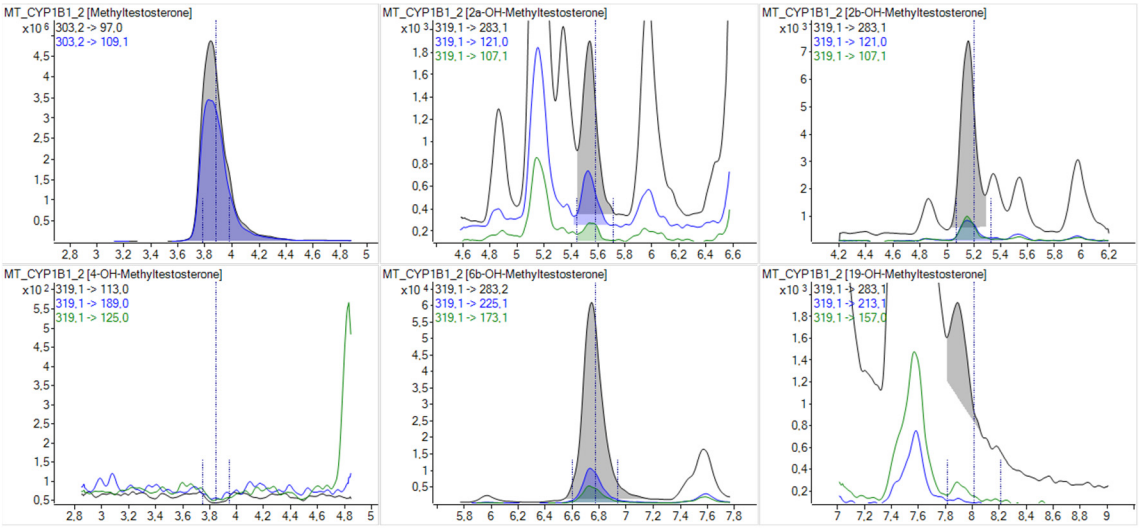

Figure 97: Chromatograms MRM of MT, 2αOHMT, 2βOHMT 4OHMT, 6βOHMT and 19OHMT after 24-hour incubation of MT with CYP1B1 (sample CYP1B1_2)

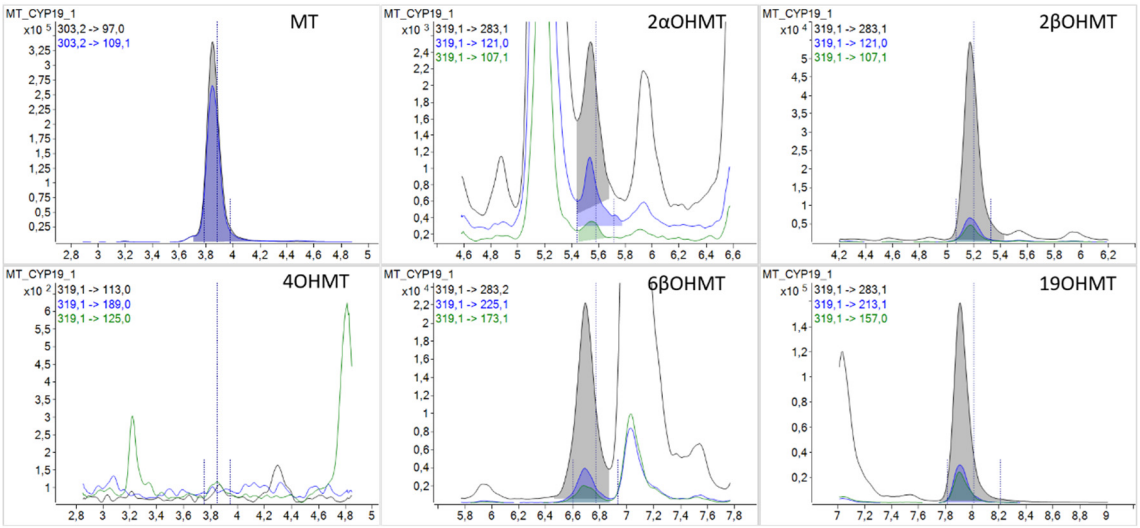

Figure 98: Chromatograms MRM of MT, 2αOHMT, 2βOHMT 4OHMT, 6βOHMT and 19OHMT after 24-hour incubation of MT with aromatase (sample CYP19_1)

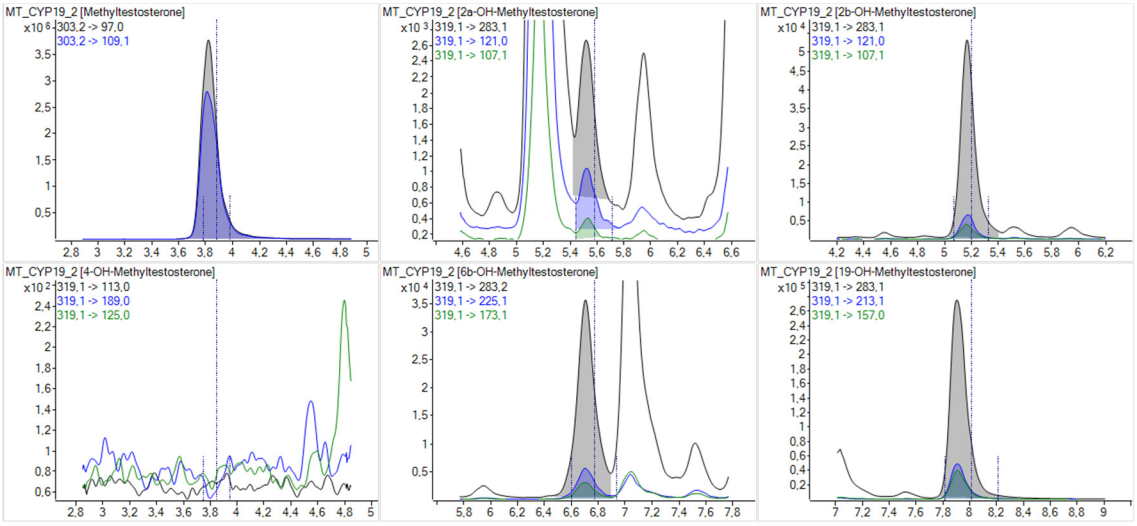

Figure 99: Chromatograms MRM of MT, 2αOHMT, 2βOHMT 4OHMT, 6βOHMT and 19OHMT after 24-hour incubation of MT with aromatase (sample CYP19_2)

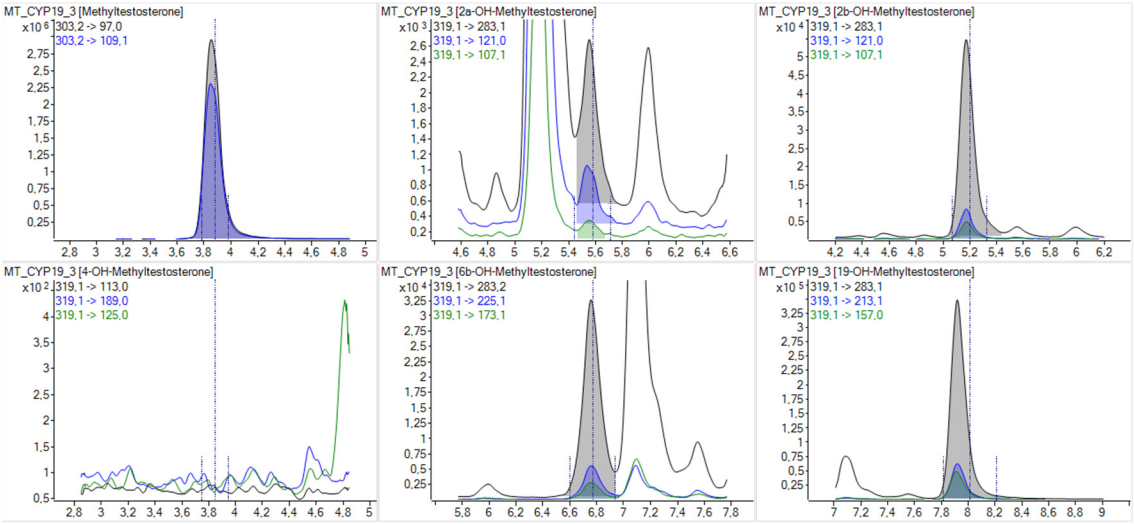

Figure 100: Chromatograms MRM of MT, 2αOHMT, 2βOHMT 4OHMT, 6βOHMT and 19OHMT after 24-hour incubation of MT with aromatase (sample CYP19_3)